Cross-linking Methods for 3D Printable Hydrogel Materials

Dylan Karis

A dissertation
submitted in partial fulfillment of the
requirements for the degree of

Doctor of Philosophy

University of Washington

2020

Reading Committee:
Alshakim Nelson, Chair
Matthew Golder
Joshua Vaughan

Program Authorized to Offer Degree:
Chemistry

University of Washington

Abstract

Cross-linking Methods for 3D Printable Hydrogel Materials

Dylan Karis

Chair of the Supervisory Committee:
Professor Alshakim Nelson
Department of Chemistry

Stimuli-responsive hydrogels have gained increased attention for a broad range of biomedical and biotechnological applications. Synthetic polymeric systems are an attractive platform as they afford tunability through the control of monomer side-chains and block composition. Additive manufacturing, as a versatile method of fabrication, is widely used in bioprinting however, the range of functional materials is limited. This dissertation describes the research on the design and development of novel polymer hydrogels and the characterization of rheological characteristics to enable extrusion-based additive manufacturing applications. Chapter 1 is an introduction to additive manufacturing and stimuli-responsive polymeric hydrogels. The study of Chapter 2 represents our work on developing a novel cross-linkable hydrogel based on alkyl glycidyl ether monomers. The resulting gel has tunable stiffness based on photoinitiator

concentration and UV irradiation length. Chapter 3 focuses on the exploration of telechelic functionalization of F127 to modify the gelation temperature and rheology. The only modifications that resulted in a noticeable change were the addition of a urea spacer and formulation of boronic acid chain-ends with galactose functionalized F127 or curdlan polysaccharide. The work of Chapter 4 discusses the influence a water-soluble dithiol has on the competition between chain-extension and polymerization on a methacrylated F127 hydrogel. When the dithiol is formulated in excess, slow thiol-ene occurs over the course of days to increase the molecular weight of F127 chains before UV cure. Careful control of equilibration prior to UV cure affords a gel that is stretchable and suturable when extruded through a coaxial nozzle.

TABLE OF CONTENTS

LIST OF FIGURES

LIST OF TABLES

ACKNOWLEDGEMENTS

First and foremost, I would like to thank my advisor, Dr. Alshakim Nelson, for his help and guidance during my graduate school life at the University of Washington. Al's enthusiasm for science and research is contagious and when meeting with him, you feel motivated and encouraged that you can accomplish the necessary experiments to move forward. Besides chemistry, he has also been an excellent role model on what a good research leader looks like and sets the standard that I hope to achieve as a mentor in the future. I believe the experience in research, collaboration, and the ability to communicate scientifically that I received during my Ph.D. will be of value for the rest of my career.

Also, I would like to thank other group members in the Nelson lab. Ryan Shafranek, Trevor Johnston, and Amrita Basu for being part of the first-year crew and working together to figure out "this whole grad school thing." Dr. Rob Ono and Dr. Abhijit Saha for being excellent postdocs in getting the lab started. Jenn Wong, Chris Fellin, and Patrick Smith for being there in the office to bounce ideas off and discuss research as well as being pillars of positivity when I am having a particularly bad day.

Additionally, I am indebted to the professors who gave me helpful suggestions and discussions during my exams and on my research projects, including all of my committee members, Dr. AJ Boydston, Dr. Forrest Michael, Dr. Gojko Lalic, Dr. Joshua Vaughan, Dr. Cole DeForest, Dr. Niels Anderson, and Dr. Matt Golder.

Finally, I would like to thank my parents, brother, and sister who have provided support in various forms throughout the years.

Chapter 1. INTRODUCTION INTO STIMULI-RESPONSIVE HYDROGELS FOR DIRECT-INK-WRITE ADDITIVE MANUFACTURING

1.1 Introduction into Extrusion-Based Additive Manufacturing

A surprise to some, Additive Manufacturing (AM) or 3D Printing (3DP) has existed since Hideo Kodama first designed a rapid prototyping system using a photopolymer resin.[1] Since then, the technology has been commercialized and diversified into several economic sectors such as medical and aerospace. Forbes magazine recently highlighted future potential by saying, "Additive manufacturing plays a major role in the Industry 4.0 revolution; it will help upend traditional economies of scale, making microfactories economically efficient; and it's already contributing to reshape global supply chains, strengthening local networks."[2] In a separate article they also claim that the expected market for 3D printing technologies will reach a revenue of $35.6 billion by 2024.[3] One of the reasons AM has become popular is the ability to fabricate parts with complex geometries without the need for molds and complicated tooling as is required in conventional methods. Additionally, lattice frameworks allow one to craft a part with less material reducing the material cost and weight. The facile progression of moving from CAD model to fabricated part has innovated the iterative prototyping process to occur in the span of days rather than months. More importantly, recent developments have expanded beyond prototyping with advancements in the fields of biomedicine with tissue engineering[4] and implantable devices,[5] automotive and aerospace with lightweight and strong parts,[6] construction for rapid house erection in areas where low-cost housing is necessary,[7] among many more. Future improvements in the speed of AM will continue to revolutionize the way we think about manufacturing.

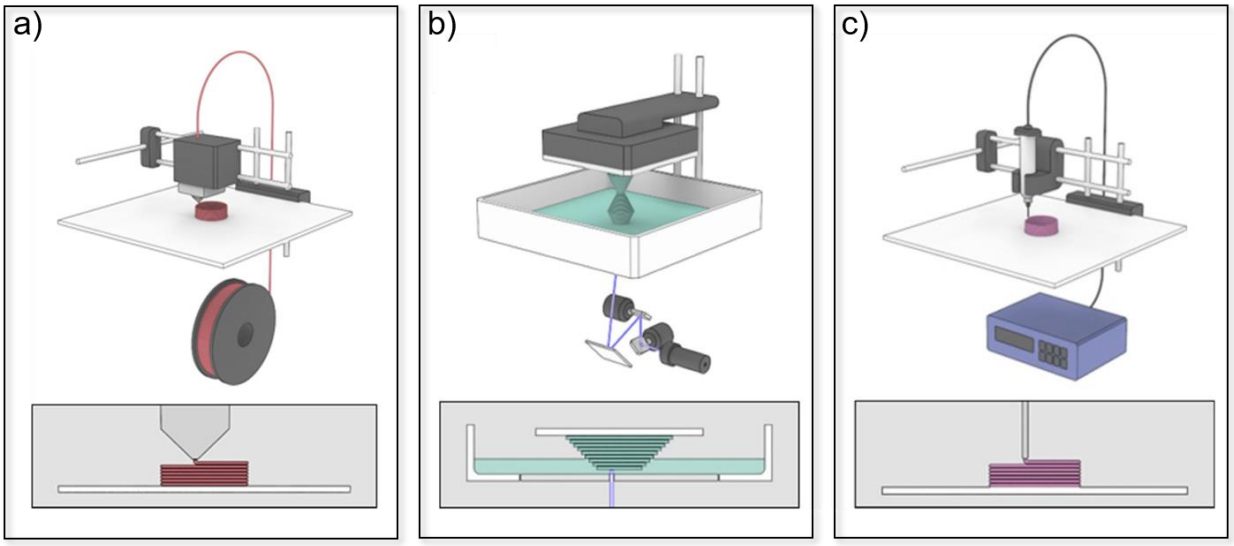

Figure 1.1 Schematic of (a) FFF, (b) SLA, and (c) DIW additive manufacturing methods.[8] Copyright 2019 (Adapted with permission from Elsevier)

A wide range of printers are available and span different deposition methods (Figure 1.1) such as Fused Filament Fabrication (FFF) which utilizes the melting transition temperature of thermoplastic polymers such as PLA or ABS, Stereolithography (SLA) which involves a rastering laser to rapidly polymerize a monomeric liquid resin, and Direct-ink-Writing (DIW) that relies on a material's viscoelastic properties to deposit a shear-thinning gel with rapid recovery. Among these FFF is likely the most familiar to the average consumer as a means to create keychains and coasters. However, this method has been proven to be incredibly versatile as it has been shown to be used in personalized prosthetic development[9] and as a model for minor surgical training.[10] Stereolithography is where AM was initially pioneered and involves a laser rastered across the surface of a monomeric resin tank to rapidly polymerize each layer. One drawback of these types of monomers is their limited scope, generally requiring acrylates to achieve the fast gel point required. In exploring new materials, our group has investigated the use of bovine serum albumin (BSA) formulated with PEGDA as a step towards achieving bio-sourced and biodegradable

photopolymers for AM. These materials showed moduli comparable to commercial resins and show good cell viability after 21 days.[11]

Particularly interesting for 3D bioprinting is DIW where a hydrogel is extruded through a pneumatically or screw-driven mechanism to deposit an ink layer-by-layer. This technique is attractive because it allows for the inclusion of bio-based materials and a relatively benign deposition method to afford materials capable of seeding cells for tissue engineering[12] or bioreactor fabrication.[13] Early research in this area involved the printing of gelatin and alginate which are excellent bio-polymers, however, they are not tailored to AM and require precise temperature control or support baths. An alternative strategy is to use synthetic polymers which grant tunability in the mechanical properties required of AM at the cost of reduced bioactivity. However, starting from a synthetic foundation allows for the expansion of functionality in addition to tunable mechanical properties which has been demonstrated in recent years through the development of stimuli-responsive "smart" polymers. The scope of innovation relies on a collaborative effort between chemists, engineers, and medical professionals to design stimuli-responsive "smart" polymers that replace the materials originally intended for traditional fabrication methods.

1.2 Introduction into Stimuli-Responsive Hydrogels for DIW 3DP

Since the advancement of additive manufacturing as a viable alternative to traditional manufacturing practices, there needs new design considerations for future polymers materials. Given the wide range of printing techniques, the processing conditions depend on the method used and gives chemists an opportunity to expand the scope of available functional polymers. As an example, extrusion-based printers either require a thermoplastic polymer (FFF) or a shear-thinning gel (DIW). Temperature can be controlled during the print process through localized heating either at the print-head, cartridge, or build plate. In DIW, gelatin is a commonly used biopolymer that

requires a heated cartridge to allow for the polymer to flow and a cooled build plate to afford a soft gel. The printed part often has low resolution which have been addressed by many groups by using viscosity modifiers such as laponite[14] and alginate.[15]

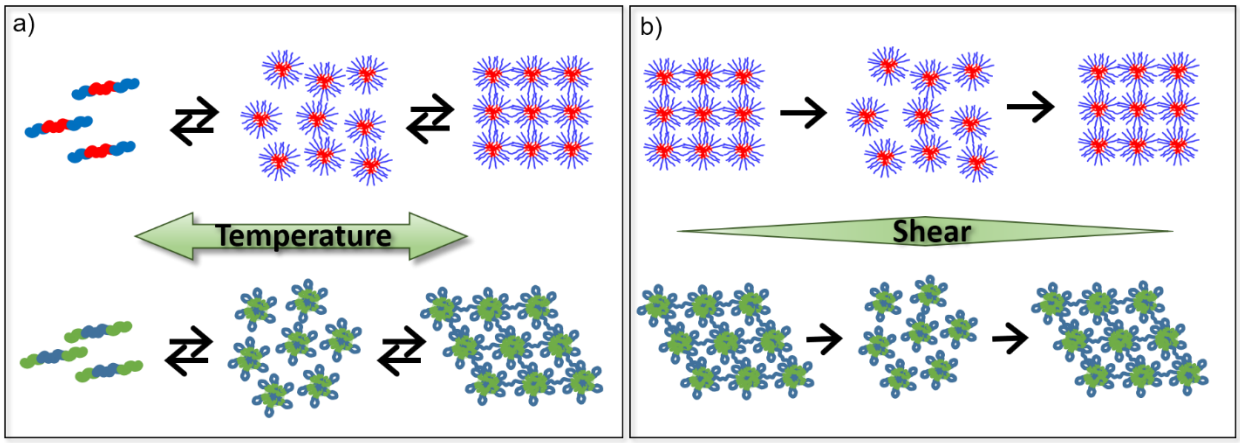

Figure 1.2 Cartoon comparing the self-assembly behavior of core shell micelles vs flower-like micelles.

a) F127, ABA-type triblock (top) assembles into core-shell micelles that pack into a face-centered-cubic lattice structure to form a hydrogel network. Alkyl glycidyl ether, BAB-type assembles into flower-like micelles that rely on bridging to form hydrogel networks. b) F127 micelles slide past one another in response to shear whereas alkyl glycidyl ether's hydrophobic blocks pull-out of the micelle core.

Alternatively, temperature-responses can be taken advantage of as in the case of Pluronic F127 hydrogels. These polymers consist of PEO and PPO blocks and by tailoring the hydrophobicity of PPO with the hydrophilicity of PEO micelles will form and given sufficient concentration will gel. Similarly, alkyl glycidyl ethers polymerized from a PEG core will form flower-like micelles and will undergo a similar transition as F127 (Figure 1.2).[16–18] The transition from solution to gel is reversible as the soluble unimers pack into micelles which allows for the facile incorporation of additives such as composites or living cells at low temperature and printing at room temperature. Both F127 and alkyl glycidyl ether copolymers are shear-thinning which provides control of filament deposition through shear pressure rather than temperature to grant

increased control. Additional design considerations must also be met such as the yield stress, or the force required to extrude the filament as well as recovery time to go from a free-flowing liquid back to a gel. For gels that require large amounts of force, die swell becomes an issue but too low and the gel will not be self-supporting and spread beyond the desired dimensions. Similarly, a slow recovery will also result in poor resolution and therefore a rapid re-gelation is necessary. Many of these issues may be solved through the optimization of polymer composition by altering the block lengths or side-chain moieties.

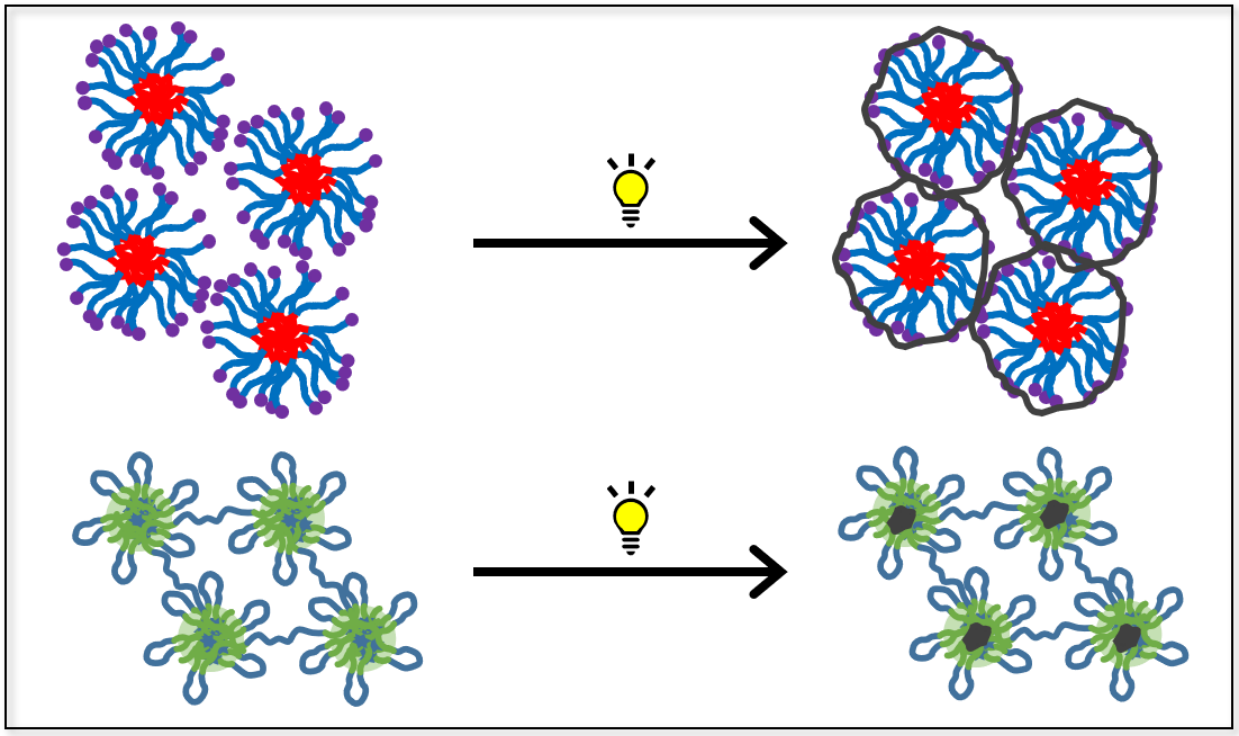

Figure 1.3 Cartoon depiction of light-responsive F127 (top) and alkyl glycidyl ether (bottom) triblock copolymers.

The chain-end determines where cross-linking takes place, for F127, the hydrophilic periphery is polymerized. Alkyl glycidyl ether's cross-linking is in the hydrophobic core.

Once the needs of the basic printing requirements have been met there is the opportunity to expand the scope of functionality as stimuli-responsive "smart" materials. While there are many strategies to accomplish this task, of note is through chemical modification at the chain-ends or

the sidechains of the polymer. For example, Frey and Obermeier have copolymerized ethylene oxide with allyl glycidyl ether and through thiol-ene "click" chemistry append various functionalities on the allyl ether alkene.[19] On a simpler note, cross-linking may be achieved through methacrylation of the alcohol at the chain-ends of F127[13,20–25] and alkyl glycidyl ether triblock copolymers.[26] This affords a material that is light-responsive to covalently fix the hydrogel which is necessary for robust 3D printed constructs. Interestingly, as shown in Figure 1.3, one may expect that polymerization taking place in the hydrophobic core vs the hydrophilic periphery would be different. However, the rheological shear modulus is comparable, and both result in a hydrogel that can be manipulated by hand without breaking.

The development of synthetic stimuli-responsive polymer hydrogels for DIW 3DP applications is discussed in the following chapters. Chapter 2 covers the initial work of our lab in the design of alkyl glycidyl ether triblock copolymers as alternatives to F127. Chapter 3 is a survey of chain-end functionalized F127 and the exploration of their gelation and rheological properties. Finally, chapter 4 is the in-depth investigation of the effect that a water-soluble dithiol has on the hydrogel network of methacrylated F127 gels.

1.3 REFERENCES

(1) Kodama, H. Automatic Method for Fabricating a Three-Dimensional Plastic Model with Photo-Hardening Polymer. *Rev. Sci. Instrum.* **1981**, *52* (11), 1770–1773. https://doi.org/10.1063/1.1136492.

(2) Annunziata, M. 2020: The Year Ahead In 3D (Printing) https://www.forbes.com/sites/marcoannunziata/2019/12/17/2020-the-year-ahead-in-3d-printing/#5f164e407fdc (accessed May 12, 2020).

(3) McCue, T. J. Significant 3D Printing Forecast Surges To $35.6 Billion

https://www.forbes.com/sites/tjmccue/2019/03/27/wohlers-report-2019-forecasts-35-6-billion-in-3d-printing-industry-growth-by-2024/#39fd3efb7d8a (accessed May 13, 2020).

(4) Gleadall, A.; Visscher, D.; Yang, J.; Thomas, D.; Segal, J. Review of Additive Manufactured Tissue Engineering Scaffolds: Relationship between Geometry and Performance. *Burn. Trauma* **2018**, *6*. https://doi.org/10.1186/s41038-018-0121-4.

(5) Youssef, A.; Hollister, S. J.; Dalton, P. D. Additive Manufacturing of Polymer Melts for Implantable Medical Devices and Scaffolds. *Biofabrication* **2017**, *9* (1), 012002. https://doi.org/10.1088/1758-5090/aa5766.

(6) Uriondo, A.; Esperon-Miguez, M.; Perinpanayagam, S. The Present and Future of Additive Manufacturing in the Aerospace Sector: A Review of Important Aspects. *Proc. Inst. Mech. Eng. Part G J. Aerosp. Eng.* **2015**, *229* (11), 2132–2147. https://doi.org/10.1177/0954410014568797.

(7) Delgado Camacho, D.; Clayton, P.; O'Brien, W. J.; Seepersad, C.; Juenger, M.; Ferron, R.; Salamone, S. Applications of Additive Manufacturing in the Construction Industry – A Forward-Looking Review. *Autom. Constr.* **2018**, *89*, 110–119. https://doi.org/10.1016/j.autcon.2017.12.031.

(8) Shafranek, R. T.; Millik, S. C.; Smith, P. T.; Lee, C.-U.; Boydston, A. J.; Nelson, A. Stimuli-Responsive Materials in Additive Manufacturing. *Prog. Polym. Sci.* **2019**, *93*, 36–67. https://doi.org/10.1016/j.progpolymsci.2019.03.002.

(9) Barrios-Muriel, J.; Romero-Sánchez, F.; Alonso-Sánchez, F. J.; Salgado, D. R. Advances in Orthotic and Prosthetic Manufacturing: A Technology Review. *Materials (Basel).* **2020**, *13* (2), 295. https://doi.org/10.3390/ma13020295.

(10) Luque, M. C.; Calleja-Hortelano, A.; Romero, P. E. Use of 3D Printing in Model

Manufacturing for Minor Surgery Training of General Practitioners in Primary Care. *Appl. Sci.* **2019**, *9* (23), 5212. https://doi.org/10.3390/app9235212.

(11) Smith, P. T.; Narupai, B.; Tsui, J. H.; Millik, S. C.; Shafranek, R. T.; Kim, D. H.; Nelson, A. Additive Manufacturing of Bovine Serum Albumin-Based Hydrogels and Bioplastics. *Biomacromolecules* **2020**, *21* (2), 484–492. https://doi.org/10.1021/acs.biomac.9b01236.

(12) Kang, H. W.; Lee, S. J.; Ko, I. K.; Kengla, C.; Yoo, J. J.; Atala, A. A 3D Bioprinting System to Produce Human-Scale Tissue Constructs with Structural Integrity. *Nat. Biotechnol.* **2016**, *34* (3), 312–319. https://doi.org/10.1038/nbt.3413.

(13) Saha, A.; Johnston, T. G.; Shafranek, R. T.; Goodman, C. J.; Zalatan, J. G.; Storti, D. W.; Ganter, M. A.; Nelson, A. Additive Manufacturing of Catalytically Active Living Materials. *ACS Appl. Mater. Interfaces* **2018**, *10* (16), 13373–13380. https://doi.org/10.1021/acsami.8b02719.

(14) Jin, Y.; Liu, C.; Chai, W.; Compaan, A.; Huang, Y. Self-Supporting Nanoclay as Internal Scaffold Material for Direct Printing of Soft Hydrogel Composite Structures in Air. *ACS Appl. Mater. Interfaces* **2017**, *9* (20), 17456–17465. https://doi.org/10.1021/acsami.7b03613.

(15) Gao, T.; Gillispie, G. J.; Copus, J. S.; Kumar, A. P. R.; Seol, Y. J.; Atala, A.; Yoo, J. J.; Lee, S. J. Optimization of Gelatin-Alginate Composite Bioink Printability Using Rheological Parameters: A Systematic Approach. *Biofabrication* **2018**, *10* (3), 034106. https://doi.org/10.1088/1758-5090/aacdc7.

(16) Zhang, M.; Vora, A.; Han, W.; Wojtecki, R. J.; Maune, H.; Le, A. B. A.; Thompson, L. E.; McClelland, G. M.; Ribet, F.; Engler, A. C.; Nelson, A. Dual-Responsive Hydrogels for Direct-Write 3D Printing. *Macromolecules* **2015**, *48* (18), 6482–6488.

https://doi.org/10.1021/acs.macromol.5b01550.

(17) Karis, D. G.; Ono, R. J.; Zhang, M.; Vora, A.; Storti, D.; Ganter, M. A.; Nelson, A. Cross-Linkable Multi-Stimuli Responsive Hydrogel Inks for Direct-Write 3D Printing. *Polym. Chem.* **2017**, *8* (29), 4199–4206. https://doi.org/10.1039/c7py00831g.

(18) Fellin, C. R.; Adelmund, S. M.; Karis, D. G.; Shafranek, R. T.; Ono, R. J.; Martin, C. G.; Johnston, T. G.; DeForest, C. A.; Nelson, A. Tunable Temperature- and Shear-Responsive Hydrogels Based on Poly(Alkyl Glycidyl Ether)S. *Polym. Int.* **2019**, *68* (7), 1238–1246. https://doi.org/10.1002/pi.5716.

(19) Obermeier, B.; Frey, H. Poly(Ethylene Glycol-Co-Allyl Glycidyl Ether)s: A PEG-Based Modular Synthetic Platform for Multiple Bioconjugation. *Bioconjug. Chem.* **2011**, *22* (3), 436–444. https://doi.org/10.1021/bc1004747.

(20) Millik, S. C.; Dostie, A. M.; Karis, D. G.; Smith, P. T.; McKenna, M.; Chan, N.; Curtis, C. D.; Nance, E.; Theberge, A. B.; Nelson, A. 3D Printed Coaxial Nozzles for the Extrusion of Hydrogel Tubes toward Modeling Vascular Endothelium. *Biofabrication* **2019**, *11* (4), 045009. https://doi.org/10.1088/1758-5090/ab2b4d.

(21) Wong, J.; Gong, A. T.; Defnet, P. A.; Meabe, L.; Beauchamp, B.; Sweet, R. M.; Sardon, H.; Cobb, C. L.; Nelson, A. 3D Printing Ionogel Auxetic Frameworks for Stretchable Sensors. *Adv. Mater. Technol.* **2019**, *4* (9), 1900452. https://doi.org/10.1002/admt.201900452.

(22) Smith, P. T.; Basu, A.; Saha, A.; Nelson, A. Chemical Modification and Printability of Shear-Thinning Hydrogel Inks for Direct-Write 3D Printing. *Polymer (Guildf).* **2018**, *152*, 42–50. https://doi.org/10.1016/j.polymer.2018.01.070.

(23) Basu, A.; Saha, A.; Goodman, C.; Shafranek, R. T.; Nelson, A. Catalytically Initiated Gel-

in-Gel Printing of Composite Hydrogels. *ACS Appl. Mater. Interfaces* **2017**, *9* (46), 40898–40904. https://doi.org/10.1021/acsami.7b14177.

(24) Johnston, T. G.; Yuan, S. F.; Wagner, J. M.; Yi, X.; Saha, A.; Smith, P.; Nelson, A.; Alper, H. S. Compartmentalized Microbes and Co-Cultures in Hydrogels for on-Demand Bioproduction and Preservation. *Nat. Commun.* **2020**, *11* (1), 1–11. https://doi.org/10.1038/s41467-020-14371-4.

(25) Müller, M.; Becher, J.; Schnabelrauch, M.; Zenobi-Wong, M. Nanostructured Pluronic Hydrogels as Bioinks for 3D Bioprinting. *Biofabrication* **2015**, *7* (3), 035006. https://doi.org/10.1088/1758-5090/7/3/035006.

(26) Johnston, T. G.; Fellin, C. R.; Carignano, A.; Nelson, A. Poly(Alkyl Glycidyl Ether) Hydrogels for Harnessing the Bioactivity of Engineered Microbes. *Faraday Discuss.* **2019**. https://doi.org/10.1039/c9fd00019d.

Chapter 2. CROSS-LINKABLE MULTI-STIMULI-RESPONSIVE HYDROGEL INKS FOR DIRECT-WRITE 3D PRINTING

2.1 ABSTRACT

Triple stimuli-responsive ABA triblock copolymer hydrogels composed of poly(allyl glycidyl ether)-*stat*-poly(alkyl glycidyl ether)-*block*-poly(ethylene glycol)-*block*-poly(allyl glycidyl ether)-*stat*-poly(alkyl glycidyl ether) were synthesized using controlled ring-opening polymerization of glycidyl ethers. These polymers form triple stimuli-responsive hydrogels that respond to temperature, pressure (shear-thinning), and UV light. The stimuli-responsive behaviors of the gels were dependent upon the composition and molecular weight of the 'A' blocks of the triblock copolymers. The hydrogels were analyzed rheometrically to characterize the stimuli-responsive properties. The optimized compositions were 3D printed using a direct-write 3D printer to afford robust 3D objects. We anticipate these materials creating new opportunities in the biomedical and biotechnological fields, by enabling the simple and rapid fabrication of 3D hydrogels.

2.2 INTRODUCTION

Stimuli-responsive hydrogels are of significant interest for their ability to adapt or change with their environment. These materials also represent an emerging class of materials suitable as bio-inks for direct-write 3D printing. In this method of 3D printing, a syringe fitted with a nozzle is rastered across a surface as it dispenses an ink. An ideal material for printing under ambient conditions is a stimuli-responsive material that demonstrates shear-thinning behavior in response to applied pressure.[1–16] Shear-thinning is a behavior of non-Newtonian fluids whereby a shear response governs a decrease in viscosity allowing normally thick liquids or gels to flow freely.[17–

[21] The most common hydrogel inks used in direct-write 3D printing are hydrogels based on calcium alginate or F-127.[22–29] Other examples of shear-thinning inks include colloidal suspensions[30–37] and polyelectrolyte gels.[38–41] All of these materials can be printed at ambient temperatures into 3D objects as a consequence of their shear-thinning behavior.

The Lewis and Zenobi-Wong groups have reported the direct-write 3D printing of hydrogel inks composed of Pluronic F-127 which is a commercially available ABA triblock copolymer of poly(ethylene glycol)-*block*-poly(propylene oxide)-*block*-poly(ethylene glycol) (PEG-*b*-PPO-*b*-PEG).[42] In addition to the shear-thinning behavior of F127 hydrogels, these materials are also thermo-responsive due to the lower critical solution temperature (LCST) behavior of the PPO block (~20 °C). When prepared as a 25 wt % aqueous solution of F-127, the polymers exist as soluble unimers at 5 °C and afford a free-flowing solution. However, as the temperature is increased to 25 °C, the solubility of PPO in water decreases, which drives the formation of micelles comprised of a hydrophobic PPO core.[43–49] The micelles pack into a face-centered cubic structure in water resulting in a gel. This property of the hydrogel is particularly advantageous when loading the hydrogel ink into the ink cartridge or the syringe of a direct-write 3D printer. Specifically, the hydrogel ink can be poured into the cartridge while in its liquid state (5 °C) and then allowed to warm to room temperature where it can be printed while in its gel state.

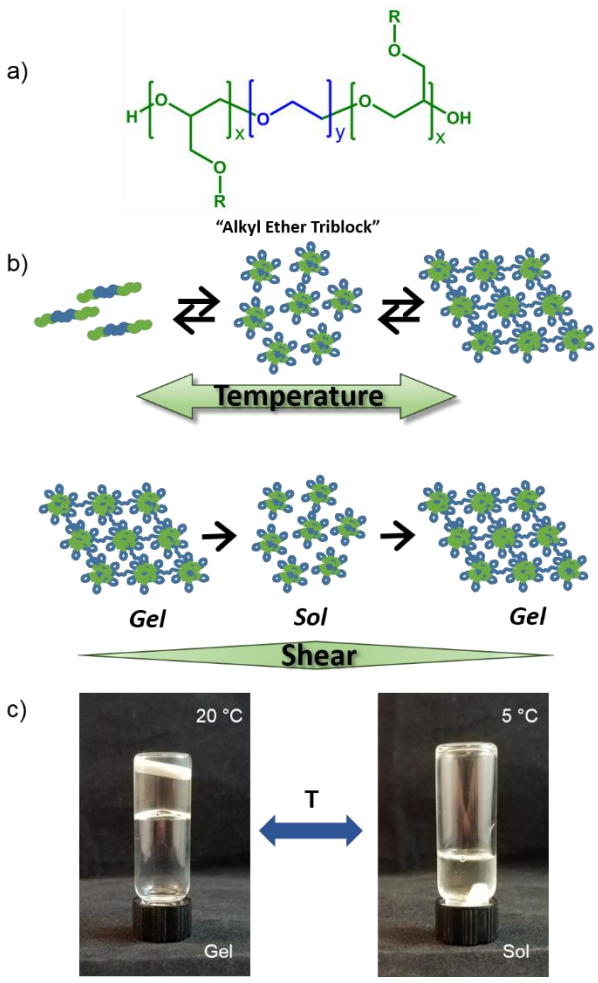

Figure 2.4 Overview of alkyl glycidyl ether triblock copolymers

a) Poly(alkyl glycidyl ether)-block-poly(ethylene glycol)-block-poly(alkyl glycidyl ether) triblock copolymer. b) Cartoon representation of temperature and shear response of alkyl glycidyl ether triblocks. c) Pictures that show a 20 wt % polymer hydrogel at 20 and 5 °C in the gel and sol states respectively.

We have previously demonstrated[50] that ABA triblock copolymers with the composition, poly(isopropyl glycidyl ether)-*b*-poly(ethylene glycol)-*b*-poly(isopropyl glycidyl ether) (PiPGE-*b*-PEG-*b*-PiPGE) forms dual-stimuli responsive hydrogels. These hydrogels reversibly respond to both temperature (due to the LCST of the iPGE block) and applied pressure (Figure 2.1). These hydrogels behave similarly to F-127 hydrogels but possess a higher modulus at lower polymer concentration. Thus, the 3D printed objects are better suited to retain their shape after printing

when compared to F-127 hydrogels at the same polymer concentration. However, in the absence of cross-linked polymer chains after printing, the 3D printed objects derived from F-127 and PiPGE-b-PEG-b-PiPGE readily dissolve when submerged into water.

Herein, we describe a 3D printable triblock copolymer hydrogel that responds to temperature and pressure (shear thins), and is also capable of cross-linking upon exposure to 365 nm UV light. Allyl-containing triblock copolymers[51–54] were synthesized and formulated into hydrogels suitable for direct-write 3D printing. We initially hypothesized that thiol-ene reactions between these polymers and a multivalent thiol would be necessary to enable inter-polymer chain cross-linking; however, we discovered that multivalent thiols were not necessary to covalently bind the polymers. The triblock copolymers were prepared by anionic copolymerization of allyl glycidyl ether with isopropyl or ethyl glycidyl ether from a poly(ethylene glycol) macroinitiator. Under ambient conditions, these ABA triblock copolymers possess two temperature-responsive hydrophobic blocks which are likely to form flower-like micelles and bridged micelles in aqueous solution.[55–58]

2.3 Results and Discussion

Living anionic polymerization is an effective method for the ring-opening polymerization of glycidyl ether derivatives to afford polymers of controlled molecular weight and polydispersity (Figure 2.2). Previously, we observed that PiPGE-*b*-PEG-*b*-PiPGE triblock copolymers formed temperature responsive hydrogels that were also shear thinning.[50] Therefore, we began the current investigation by synthesizing PAGE-*b*-PEG-*b*-PAGE with the aim of utilizing the allyl side-chains in thiol-ene reactions to enable cross-linking of the polymer chains. Triblock copolymers of PAGE-*b*-PEG-*b*-PAGE were synthesized via anionic ring-opening

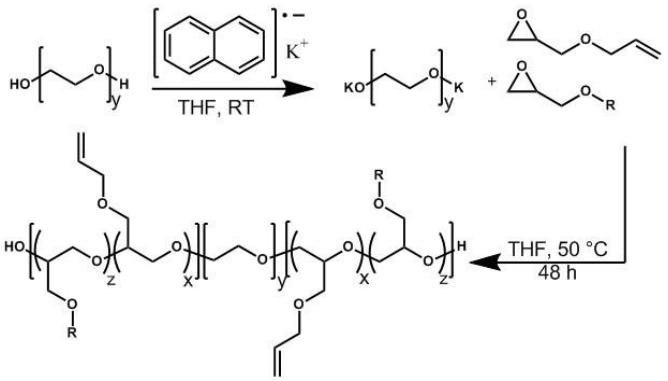

Figure 2.5 Synthesis of alkyl glycidyl ether statistical copolymers

Synthesis of poly(alkyl glycidyl ether-*stat*-allyl glycidyl ether)-*block*-poly(ethylene glycol)-*block*-poly(alkyl glycidyl ether-*stat*-allyl glycidyl ether). When z is no zero, R represents an ethyl or isopropyl group. The compositions of the polymers synthesized for this study are described in Table 2.1

Table 2.1 Polymer compositions with different monomer ratios

Composition	Alkyl Ethers	P(R)GE/PAGE-*b*-PEG-*b*-P(R)GE/PAGE[a]	DP AGE[a]	DP iPGE[a]	DP EGE[a]	Đ[b]
Polymer **1**	AGE	1.4k-*b*-8k-*b*-1.4k	24	-	-	1.11
Polymer **2**	EGE	1.6k-*b*-8k-*b*-1.6k	-	-	32	1.11
Polymer **3**	AGE/iPGE	1.2k-*b*-8k-*b*-1.2k	2.4	17.8	-	1.10
Polymer **4**	AGE/iPGE	1.4k-*b*-8k-*b*-1.4k	4.4	19.2	-	1.11
Polymer **5**	AGE/iPGE	1.7k-*b*-8k-*b*-1.7k	16	13.2	-	1.12
Polymer **6**	AGE/EGE	1.7k-*b*-8k-*b*-1.7k	19.2	-	11.2	1.11

[a]Determined by NMR
[b]Determined by GPC

polymerization using PEG as the initiator and potassium naphthalenide as the base (Table 2.1). The block lengths were controlled by varying the molar ratio of allyl glycidyl ether monomer to PEG macroinitiator. As noted by Lynd and co-workers,[59] during the polymerization, some of the allyl side chains isomerized to the vinyl form. While this isomerization can be suppressed by performing the polymerization at more moderate temperatures, we did not observe complete suppression of the vinylic side chains. The degree of polymerization was determined using ^{1}H NMR spectroscopy by comparing the integration values of the ethylene glycol protons (3.4-3.6 ppm) relative to the allyl and vinyl protons at 4, 5.2, and 5.9 ppm, respectively (Figure 2.12). The

resulting Mn for polymer 1 was 1.4k-*b*-8k-*b*-1.4k g/mol. The degree of polymerization (DP) was less than the theoretical value suggesting there may have been homopolymer impurities and/or unreacted monomer in the initial crude product, which was removed after purification by precipitation.

Figure 2.6 $PAGE_{18.5}$-*b*-PEG_{181}-*b*-$PAGE_{18.5}$ (polymer **1**) 15 wt% concentration hydrogel

Unlike the PiPGE-*b*-PEG-*b*-PiPGE (DP 15) triblock copolymers which exhibited a gel-to-sol transition at 16 °C, the PAGE-*b*-PEG-*b*-PAGE block copolymers did not form thermoresponsive hydrogels. In fact, the hydrogels formed with polymer **1** were brittle and inhomogeneous (Figure 2.3). Therefore, in order to combine the thermo-responsiveness of PiPGE-*b*-PEG-*b*-PiPGE with the cross-linkable functionality of PAGE-*b*-PEG-*b*-PAGE, statistical copolymers of PiPGE-*stat*-PAGE-*b*-PEG-*b*-PiPGE-*stat*-PAGE were synthesized. The polymer compositions were altered by changing the iPGE and AGE monomer feed ratios, as well as the molar ratios of the monomers to PEG macroinitiator. The polymer composition was determined using ^{1}H NMR spectroscopy by comparing the integration values of the ethylene glycol backbone (3.4-3.6 ppm) and allyl, vinyl, and methyl protons at 4, 5.2, 5.9, and 1.15 ppm, respectively, from the allyl glycidyl ether unit and isopropyl glycidyl ether unit (Figure 2.14). The resulting Mn for polymers **3**, **4**, and **5** were 1.2k-*b*-8k-*b*-1.2k g/mol (DP = 2.4 for AGE and DP = 17.8 for iPGE), 1.4k-*b*-8k-*b*-1.4k g/mol (DP = 4.4 for AGE and DP = 19.2 iPGE), and 1.7k-*b*-8k-*b*-1.7k g/mol (DP

= 16 for AGE and DP = 13.2 for iPGE), respectively. Generally, the allyl-iPGE co-polymers **3**, **4**, and **5** performed poorly in forming homogeneous hydrogels.

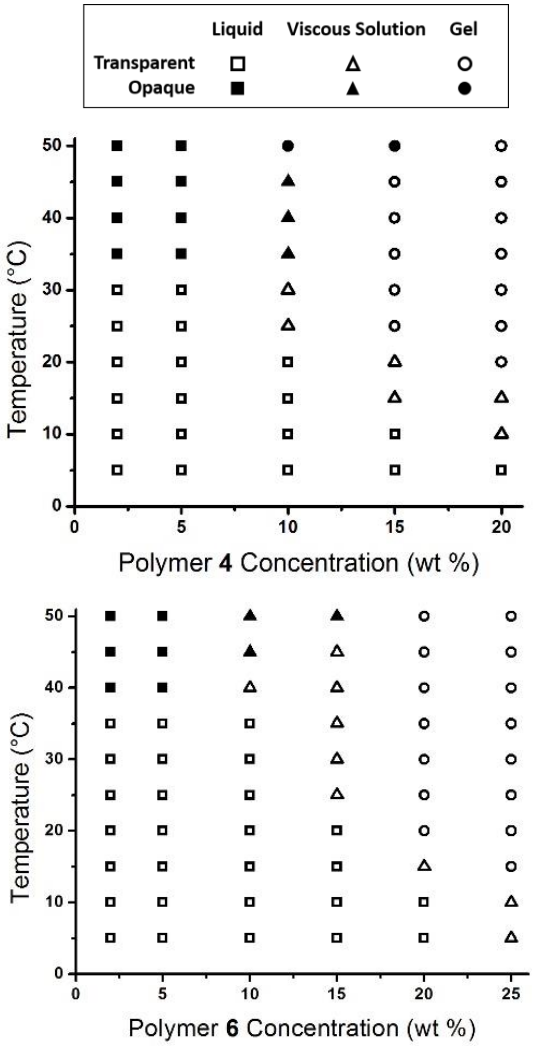

Figure 2.7 Temperature-concentration phase diagrams summarizing the solution and hydrogel properties of polymers (a) **4** and (b) **6**.

Ethyl and allyl glycidyl ether were also co-polymerized to afford PEGE-*stat*-PAGE-*b*-PEG-*b*-PEGE-*stat*-PAGE (polymer **6**). Analysis by ^{1}H NMR spectroscopy showed that polymer **6** was successfully polymerized under the same conditions used to synthesize the iPGE copolymers, and the composition was determined by ^{1}H NMR spectroscopy using the integration values of the ethylene glycol backbone (3.4-3.6 ppm) and the allyl, vinyl, and methyl protons at 4, 5.2, 5.9, and

1.2 ppm, respectively (Figure 2.15). The resulting Mn for polymer **6** was 1.7k-*b*-8k-*b*-1.7k g/mol (DP = 11.2 for PEGE and DP = 19.2 PAGE).

Phase diagrams based on polymer concentration and solution temperature were constructed to summarize the physical properties of the polymer solutions at temperatures ranging from 5 to 50 °C and polymer concentrations between 2 and 25 wt %. The vial inversion method was used to ascertain whether each sample was a liquid, viscous liquid, or a gel. Polymers **4** and **6** demonstrated the best performance as homogeneous hydrogels that undergo gel-to-sol transitions. As shown in Figure 2.4, Polymer **4** in water remained as a clear solution from 5 to 30 °C at 2 to 10 wt %, but the sample then became turbid above 35 °C. At 20 wt %, the mixture had a slow transition from a clear solution at 5 °C to a viscous liquid until it gelled at 20 °C. This polymer did not form homogenous hydrogels at 25 wt % and above. Polymer **6**, which had a higher allyl glycidyl ether composition with some ethyl glycidyl ether incorporated, also existed as a free-flowing solution from 5 to 35 °C at 2 to 10 wt % concentrations. In comparison to polymer **4**, a 20 wt % mixture of polymer **6** demonstrated a sharper transition wherein the sample was a clear solution at 5 and 10 °C and became a gel at 20 °C. This polymer was homogenous at 25 wt % which suggested that EGE was more soluble than iPGE. The turbidity observed at the higher temperatures was attributed to the formation of larger light-scattering aggregates. Interestingly, these aggregates are not present at higher concentrations of polymer. We hypothesize that the dynamics of polymer chains changes with concentration, and the origins of these differences will be reported in due time.

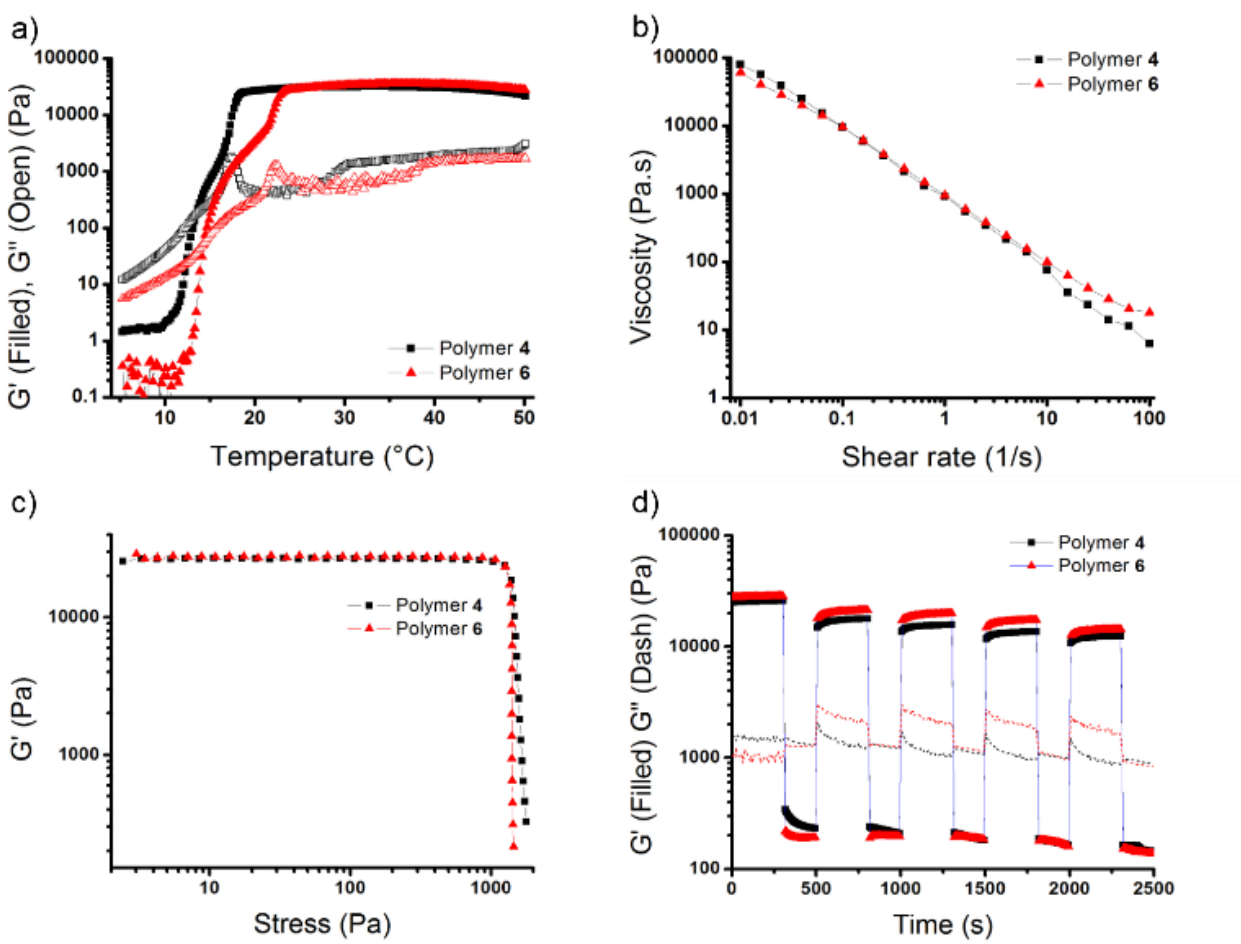

Figure 2.8 Rheological experiments on polymer **4** and **6**

Rheology performed on 18 wt% polymer **4** (black) and 20 wt% polymer **6** (red) hydrogels a) Dynamic oscillatory temperature ramp experiment showing storage (filled) and loss (open) moduli. b) Viscosity versus shear rate profile showing non-Newtonian behavior and shear-thinning properties. c) Modulus versus stress showing the yield stress. d) Cyclic shear-thinning experiment showing G', storage modulus, response and instantaneous recovery to high (100%) and low (1%) oscillatory strains. The solid lines show storage modulus of the polymer and the dotted lines represent loss modulus. Experiments b-d were run at 25 °C

These hydrogels were further characterized by rheometry. Figure 2.5a compares the dynamic elastic (G') and viscous (G") moduli for 18 wt % concentration of polymer **4**, as well as a 20 wt % concentration of polymer **6**. The results confirmed that both hydrogels exhibit a reversible sol-gel transition. The gelation temperature (which is defined by the intersection of the

G' and G" curves) was below room temperature for polymers **4** and **6** (13.5 and 14.3 °C, respectively). Thus, at ambient temperature, the material occupied a gel state, but when the sample was brought to a temperature below its gelation temperature, the material was a liquid. This reversible temperature response is an important feature of these hydrogel inks as the ink can be transferred into the 3D printer in its liquid state by cooling below its T_{gel}, but then printed at room temperature in its gel state.

An ideal material for extrusion through a small diameter nozzle in direct-write 3D printing is a shear-thinning polymer ink. Therefore, we investigated the shear-thinning behavior and the gel yield stress at 25 °C. Figure 2.5b shows that the hydrogels corresponding to polymer **4** and polymer **6** have linearly decreasing shear viscosities as the shear rate increases. The viscosity versus shear rates are similar between the 18 wt % polymer **4** and 20 wt % polymer **6**. These results indicate the gels are non-Newtonian fluids and shear-thinning.

We further investigated the gel yield stress, an important parameter that correlates to the force necessary for gel extrusion. The gel yield stress also provides an indirect indication of the gel strength as it supports subsequent stacked layers during 3D printing. In other words, a gel with a higher yield stress can support more stacked layers without printing defects such as sagging than a gel with a low yield stress. Hydrogels of polymers **4** and **6** have a yield stress of 1.27 kPa at 18 wt % and 1.25 kPa at 20 wt %, respectively. Figure 2.5c suggests that the incorporation of ethyl glycidyl ether instead of isopropyl glycidyl ether allows for higher allyl glycidyl ether incorporation to obtain nearly identical yield stress results. These results suggest that these polymer compositions will have similar printing performance and printing quality.

The shear-thinning and yielding behavior of these hydrogels originates from the dynamic character of the self-assembled structures formed by the triblock copolymers in aqueous media.

As the gel experiences static or dynamic shear stresses, the viscoelastic behavior of the gel changes as the mobility of the physically cross-linked polymers attenuates the applied stresses. The reversible (and self-healing) nature of the physical cross-links that exist within these hydrogel networks manifests itself in the instantaneous response of the gel modulus to changes in the applied strain as illustrated in Figure 2.5d. In this experiment, 18 wt % polymer **4** and 20 wt % polymer **6** hydrogels were subjected to 5 consecutive cycles of low (1%) strain for 5 min followed by high (100%) strain for 3 min. All of the hydrogels exhibited a marked decrease in the G' moduli at high strains and immediate recovery at low strains for each cyclic testing. Polymer **4** had G' moduli of ~17.5 kPa and 0.2 kPa at 1% and 100% strains, respectively. Polymer **6**, being a slightly stronger gel with higher concentration, had G' moduli of ~20.8 kPa and 0.2 kPa at 1% and 100% strains, respectively. All the hydrogels demonstrated the G' response to high and low strains occurred in less than 15 seconds. This rapid and reversible shear-thinning behavior is attributed to the disruption of the physical network under large shear deformations while the recovery was due to the rapid reformation of the transient network, which was promoted by hydrophobic interactions. Furthermore, our hydrogels displayed minimal mechanical hysteresis between strain cycles. The small degree of hysteresis between the first and second cycles was likely due to the initial equilibration at 0% strain for 8 minutes leading to the observed higher G' in the first cycle. This rapid and reversible modulus response to shear stress suggested that these hydrogels can be extruded from a nozzle but then quickly regain the mechanical integrity required to support subsequent printed layers.

We initially hypothesized that thiol-ene reactions or alternative polymerization schemes[60] would be necessary to cross-link the polymer chains in the presence of a photoradical generator (2-hydroxy-2-methyl propiophenone). However, our data show that in the absence of any dithiol

cross-linking molecule, the triblock copolymers can undergo photo-initiated cross-linking. We postulate that the allyl groups can undergo radical-initiated cross coupling to form carbon-carbon bonds that bridge polymer chains. Thus, for this hydrogel system, thiol-ene mediated cross-linking is not necessary to afford a covalently fixed structure. In fact, when the photo-initiated reaction was performed in the presence of dithiols, we only saw an increase in the modulus at high (5 wt % of the polymer mass) loading and the addition of dithiol added turbidity to the gel.(Figure 2.6 and S2.7).

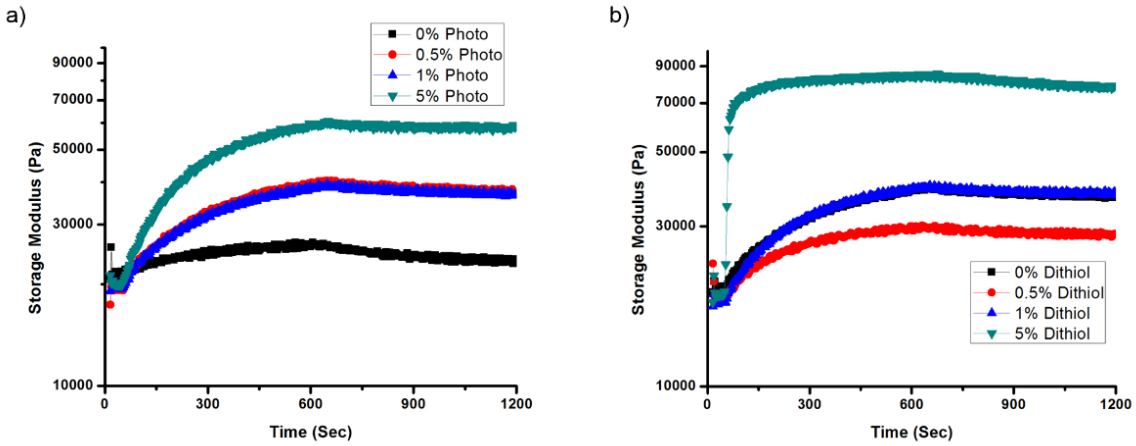

Figure 2.9 Photorheology of polymer **4** with and without ethanedithiol

Dynamic oscillatory UV cure experiment showing an increase in storage modulus when lamp is turned on at the 60 second mark for 10 minutes of irradiation. Experiment performed on a) polymer **4** with different photoinitiator concentrations based on polymer weight. b) polymer **4** with 1 wt% photoinitiator and different concentrations of ethanedithiol based on polymer weight.

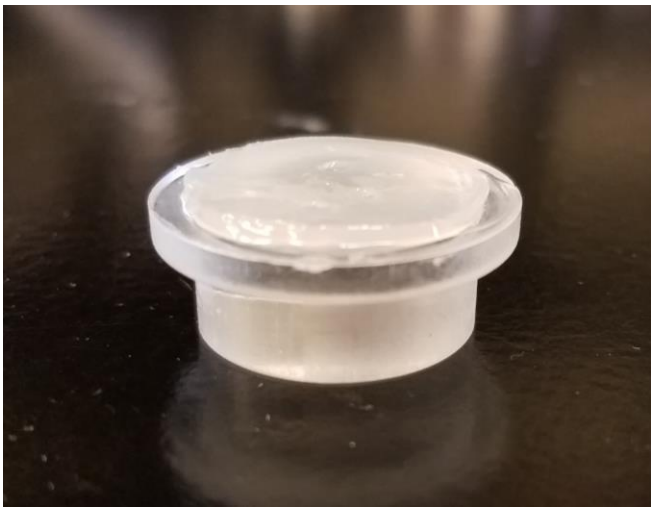

Figure 2.10 Picture of polymer **4** with ethanedithiol

Cross-linked polymer **4** with 5 wt% ethanedithiol of the polymer mass after UV curing experiment. Addition of dithiol adds turbidity to the gel.

Rheometrical experiments with in-situ UV curing were performed to evaluate the photo-initiated cross-linking of the allyl side-chains. Polymers **4** and **6** were formulated as hydrogels with photoinitiator concentrations that varied from 0 to 5 wt % of the polymer mass. (Figure 2.8). Polymer **6** possesses a higher allyl glycidyl ether composition, and therefore, a higher storage modulus after UV curing as a consequence of the increased cross-link density.

The elastic modulus of the hydrogel was also dependent upon the UV exposure time and photo-initiator concentration (Figure 2.9). When 1 wt % photoinitiator (relative to the polymer) was added to the polymer **6** hydrogel, the cross-linking reached its peak in 400 s to afford a modulus of 80 kPa. Continued UV exposure beyond this time did not change the G' modulus. Adjusting to shorter cure times reduced the cross-linking density, and afforded G' of 40 kPa and 68 kPa for 60 and 200 s cure times, respectively. The introduction of covalent bonds between the polymer chains significantly changes the dynamic character of the triblock copolymer chains of the hydrogel. The crosslinked polymer network no longer exhibits the shear-thinning behavior that was originally required for printing.

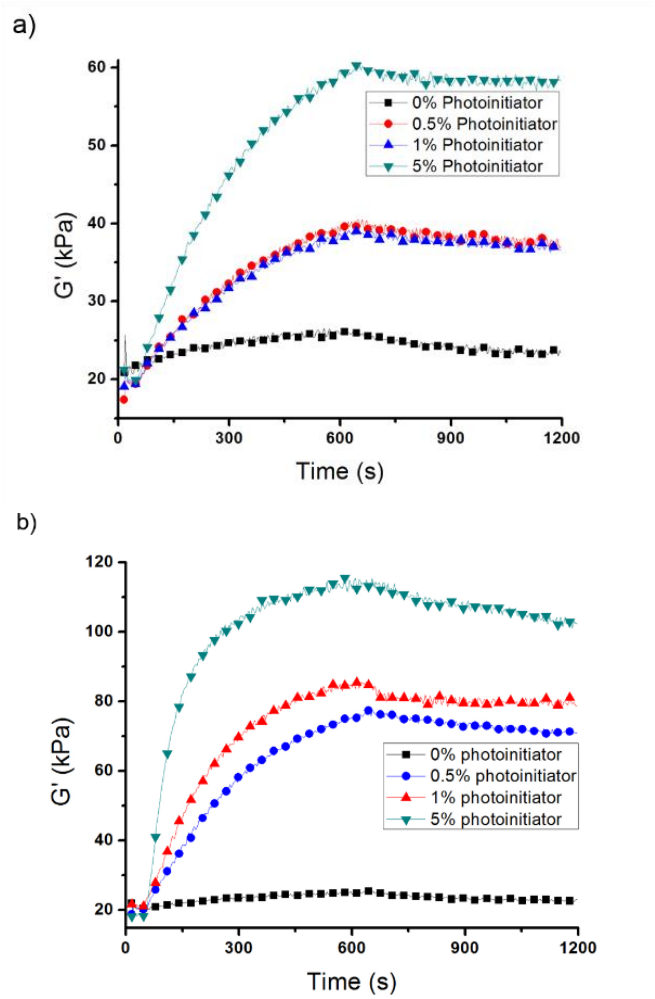

Figure 2.11 Photorheology of polymer **4** and **6** with different photoinitiator concentrations

Dynamic oscillatory UV cure experiment showing increase in storage modulus when lamp is turned on at the 60 s mark for 10 min of irradiation. Experiment performed on (a) 18 wt% polymer **4** and (b) 20 wt% polymer **6** hydrogels with different photoinitiator concentrations based on polymer weight.

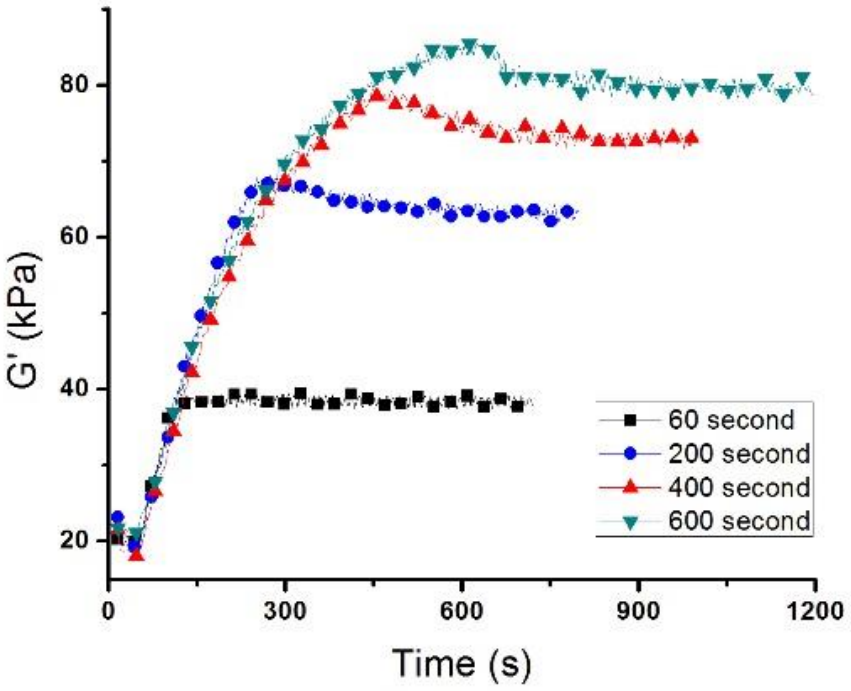

Figure 2.12 Photorheology of polymer **6** with different UV cure times

Dynamic oscillatory UV cure experiment showing tunability of G' moduli by altering length of UV irradiation. Experiment performed on polymer **6** at 20 wt% concentration and 1% photoiniator concentration based on polymer weight with 60 s dwell time followed by 60 to 600 s cure times and a 10 min post-cure at constant strain.

We demonstrated the ability to 3D print the hydrogels into multi-layer 3D objects. The hydrogel inks were transferred into the syringe for the direct-write 3D printer by cooling the gel to 5 °C and pouring the solution into the syringe barrel. Upon warming to ambient temperature, the ink became a gel which were printed via extrusion through a 210, 260, or 410 µm diameter nozzle. Figure 2.9 shows that the 3D printing of layered grid structures was successful for polymer **6** (see Figure 2.10 for Polymer **4**). Layer thickness could be controlled by modifying the nozzle diameter, as well as the print speed. As the speed at which the nozzle moved across the printing surface increased, the diameter of the printed strand decreased. Additionally, grid structures up to 40 printed layers in thickness were demonstrated with excellent fidelity. The printed objects were

cured for 10 minutes using 365 nm LED bulbs, which afforded robust structures that could easily be gripped by tweezers or manipulated by hand. These cross-linked structures could also be submerged into water without any visual disintegration.

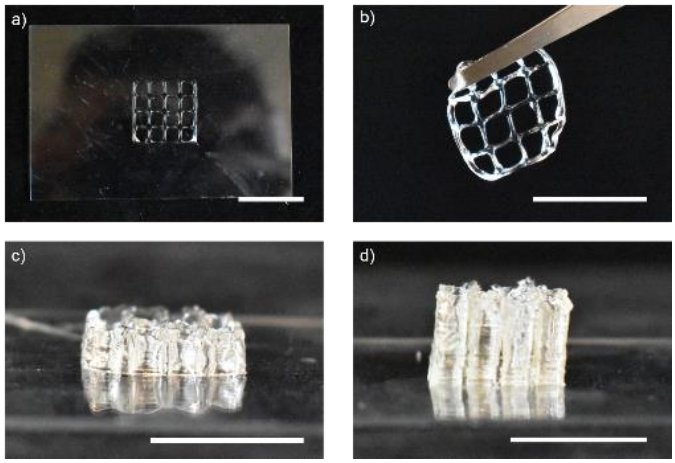

Figure 2.13 3D printed grids of polymer **6**

a) Grid printed with 0.21 mm ID nozzle at 5 mm/s. b) cross-linked gel of a. c) 20-layer grid printed at 5 mm/s d) 40-layer grid printed with 0.41 mm ID nozzle at 10 mm/s. Structures a-c were printed with polymer **6** at 20 wt% and d was printed at 25 wt% from a direct-write printer (scale bar 2 mm).

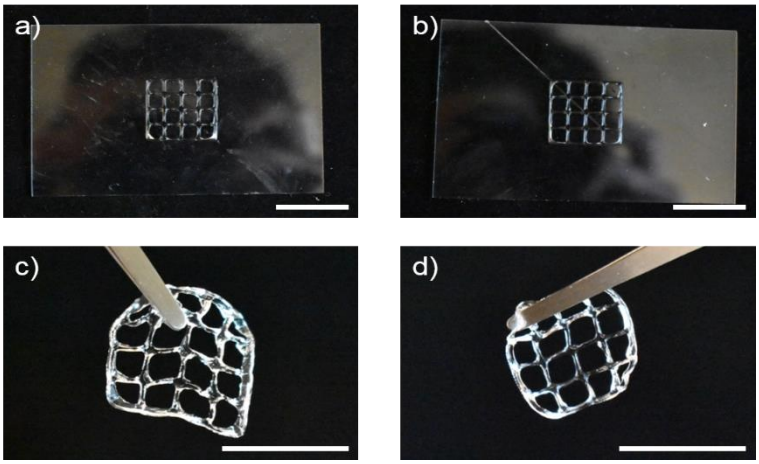

Figure 2.14 3D printed grids of polymer **4**

a) Grid printed with 0.26 mm ID nozzle. b) grid printed with 0.41 mm ID nozzle. c,d) cross-linked gels of a and b respectively. All structures were printed from a direct-write printer at 5 mm/s (scale bar 2 mm).

2.4 CONCLUSIONS

Living anionic ring-opening polymerization of glycidyl ethers was used to synthesize PiPGE-*stat*-PAGE-*b*-PEG-*b*-PiPGE-*stat*-PAGE and PEGE-*stat*-PAGE-*b*-PEG-*b*-PEGE-*stat*-PAGE triblock copolymers. These polymers self-assembled in aqueous media to afford triple stimuli-responsive triblock copolymers hydrogels, which respond to temperature, pressure, and UV light. The stimuli-responsive capabilities of these hydrogels are critical to the printability of these materials using a direct-write 3D printer: (1) the temperature response facilitates easy handling and transfer of the gel, (2) the pressure (or shear-thinning) response allow the material to be printed at ambient temperature, and (3) the light response facilitates cross-linking of the polymer chains afford a robust 3D object. Interestingly, these allyl-containing polymers were readily cross-linked in the presence of a photo-initiator and did not require the addition of other additives to cross-link the polymer chains. These hydrogels afforded inks that were suitable for direct-write 3D printing to create 3D objects. The hydrogels based on these triblock copolymers provide a platform to expand the set of materials available for direct-write 3D printing, and demonstrates that the properties of the hydrogels, such as the modulus, can be tuned based on the compositional make-up of the polymer. We are currently exploring the application of these materials for biotechnology applications which require robust 3D hydrogels, and will report these results in due time.

2.5 EXPERIMENTAL

2.5.1 *Calculation of Mn*

Number average molecular weight was calculated using ^{1}H NMR and an example for a copolymer of PiPGE-*stat*-PAGE-*b*-PEG-*b*-PiPGE-*stat*-PAGE is given. The M_n of PEG is 8k Da which corresponds to approximately 182 ethylene glycol units per macroinitiator. If we use Figure 2.14 as the example spectrum then the number of isopropyl and allyl glycidyl ether units can be calculated by finding the PEG to PiPGE and PEG to PAGE ratio. The integration for the peak at 2 ppm corresponds to the methyl groups on iPGE and is usually set to 1. The peaks between 3.2 and 3.9 correspond to protons e-m and were integrated to a value of 8, and the peaks at 4, 5.1 to 5.3, and 5.9 ppm corresponding to proton a-d equaled a total of 0.125. Since iPGE and AGE have peaks that overlap in the 3.5 ppm region, their contribution to the overall integration must be subtracted as shown below.

$$\frac{182\ ethylene\ glycol\ units}{\left(\frac{6\ PiPGE\ CH_3}{4\ PEG\ CH_2}\right) * (8 - 1 - 0.125)} = 17.6\ iPGE\ units$$

Then, the integrations for PAGE allyl and vinyl protons at 4, 5.1 to 5.3, and 5.9 ppm can be summed and multiplied by the number of iPGE units to give the number of AGE units as shown below.

$$0.125 * \frac{6\ PiPGE\ CH_3}{5\ PAGE\ CH_2 + CH} * 17.6 = 2.6\ AGE\ units$$

2.5.2 *Materials and Instrumentation.*

All chemicals and solvents, unless otherwise stated, were purchased from Sigma-Aldrich or Fisher Scientific and used without further purification. Poly(ethylene glycol) (PEG, Mn 8,000) was dried under vacuum at 50 °C overnight in a flask prior to use. Allyl glycidyl ether (AGE, 99%, Acros), isopropyl glycidyl ether (iPGE, 98%), and ethyl glycidyl ether (EGE, 98%, TCI America)

were dried over CaH_2, distilled into a flask containing butyl magnesium chloride solution (2M in THF), distilled, and stored under an inert atmosphere. Dry tetrahydrofuran was obtained by purification over alumina column on a Pure Process Technology purification system. Potassium naphthalenide was prepared by dissolving naphthalene (5 g) in THF (50 mL) and adding potassium (1.5 g) and storing in an inert atmosphere. ^{1}H NMR spectra were obtained on a Bruker Avance 300 or 500 MHz spectrometer.

Gel permeation chromatography was performed using a Waters chromatograph equipped with two 10 µm Malvern columns (300 mm X 7.8 mm) connected in series with increasing pore size (1000, 10000 Å), using chloroform as the eluent, and calibrated with poly(ethylene glycol) standards (102 to 40000 g/mol). Relative molecular weights were measured in chloroform using poly(ethylene glycol) standards and a refractive index detector (flow rate: 1 mL/min).

2.5.3 *Synthesis of poly(allyl glycidyl ether)-b-poly(ethylene glycol)-b-poly(allyl glycidyl ether) (PAGE-b-PEG-b-PAGE)*

PEG (10 g, 1.25 mmol, M_n = 8,000 g/mol) was dried under reduced pressure in a reaction vessel at 50 °C overnight. THF (100 mL) was added under an argon atmosphere to dissolve PEG at room temperature. Potassium naphthalenide solution was titrated into the flask until a slight green color persisted, indicating that the hydroxyl groups of the PEG have been fully deprotonated. The reaction vessel was then warmed to 30 °C and AGE (4 mL, 34 mmol) was added via buret. The reaction was left to stir for 48 h and was quenched with degassed acidic methanol (10 mL, 1 v/v % acetic acid). The reaction mixture was concentrated under reduced pressure and added to cold diethyl ether to precipitate. The resulting suspension was poured into centrifuge tubes and spun at 4400 rpm for 10 min. The supernatant was decanted and resulting material was dried in a vacuum oven to afford a white solid. ^{1}H NMR (500 MHz, $CDCl_3$): δ 5.86-5.95 (m, 1 H, CH_2-

C*H*=CH_2), 5.15-5.30 (m, 2 H, CH_2-CH=C*H*$_2$), 4.01 (s, 2 H, O-C*H*$_2$-CH=CH_2), 3.47-3.89 (m, 4 H, + 5 H, PEG backbone, PAGE backbone). M_n = 10800 g/mol (determined by ^{1}H NMR 500 MHz, $CDCl_3$). Đ = 1.11 (determined by SEC using RI detection and $CHCl_3$ as eluent).

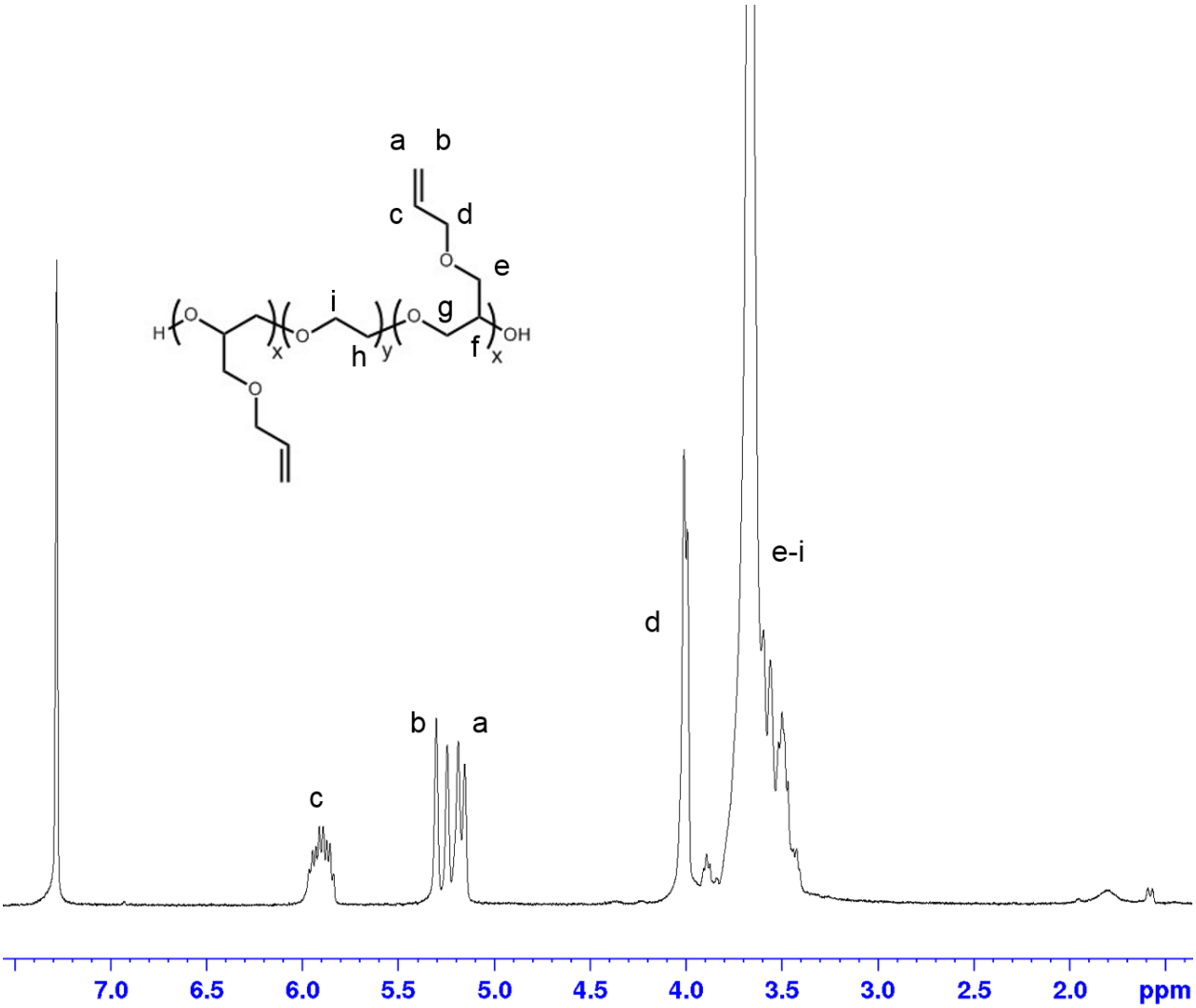

Figure 2.15 ^{1}H NMR spectrum of PAGE-*b*-PEG-*b*-PAGE (polymer **1**) triblock (500 MHz, 293 K, $CDCl_3$).

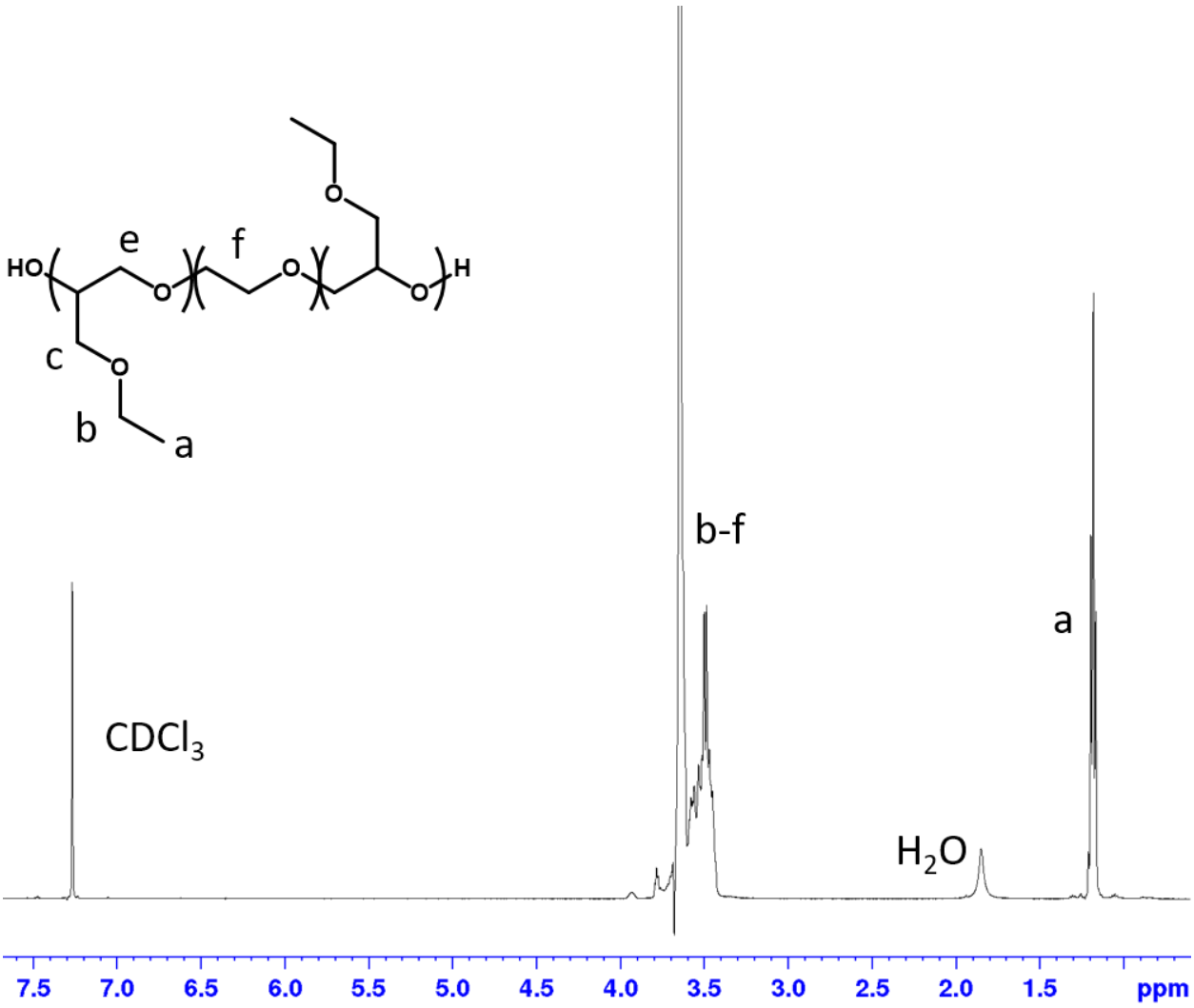

Figure 2.16 ^{1}H NMR spectrum of PEGE-*b*-PEG-*b*-PEGE (polymer **2**) triblock (500 MHz. 293 K, $CDCl_3$).

2.5.4 *Synthesis of poly(ethyl glycidyl ether)-b-poly(ethylene glycol)-b-poly(ethyl glycidyl ether) (PEGE-b-PEG-b-PEGE)*

PEG (10 g, 1.25 mmol, M_n = 8,000 g/mol) was dried under reduced pressure in a reaction vessel at 50 °C overnight. THF (100 mL) was added under an argon atmosphere to dissolve PEG at room temperature. Potassium naphthalenide solution was titrated into the flask until a slight green color persisted, indicating that the hydroxyl groups of the PEG have been fully deprotonated. The reaction vessel was then warmed to 50 °C and EGE (4.8 mL, 44 mmol) was added via buret.

The reaction was left to stir for 48 h and was quenched with degassed acidic methanol (10 mL, 1 v/v % acetic acid). The reaction mixture was concentrated under reduced pressure and added to cold diethyl ether to precipitate. The resulting suspension was poured into centrifuge tubes and spun at 4400 rpm for 10 min. The supernatant was decanted and resulting material was dried in a vacuum oven to afford a white solid. ^{1}H NMR (500 MHz, $CDCl_3$): δ 3.48-3.92 (m, 4 H, + 7 H, PEG backbone, PEGE backbone), 1.18-1.19 (m, 3 H, O-$CH_2C\mathit{H}_3$). M_n = 11300 g/mol (determined by ^{1}H NMR 500 MHz, $CDCl_3$). Đ = 1.11 (determined by SEC using RI detection and $CHCl_3$ as eluent).

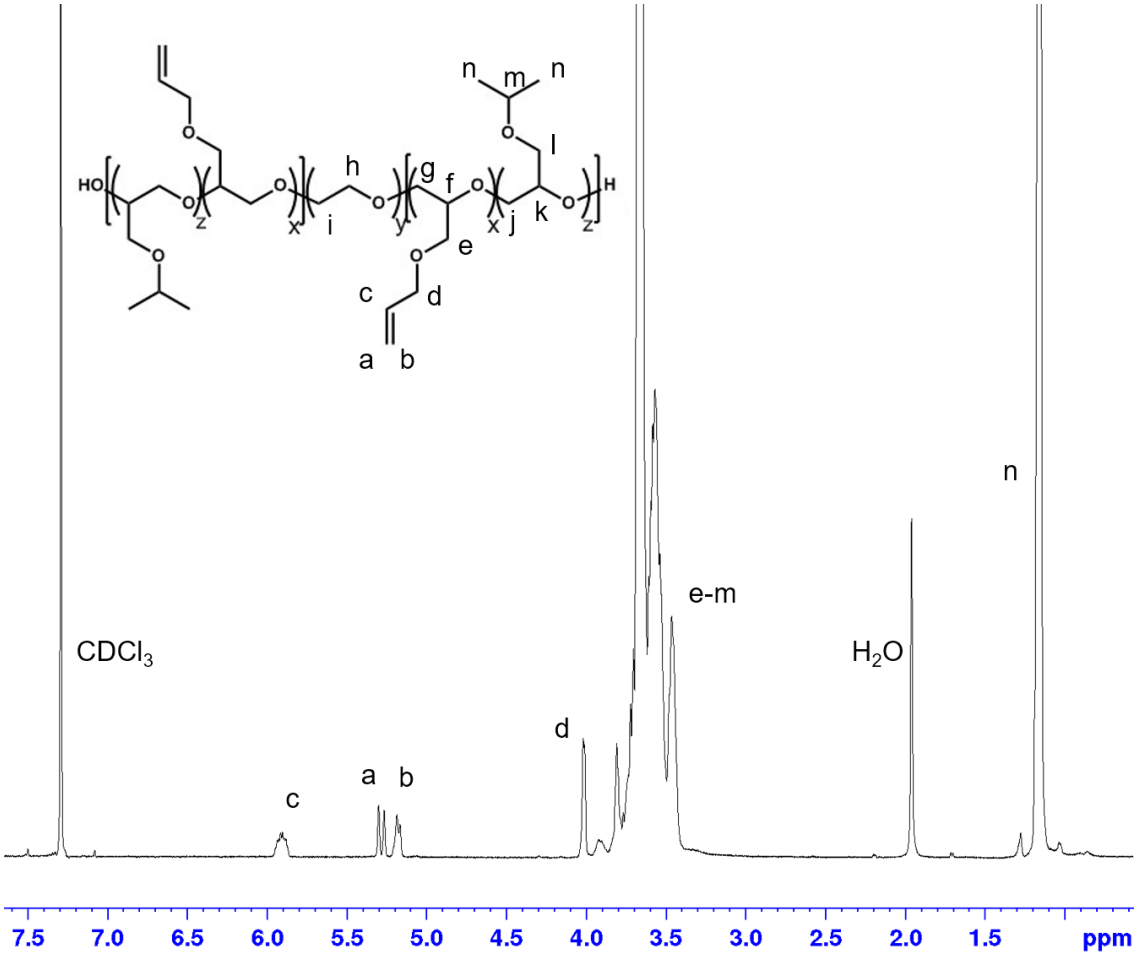

Figure 2.17 ^{1}H NMR spectrum of PiPGE-*stat*-PAGE-*b*-PEG-*b*-PiPGE-*stat*-PAGE (polymer **3**) triblock (500 MHz, 293 K, $CDCl_3$).

2.5.5 *Synthesis of poly(isopropyl glycidyl ether)-stat-poly(allyl glycidyl ether)-b-poly(ethylene glycol)-b-poly(isopropyl glycidyl ether)-stat-poly(allyl glycidyl ether) (PiPGE-stat-PAGE-b-PEG-b-PiPGE-stat-PAGE)*

PEG (10 g, 1.25 mmol, M_n = 8,000 g/mol) was dried under reduced pressure in a reaction vessel at 50 °C overnight. THF (100 mL) was added under an argon atmosphere to dissolve PEG at room temperature. Potassium naphthalenide solution was titrated into the flask until a slight green color persisted, indicating that the hydroxyl groups of the PEG have been fully deprotonated. The reaction vessel was then warmed to 30 °C AGE (0.72 mL, 6.1 mmol) and iPGE (3.3 mL, 26 mmol) were added via burets. The reaction was left to stir for 48 h and was quenched with degassed acidic methanol (10 mL, 1 v/v % acetic acid). The reaction mixture was concentrated under reduced pressure and added to cold diethyl ether to precipitate. The resulting suspension was poured into centrifuge tubes and spun at 4400 rpm for 10 min. The supernatant was decanted and resulting material was dried in a vacuum oven to afford a white solid. ^{1}H NMR (500 MHz, $CDCl_3$): δ 5.88-5.97 (m, 1 H, CH_2-C*H*=CH_2), 5.16-5.28 (m, 2 H, CH_2-CH=C*H*$_2$), 3.99 (s, 2 H, O-C*H*$_2$-CH=CH_2), 3.47-3.89 (m, 4 H, + 5 H, + 6 H, PEG backbone, PAGE backbone, PiPGE backbone), 1.14-1.21 (d, 6 H, O-CH-2C*H*$_3$). M_n = 10700 g/mol (determined by ^{1}H NMR 500 MHz, $CDCl_3$). Đ = 1.11 (determined by SEC using RI detection and $CHCl_3$ as eluent).

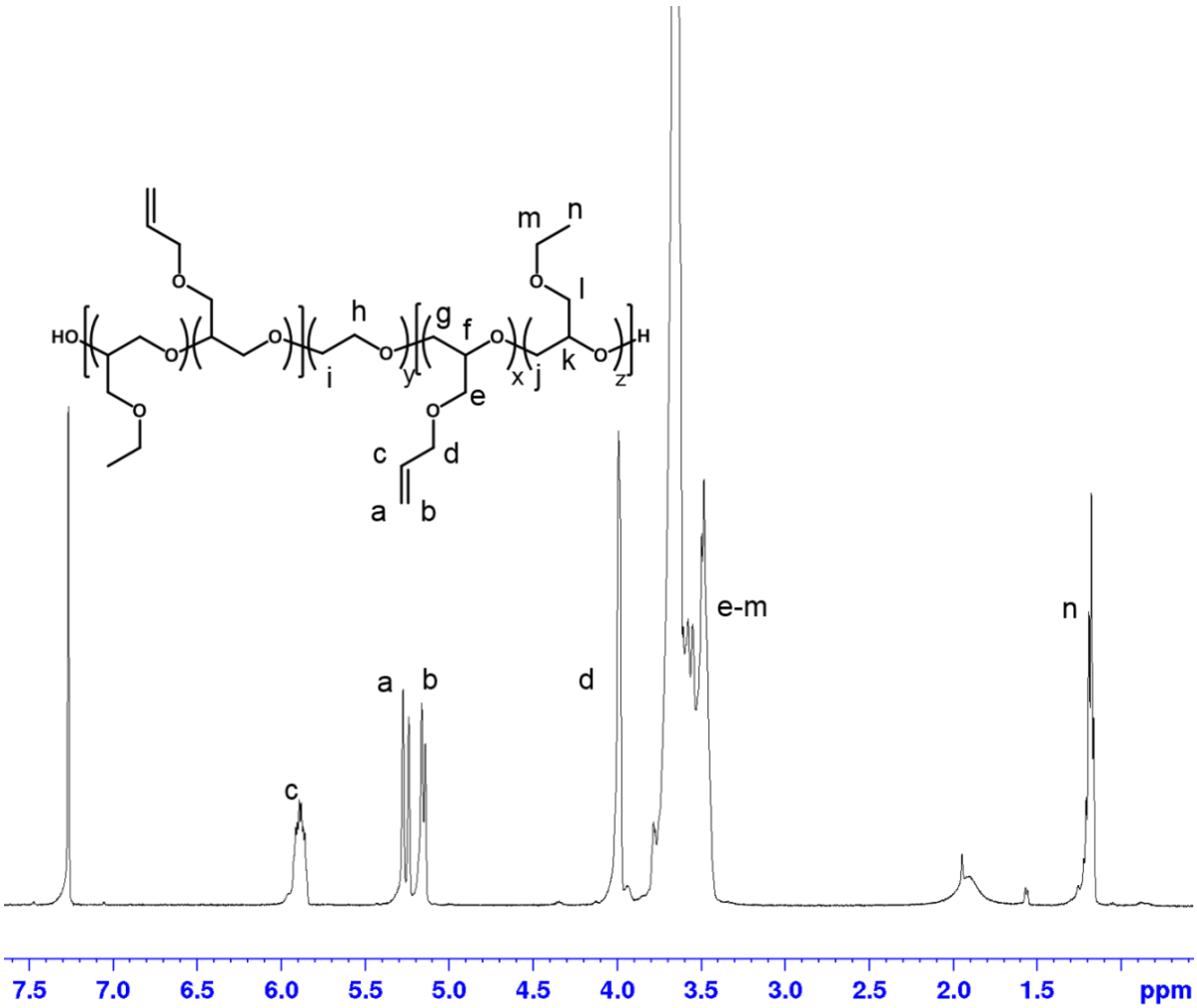

Figure 2.18 ^{1}H NMR spectrum of PEGE-*stat*-PAGE-*b*-PEG-*b*-PEGE-*stat*-PAGE (polymer **6**) triblock (500 MHz, 293 K, $CDCl_3$).

2.5.6 *Synthesis of poly(ethyl glycidyl ether)-stat-poly(allyl glycidyl ether)-b-poly(ethylene glycol)-b-poly(ethyl glycidyl ether)-stat-poly(allyl glycidyl ether) (PEGE-stat-PAGE-b-PEG-b-PEGE-stat-PAGE)*

PEG (10 g, 1.25 mmol, M_n = 8,000 g/mol) was dried under reduced pressure in a reaction vessel at 50 °C overnight. THF (100 mL) was added under an argon atmosphere to dissolve PEG at room temperature. Potassium naphthalenide solution was titrated into the flask until a slight green color persisted, indicating that the hydroxyl groups of the PEG have been fully deprotonated. The reaction vessel was then warmed to 30 °C AGE (3.1 mL, 26 mmol) and EGE (1.8 mL, 15

mmol) were added via burets. The reaction was left to stir for 48 h and was quenched with degassed acidic methanol (10 mL, 1 v/v % acetic acid). The reaction mixture was concentrated under reduced pressure and added to cold diethyl ether to precipitate. The resulting suspension was poured into centrifuge tubes and spun at 4400 rpm for 10 min. The supernatant was decanted and resulting material was dried in a vacuum oven to afford a white solid. ^{1}H NMR (500 MHz, $CDCl_3$): δ 5.88-5.89 (m, 1 H, CH_2-C*H*=CH_2), 5.14-5.27 (m, 2 H, CH_2-CH=C*H*$_2$), 3.98 (s, 2 H, O-C*H*$_2$-CH=CH_2), 3.48-3.89 (m, 4 H, + 5 H, + 7 H, PEG backbone, PAGE backbone, PEGE backbone), 1.18 (m, 3 H, O-CH-C*H*$_3$). M_n = 11300 g/mol (determined by ^{1}H NMR 500 MHz, $CDCl_3$). Đ = 1.11 (determined by SEC using RI detection and $CHCl_3$ as eluent).

2.5.7 *Rheological Experiments.*

Dynamic oscillatory experiments were performed on a TA Instruments Discovery HR-2 equipped with a 20 mm parallel plate geometry. Samples, which were equilibrating in an ice bath for at least 10 minutes, were carefully loaded onto the Peltier plate at 5 °C. A preshear experiment was applied to ensure bubbles were eliminated from the sample cell. The sample was equilibrated at 25 °C for 8 minutes. Strain sweep experiments were performed, and all experiments were conducted using a strain value in the linear viscoelastic regime. Temperature ramp experiments were performed at 1 Hz from 5-50 °C at 2 °C/min. Cyclic strain sweep experiments were conducted to investigate the shear-thinning and recovery behavior of the hydrogels. Samples were loaded on a 20 mm parallel plate geometry at 5 °C and a preshear experiment was performed to eliminate bubbles from the sample. Cyclic shear thinning tests(frequency 1 Hz) were performed at 25 °C using alternating strains of 1 % for 5 minutes and 100 % for 3 minutes per cycle. Viscosity versus shear rate experiments were performed with a 20 mm parallel plate geometry at 25 °C. Gel yield strains were measured under oscillatory strain (frequency 1 Hz, 25 °C) starting with an initial strain

of 0.01 %. UV cure experiments were conducted to investigate the cross-linking behavior of the hydrogels. Samples were loaded on a 20 mm parallel plate geometry and a preshear experiment was performed to eliminate bubbles from the sample. The sample was equilibrated for 10 min to bring sample to room temperature. A 60 s dwell time (frequency 1 Hz) preceded the UV lamp (365 nm LED with irradiation intensity 5 mW/cm2) was turned on for 10 min followed by a 10 min post-cure constant oscillatory strain.

2.5.8 *3D Printing of Hydrogels.*

A direct-write printer was assembled from a Fab@Home V1 from Cornell University which enabled the printer to translate in the x, y, and z directions at 25 µm resolution. The hydrogel inks were cooled to 5 °C and poured into a Nordson Optimum 10 cc fluid dispensing barrel equipped with a Metcal conical (210, 260, or 410 µm inner diameter) precision tip nozzle. The syringe was pressurized using nitrogen gas (20 psi) to extrude the gel from the nozzle at ambient temperature. The printer was controlled with an Arduino using Marlin firmware. The G-code was made with Slic3r. Printed structures were cured in a custom-made box fitted with sunlite 365 nm A19 UV Lamp(s) for 10 min. Irradiation intensity was 2 mW/cm^2 or 3.4 mW/cm^2 for 1 or 2 lamps, respectively.

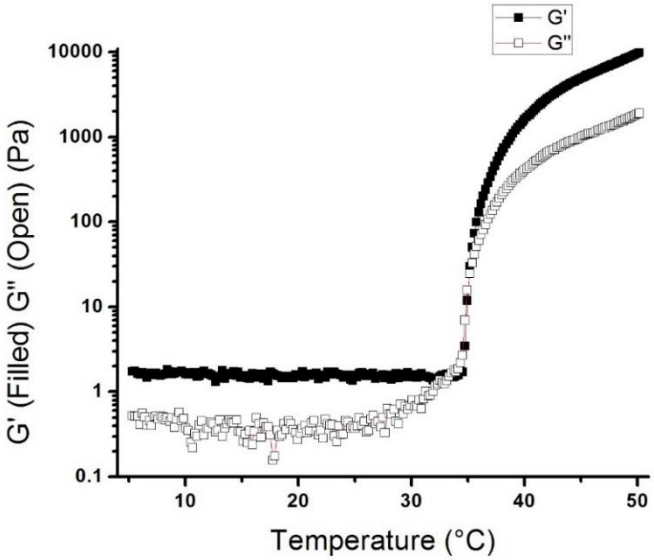

Figure 2.19 Rheological temperature ramp of polymer **2**

Dynamic oscillatory temperature ramp experiment showing storage (filled) and loss (open) moduli performed on polymer **2**. Experiment shows that PEGE-*b*-PEG-*b*-PEGE hydrogels are not viable for printing but can assist in the gelation properties of PEGE-*stat*-PAGE-*b*-PEG-*b*-PEGE-*stat*-PAGE hydrogels.

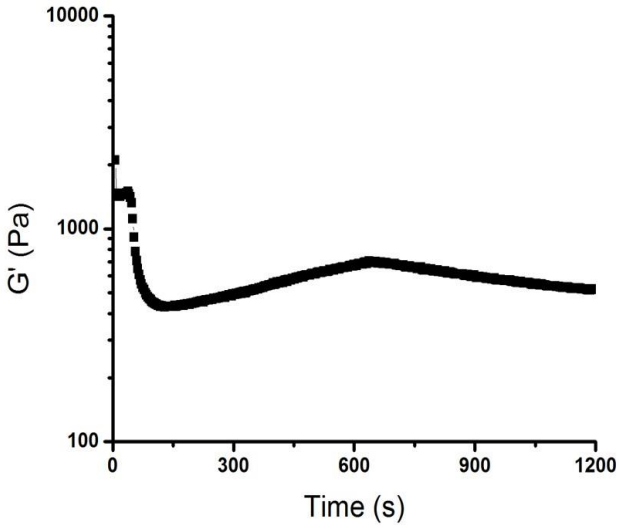

Figure 2.20 Photorheology of PiPGE-*b*-PEG-*b*-PiPGE control

Dynamic oscillatory UV cure experiment on a triblock copolymer of PiPGE-*b*-PEG-*b*-PiPGE showing no increase in storage modulus after UV lamp is turned on. The slight slope shown in the graph is due to heating of the plate during lamp irradiation.

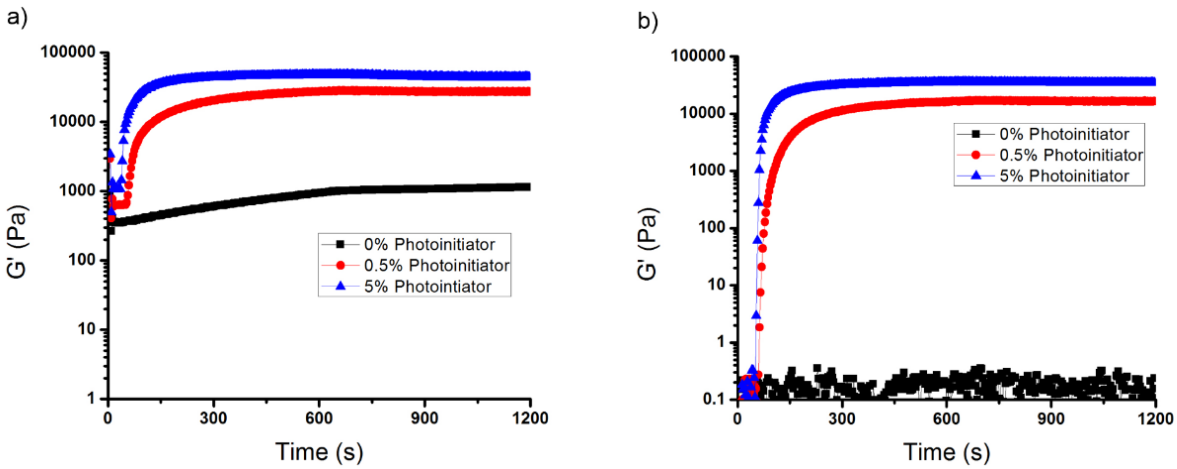

Figure 2.21 Photorheology of polymer **5** with and without DOWEX treatment

Dynamic oscillatory UV cure experiment showing increase in storage modulus when lamp is turned on at the 60 s mark for 10 min of irradiation. Experiment performed on (a) polymer **5** at 13.5 wt% and (b) polymer **5** treated with DOWEX cationic exchange resin to hydrolyze vinyl ethers. Both polymers form cross-linked networks upon exposure to UV light in the presence of phototiniator suggesting that vinyl ether itself is not necessary for cross-linking.

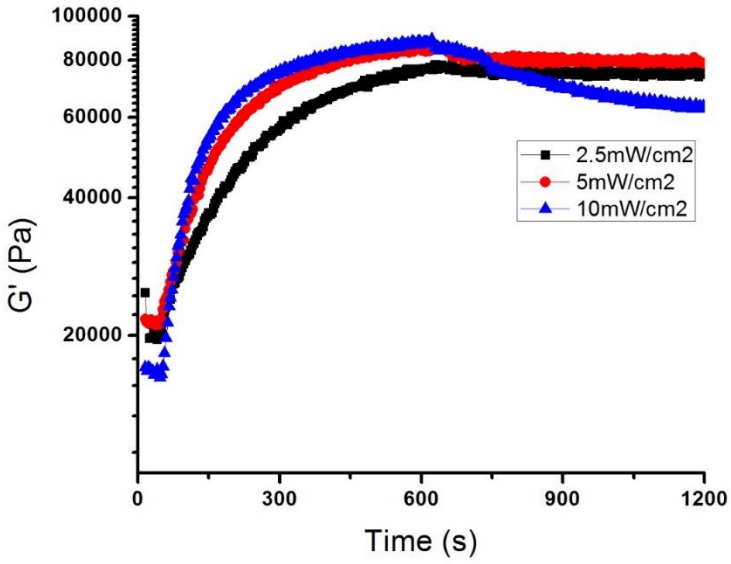

Figure 2.22 Photorheology of polymer **6** with different UV intensities

Dynamic oscillatory UV cure experiment showing increase in storage modulus when lamp is turned on at the 60 s mark for 10 min of irradiation. Experiment performed on polymer **6** at 20 wt% with 1 wt% photoinitiator with varied UV light intensities showing the rate of cross-linking can be controlled with lamp power.

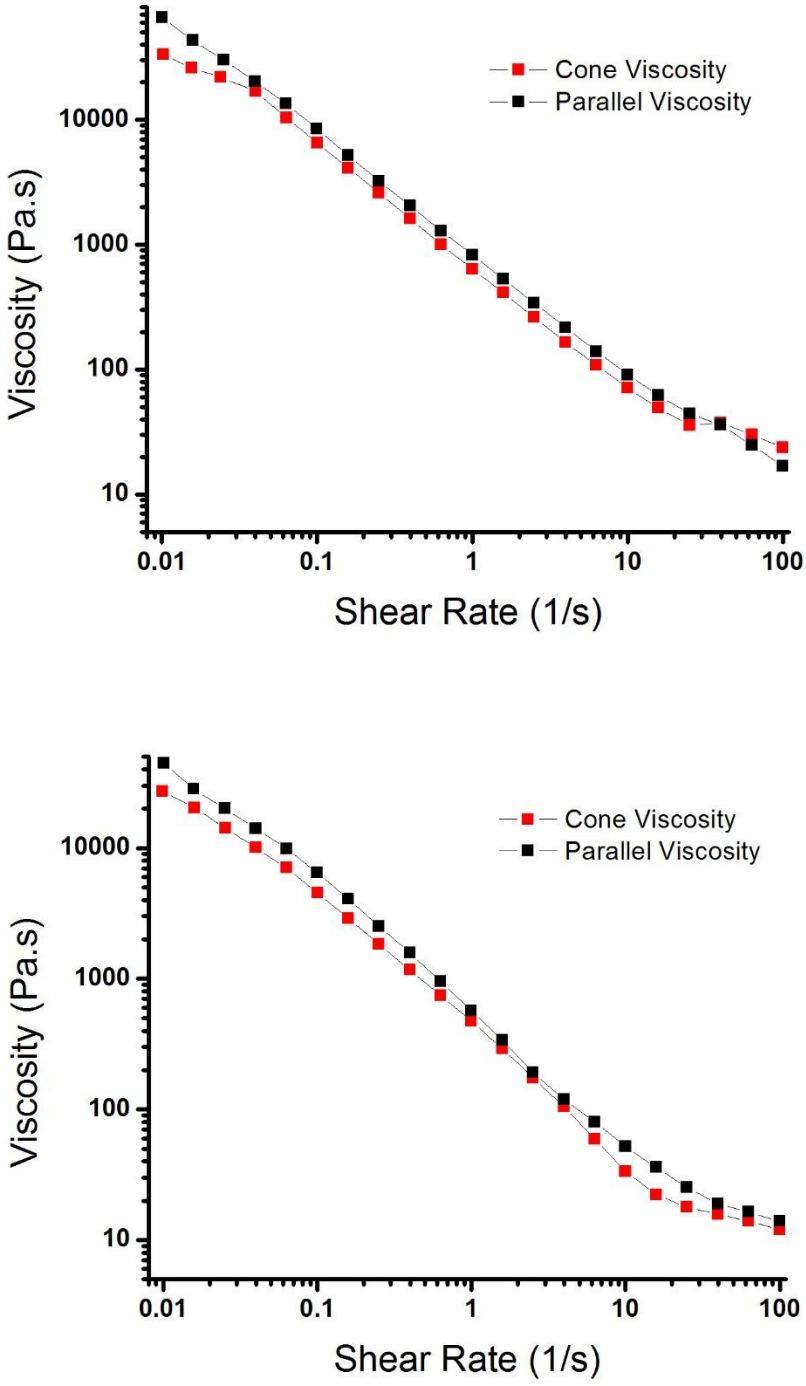

Figure 2.23 Comparison of 20 mm parallel plate and 40 mm cone and plate geometries

Viscosity vs shear rate profiles comparing 40 mm cone and plate geometry with 20 mm parallel plate geometry. Experiment performed on polymer **4** (top) at 18 wt% and polymer **6** (bottom) at 20 wt%. Graph indicates that there is not a significant difference between geometries.

2.6 ACKNOWLEDGEMENTS

"Reprinted (adapted) with permission from: Karis, D.; Ono, R.; Zhang, M.; Vora, A.; Storti, D.; Ganter, M.; and Nelson, A. Cross-Linkable Multi-Stimuli-Responsive Hydrogel Inks for Direct-Write 3D Printing. *Polymer Chemistry*, **2017**, *8*, 4199-4206. https://doi.org/10.1039/C7PY00831G. Copyright 2017 Royal Society of Chemistry."

2.7 REFERENCES

(1) Krishnamoorti, R.; Ren, J.; Silva, A. S. Shear Response of Layered Silicate Nanocomposites. *J. Chem. Phys.* **2001**, *114* (11), 4968–4973. https://doi.org/10.1063/1.1345908.

(2) Barry, R. A.; Shepherd, R. F.; Hanson, J. N.; Nuzzo, R. G.; Wiltzius, P.; Lewis, J. A. Direct-Write Assembly of 3D Hydrogel Scaffolds for Guided Cell Growth. *Adv. Mater.* **2009**, *21* (23), 2407–2410. https://doi.org/10.1002/adma.200803702.

(3) Hansen, C. J.; Saksena, R.; Kolesky, D. B.; Vericella, J. J.; Kranz, S. J.; Muldowney, G. P.; Christensen, K. T.; Lewis, J. A. High-Throughput Printing via Microvascular Multinozzle Arrays. *Adv. Mater.* **2013**, *25* (1), 96–102. https://doi.org/10.1002/adma.201203321.

(4) Lewis, J. A.; Gratson, G. M. Direct Writing in Three Dimensions. *Mater. Today* **2004**, *7* (7), 32–39. https://doi.org/10.1016/S1369-7021(04)00344-X.

(5) Pawar, G. M.; Koenigs, M.; Fahimi, Z.; Cox, M.; Voets, I. K.; Wyss, H. M.; Sijbesma, R. P. Injectable Hydrogels from Segmented PEG-Bisurea Copolymers. *Biomacromolecules* **2012**, *13* (12), 3966–3976. https://doi.org/10.1021/bm301242v.

(6) Guvendiren, M.; Lu, H. D.; Burdick, J. A. Shear-Thinning Hydrogels for Biomedical Applications. *Soft Matter*. The Royal Society of Chemistry January 14, 2012, pp 260–272. https://doi.org/10.1039/c1sm06513k.

(7) Hospodiuk, M.; Dey, M.; Sosnoski, D.; Ozbolat, I. T. The Bioink: A Comprehensive Review on Bioprintable Materials. *Biotechnology Advances*. Elsevier Inc. March 1, 2017, pp 217–239. https://doi.org/10.1016/j.biotechadv.2016.12.006.

(8) Lewis, J. A. Direct Ink Writing of 3D Functional Materials. *Adv. Funct. Mater.* **2006**, *16* (17), 2193–2204. https://doi.org/10.1002/adfm.200600434.

(9) Kirchmajer, D. M.; Gorkin, R.; In Het Panhuis, M. An Overview of the Suitability of Hydrogel-Forming Polymers for Extrusion-Based 3D-Printing. *J. Mater. Chem. B* **2015**, *3* (20), 4105–4117. https://doi.org/10.1039/c5tb00393h.

(10) Landers, R.; Mülhaupt, R. Desktop Manufacturing of Complex Objects, Prototypes and Biomedical Scaffolds by Means of Computer-assisted Design Combined with Computer-guided 3D Plotting of Polymers and Reactive Oligomers. *Macromol. Mater. Eng.* **2000**, *282* (1), 17–21. https://doi.org/10.1002/1439-2054(20001001)282:1<17::AID-MAME17>3.0.CO;2-8.

(11) Vozzi, G.; Previti, A.; De Rossi, D.; Ahluwalia, A. Microsyringe-Based Deposition of Two-Dimensional and Three-Dimensional Polymer Scaffolds with a Well-Defined Geometry for Application to Tissue Engineering. *Tissue Eng.* **2002**, *8* (6), 1089–1098. https://doi.org/10.1089/107632702320934182.

(12) Farahani, R. D.; Dubé, M.; Therriault, D. Three-Dimensional Printing of Multifunctional Nanocomposites: Manufacturing Techniques and Applications. *Adv. Mater.* **2016**, *28* (28), 5794–5821. https://doi.org/10.1002/adma.201506215.

(13) Truby, R. L.; Lewis, J. A. Printing Soft Matter in Three Dimensions. *Nature*. Nature Publishing Group December 14, 2016, pp 371–378. https://doi.org/10.1038/nature21003.

(14) Unterman, S.; Charles, L. F.; Strecker, S. E.; Kramarenko, D.; Pivovarchik, D.; Edelman, E. R.; Artzi, N. Hydrogel Nanocomposites with Independently Tunable Rheology and Mechanics. *ACS Nano* **2017**, *11* (3), 2598–2610. https://doi.org/10.1021/acsnano.6b06730.

(15) Lis, M.; Plaut, M.; Zai, A.; Cipolle, D.; Russo, J.; Fedynyshyn, T. High Performance, 3D-Printable Dielectric Nanocomposites for Millimeter Wave Devices. *ACS Appl. Mater. Interfaces* **2016**, *8* (49), 34019–34026. https://doi.org/10.1021/acsami.6b11643.

(16) Highley, C. B.; Rodell, C. B.; Burdick, J. A. Direct 3D Printing of Shear-Thinning Hydrogels into Self-Healing Hydrogels. *Adv. Mater.* **2015**, *27* (34), 5075–5079. https://doi.org/10.1002/adma.201501234.

(17) Ewoldt, R. H.; Hosoi, A. E.; McKinley, G. H. New Measures for Characterizing Nonlinear Viscoelasticity in Large Amplitude Oscillatory Shear. *J. Rheol. (N. Y. N. Y).* **2008**, *52* (6), 1427–1458. https://doi.org/10.1122/1.2970095.

(18) Thompson, P. A.; Robbins, M. O.; Grest, G. S. Structure and Shear Response in Nanometer-Thick Films. *Isr. J. Chem.* **1995**, *35* (1), 93–106. https://doi.org/10.1002/ijch.199500015.

(19) Cho, K. S.; Hyun, K.; Ahn, K. H.; Lee, S. J. A Geometrical Interpretation of Large Amplitude Oscillatory Shear Response. *J. Rheol. (N. Y. N. Y).* **2005**, *49* (3), 747–758. https://doi.org/10.1122/1.1895801.

(20) Winnik, M. A.; Yekta, A. Associative Polymers in Aqueous Solution. *Curr. Opin. Colloid Interface Sci.* **1997**, *2* (4), 424–436. https://doi.org/10.1016/s1359-0294(97)80088-x.

(21) Butler, P. Shear Induced Structures and Transformations in Complex Fluids. *Curr. Opin. Colloid Interface Sci.* **1999**, *4* (3), 214–221. https://doi.org/10.1016/S1359-0294(99)00041-2.

(22) Franco, J.; Hunger, P.; Launey, M. E.; Tomsia, A. P.; Saiz, E. Direct Write Assembly of Calcium Phosphate Scaffolds Using a Water-Based Hydrogel. *Acta Biomater.* **2010**, *6* (1), 218–228. https://doi.org/10.1016/j.actbio.2009.06.031.

(23) Fu, Q.; Saiz, E.; Tomsia, A. P. Direct Ink Writing of Highly Porous and Strong Glass Scaffolds for Load-Bearing Bone Defects Repair and Regeneration. *Acta Biomater.* **2011**, *7* (10), 3547–3554. https://doi.org/10.1016/j.actbio.2011.06.030.

(24) Luo, Y.; Wu, C.; Lode, A.; Gelinsky, M. Hierarchical Mesoporous Bioactive Glass/Alginate Composite Scaffolds Fabricated by Three-Dimensional Plotting for Bone Tissue Engineering. *Biofabrication* **2013**, *5* (1), 015005. https://doi.org/10.1088/1758-5082/5/1/015005.

(25) Fedorovich, N. E.; Swennen, I.; Girones, J.; Moroni, L.; Van Blitterswijk, C. A.; Schacht, E.; Alblas, J.; Dhert, W. J. A. Evaluation of Photocrosslinked Lutrol Hydrogel for Tissue Printing Applications. *Biomacromolecules* **2009**, *10* (7), 1689–1696. https://doi.org/10.1021/bm801463q.

(26) Song, S.-J.; Choi, J.; Park, Y.-D.; Hong, S.; Lee, J. J.; Ahn, C. B.; Choi, H.; Sun, K. Sodium Alginate Hydrogel-Based Bioprinting Using a Novel Multinozzle Bioprinting System. *Artif. Organs* **2011**, *35* (11), 1132–1136. https://doi.org/10.1111/j.1525-1594.2011.01377.x.

(27) Hong, S.; Sycks, D.; Chan, H. F.; Lin, S.; Lopez, G. P.; Guilak, F.; Leong, K. W.; Zhao, X. 3D Printing of Highly Stretchable and Tough Hydrogels into Complex, Cellularized Structures. *Adv. Mater.* **2015**, *27* (27), 4035–4040. https://doi.org/10.1002/adma.201501099.

(28) Markstedt, K.; Mantas, A.; Tournier, I.; Martínez Ávila, H.; Hägg, D.; Gatenholm, P. 3D Bioprinting Human Chondrocytes with Nanocellulose-Alginate Bioink for Cartilage Tissue Engineering Applications. *Biomacromolecules* **2015**, *16* (5), 1489–1496. https://doi.org/10.1021/acs.biomac.5b00188.

(29) Duan, B.; Hockaday, L. A.; Kang, K. H.; Butcher, J. T. 3D Bioprinting of Heterogeneous Aortic Valve Conduits with Alginate/Gelatin Hydrogels. *J. Biomed. Mater. Res. Part A* **2013**, *101A* (5), 1255–1264. https://doi.org/10.1002/jbm.a.34420.

(30) Xie, B.; Parkhill, R. L.; Warren, W. L.; Smay, J. E. Direct Writing of Three-Dimensional Polymer Scaffolds Using Colloidal Gels. *Adv. Funct. Mater.* **2006**, *16* (13), 1685–1693. https://doi.org/10.1002/adfm.200500666.

(31) Li, Q.; Lewis, J. A. Nanoparticle Inks for Directed Assembly of Three-Dimensional Periodic Structures. *Adv. Mater.* **2003**, *15* (19), 1639–1643. https://doi.org/10.1002/adma.200305413.

(32) Morissette, S. L.; Lewis, J. A.; Cesarano, J.; Dimos, D. B.; Baer, T. Solid Freeform Fabrication of Aqueous Alumina-Poly(Vinyl Alcohol) Gelcasting Suspensions. *J. Am. Ceram. Soc.* **2004**, *83* (10), 2409–2416. https://doi.org/10.1111/j.1151-2916.2000.tb01569.x.

(33) Stuecker, J. N.; Cesarano, J.; Hirschfeld, D. A. Control of the Viscous Behavior of Highly Concentrated Mullite Suspensions for Robocasting. *J. Mater. Process. Technol.* **2003**, *142* (2), 318–325. https://doi.org/10.1016/S0924-0136(03)00586-7.

(34) Smay, J. E.; Gratson, G. M.; Shepherd, R. F.; Cesarano, J.; Lewis, J. A. Directed Colloidal Assembly of 3D Periodic Structures. *Adv. Mater.* **2002**, *14* (18), 1279–1283. https://doi.org/10.1002/1521-4095(20020916)14:18<1279::AID-ADMA1279>3.0.CO;2-A.

(35) Lewis, J. A.; Smay, J. E.; Stuecker, J.; Cesarano, J. Direct Ink Writing of Three-Dimensional Ceramic Structures. *J. Am. Ceram. Soc.* **2006**, *89* (12), 3599–3609. https://doi.org/10.1111/j.1551-2916.2006.01382.x.

(36) Smay, J. E.; Cesarano, J.; Lewis, J. A. Colloidal Inks for Directed Assembly of 3-D Periodic Structures. *Langmuir* **2002**, *18* (14), 5429–5437. https://doi.org/10.1021/la0257135.

(37) Lewis, J. A. Direct-Write Assembly of Ceramics from Colloidal Inks. *Curr. Opin. Solid State Mater. Sci.* **2002**, *6* (3), 245–250. https://doi.org/10.1016/S1359-0286(02)00031-1.

(38) Ng, W. L.; Yeong, W. Y.; Naing, M. W. Polyelectrolyte Gelatin-Chitosan Hydrogel Optimized for 3D Bioprinting in Skin Tissue Engineering. *Int. J. Bioprinting* **2016**, *2* (1), 53–62. https://doi.org/10.18063/IJB.2016.01.009.

(39) Rajaram, A.; Schreyer, D. J.; Chen, D. X. B. Use of the Polycation Polyethyleneimine to Improve the Physical Properties of Alginate-Hyaluronic Acid Hydrogel during Fabrication of Tissue Repair Scaffolds. *J. Biomater. Sci. Polym. Ed.* **2015**, *26* (7), 433–445. https://doi.org/10.1080/09205063.2015.1016383.

(40) Ang, T. H.; Sultana, F. S. A.; Hutmacher, D. W.; Wong, Y. S.; Fuh, J. Y. H.; Mo, X. M.; Loh, H. T.; Burdet, E.; Teoh, S. H. Fabrication of 3D Chitosan-Hydroxyapatite Scaffolds Using a Robotic Dispensing System. *Mater. Sci. Eng. C* **2002**, *20* (1–2), 35–42. https://doi.org/10.1016/S0928-4931(02)00010-3.

(41) Gratson, G. M.; Xu, M.; Lewis, J. A. Direct Writing of Three-Dimensional Webs. *Nature* **2004**, *428* (6981), 386. https://doi.org/10.1038/428386a.

(42) Kolesky, D. B.; Truby, R. L.; Gladman, A. S.; Busbee, T. A.; Homan, K. A.; Lewis, J. A. 3D Bioprinting of Vascularized, Heterogeneous Cell-Laden Tissue Constructs. *Adv. Mater.* **2014**, *26* (19), 3124–3130. https://doi.org/10.1002/adma.201305506.

(43) Su, Y. L.; Wang, J.; Liu, H. Z. FTIR Spectroscopic Study on Effects of Temperature and Polymer Composition on the Structural Properties of PEO-PPO-PEO Block Copolymer Micelles. *Langmuir* **2002**, *18* (14), 5370–5374. https://doi.org/10.1021/la020007p.

(44) Goldmints, I.; Von Gottberg, F. K.; Smith, K. A.; Hatton, T. A. Small-Angle Neutron Scattering Study of PEO-PPO-PEO Micelle Structure in the Unimer-to-Micelle Transition Region. *Langmuir* **1997**, *13* (14), 3659–3664. https://doi.org/10.1021/la970140v.

(45) Alexandridis, P.; Holzwarth, J. F.; Hatton, T. A. Micellization of Poly(Ethylene Oxide)-Poly(Propylene Oxide)-Poly(Ethylene Oxide) Triblock Copolymers in Aqueous Solutions: Thermodynamics of Copolymer Association. *Macromolecules* **1994**, *27* (9), 2414–2425. https://doi.org/10.1021/ma00087a009.

(46) Yan-lei Su; Jing Wang, and; Liu*, H. Formation of a Hydrophobic Microenvironment in Aqueous PEO−PPO−PEO Block Copolymer Solutions Investigated by Fourier Transform Infrared Spectroscopy. **2002**. https://doi.org/10.1021/JP026160+.

(47) Hecht, E.; Hoffmann, H. Interaction of ABA Block Copolymers with Ionic Surfactants in Aqueous Solution. *Langmuir* **1994**, *10* (1), 86–91. https://doi.org/10.1021/la00013a013.

(48) Mortensen, K.; Talmon, Y. Cryo-TEM and SANS Microstructural Study of Pluronic Polymer Solutions. *Macromolecules* **1995**, *28* (26), 8829–8834. https://doi.org/10.1021/ma00130a016.

(49) Mortensen, K. Structural Studies of Aqueous Solutions of PEO - PPO - PEO Triblock Copolymers, Their Micellar Aggregates and Mesophases; a Small-Angle Neutron Scattering Study. *J. Phys. Condens. Matter* **1996**, *8* (25A), A103–A124. https://doi.org/10.1088/0953-8984/8/25A/008.

(50) Zhang, M.; Vora, A.; Han, W.; Wojtecki, R. J.; Maune, H.; Le, A. B. A.; Thompson, L. E.; McClelland, G. M.; Ribet, F.; Engler, A. C.; Nelson, A. Dual-Responsive Hydrogels for

Direct-Write 3D Printing. *Macromolecules* **2015**, *48* (18), 6482–6488. https://doi.org/10.1021/acs.macromol.5b01550.

(51) Obermeier, B.; Frey, H. Poly(Ethylene Glycol-Co-Allyl Glycidyl Ether)s: A PEG-Based Modular Synthetic Platform for Multiple Bioconjugation. *Bioconjug. Chem.* **2011**, *22* (3), 436–444. https://doi.org/10.1021/bc1004747.

(52) Lee, J.; McGrath, A. J.; Hawker, C. J.; Kim, B. S. PH-Tunable Thermoresponsive PEO-Based Functional Polymers with Pendant Amine Groups. *ACS Macro Lett.* **2016**, *5* (12), 1391–1396. https://doi.org/10.1021/acsmacrolett.6b00830.

(53) Srivastava, S.; Andreev, M.; Levi, A. E.; Goldfeld, D. J.; Mao, J.; Heller, W. T.; Prabhu, V. M.; De Pablo, J. J.; Tirrell, M. V. Gel Phase Formation in Dilute Triblock Copolyelectrolyte Complexes. *Nat. Commun.* **2017**, *8* (1), 1–9. https://doi.org/10.1038/ncomms14131.

(54) Barteau, K. P.; Wolffs, M.; Lynd, N. A.; Fredrickson, G. H.; Kramer, E. J.; Hawker, C. J. Allyl Glycidyl Ether-Based Polymer Electrolytes for Room Temperature Lithium Batteries. *Macromolecules* **2013**, *46* (22), 8988–8994. https://doi.org/10.1021/ma401267w.

(55) Kadam, V. S.; Nicol, E.; Gaillard, C. Synthesis of Flower-like Poly(Ethylene Oxide) Based Macromolecular Architectures by Photo-Cross-Linking of Block Copolymers Self-Assemblies. *Macromolecules* **2012**, *45* (1), 410–419. https://doi.org/10.1021/ma2022937.

(56) Liu, T.; Zhou, Z.; Wu, C.; Chu, B.; Schneider, D. K.; Nace, V. M. Self-Assembly of Poly(Oxybutylene)-Poly(Oxyethylene)-Poly(Oxybutylene) (B6E46B6) Triblock Copolymer in Aqueous Solution. *J. Phys. Chem. B* **1997**, *101* (43), 8808–8815. https://doi.org/10.1021/jp963810z.

(57) Zhou, Z.; Chu, B.; Nace, V. M.; Yang, Y. W.; Booth, C. Self-Assembly Characteristics of BEB-Type Triblock Copolymers. *Macromolecules* **1996**, *29* (10), 3663–3664. https://doi.org/10.1021/ma960033s.

(58) Yang, J.; Zheng, X.; Zhang, B.; Fu, R.; Chen, X. Intrinsic Fluorescence Studies of Conformational Relaxation and Its Dynamics of Triblock Copolymer during the Micellization in Selective Solvents. *Macromolecules* **2011**, *44* (4), 1026–1033. https://doi.org/10.1021/ma102243u.

(59) Lee, B. F.; Kade, M. J.; Chute, J. A.; Gupta, N.; Campos, L. M.; Fredrickson, G. H.; Kramer, E. J.; Lynd, N. A.; Hawker, C. J. Poly(Allyl Glycidyl Ether)-A Versatile and Functional Polyether Platform. *J. Polym. Sci. Part A Polym. Chem.* **2011**, *49* (20), 4498–4504. https://doi.org/10.1002/pola.24891.

(60) Hrubý, M.; Koňák, Č.; Ulbrich, K. Poly(Allyl Glycidyl Ether)- *Block* - Poly(Ethylene Oxide): A Novel Promising Polymeric Intermediate for the Preparation of Micellar Drug Delivery Systems. *J. Appl. Polym. Sci.* **2005**, *95* (2), 201–211. https://doi.org/10.1002/app.21121.

Chapter 3. CHAIN-END FUNCTIONALIZATION OF F127 POLYMER HYDROGELS

3.1 INTRODUCTION

Stimuli-responsive hydrogels have existed for quite some time and are attractive for applications in drug delivery,[1] injectables,[2] soft actuators,[3] and strain sensors.[4] One strategy to achieve a stimuli-responsive material is through chain-end functionalization of commercial polymers. This method allows for facile modification through use of established chemistry and rapid analysis without requiring extensive planning or optimization of polymerization conditions. For example, poly(ethylene glycol) (PEG) has been used extensively in hydrogels by introducing functional end-groups such as thiols,[5,6] azides,[7] or acrylates[8] for cross-linking or conjugation. However, PEG does not self-assemble in aqueous solution and requires an additional polymer before a network is formed. Another polymer of interest is the triblock copolymer poly(ethylene oxide)-*b*-poly(propylene oxide)-*b*-poly(ethylene oxide) commercially known as F127. This polymer is attractive because it self-assembles in aqueous media between 20-35 wt% without requiring additives. Derivatives of F127 have been presented in the literature such as F127-bis-urethane methacrylate (F127-BUM)[9–15] and F127-diacrylate (F127DA).[16] Both examples are light-responsive to afford a cross-linkable hydrogel, however, the part that is generated is brittle. Additionally, these hydrogels require a high concentration (over 25 wt%) to form gels that are suitable for Direct-Ink-Write (DIW) printing. Therefore, there is room for improvement of the gelation concentration, gelation temperature, and cross-linking by investigating alternative chain-end functionalities.

Among possible end-groups, of note are ionic, physical, and dynamic covalent bonds. Acid or amine chain-ends may alter the assembly behavior by providing an ionic cross-linking point

that is relatively weak and may result in lower yield stress without sacrificing a robust printed construct. Alternatively, incorporating a urea spacer into F127-BUM may provide additional strength in addition to the urethane through hydrogen bonding assembly. Another possibility is through the exploitation of binding affinity in dynamic covalent bonds that relies on an equilibrium to allow for facile breaking points but rapid recovery in self-healing applications.

Herein, we present the functionalization of F127 to generate a series of telechelic polymers and then explore the phase behavior and rheological properties. Among the end-groups studied we looked at ionic, physical, and dynamic covalent bonds, and how these interactions alter the gelation behavior by creating phase diagrams in various solvents and blends. Furthermore, rheology was utilized to investigate the change in stiffness across the polymer formulations. Ultimately the effect was less pronounced than expected and alternative projects were pursued but nonetheless the data presented herein may aid in the design of future polymeric hydrogels.

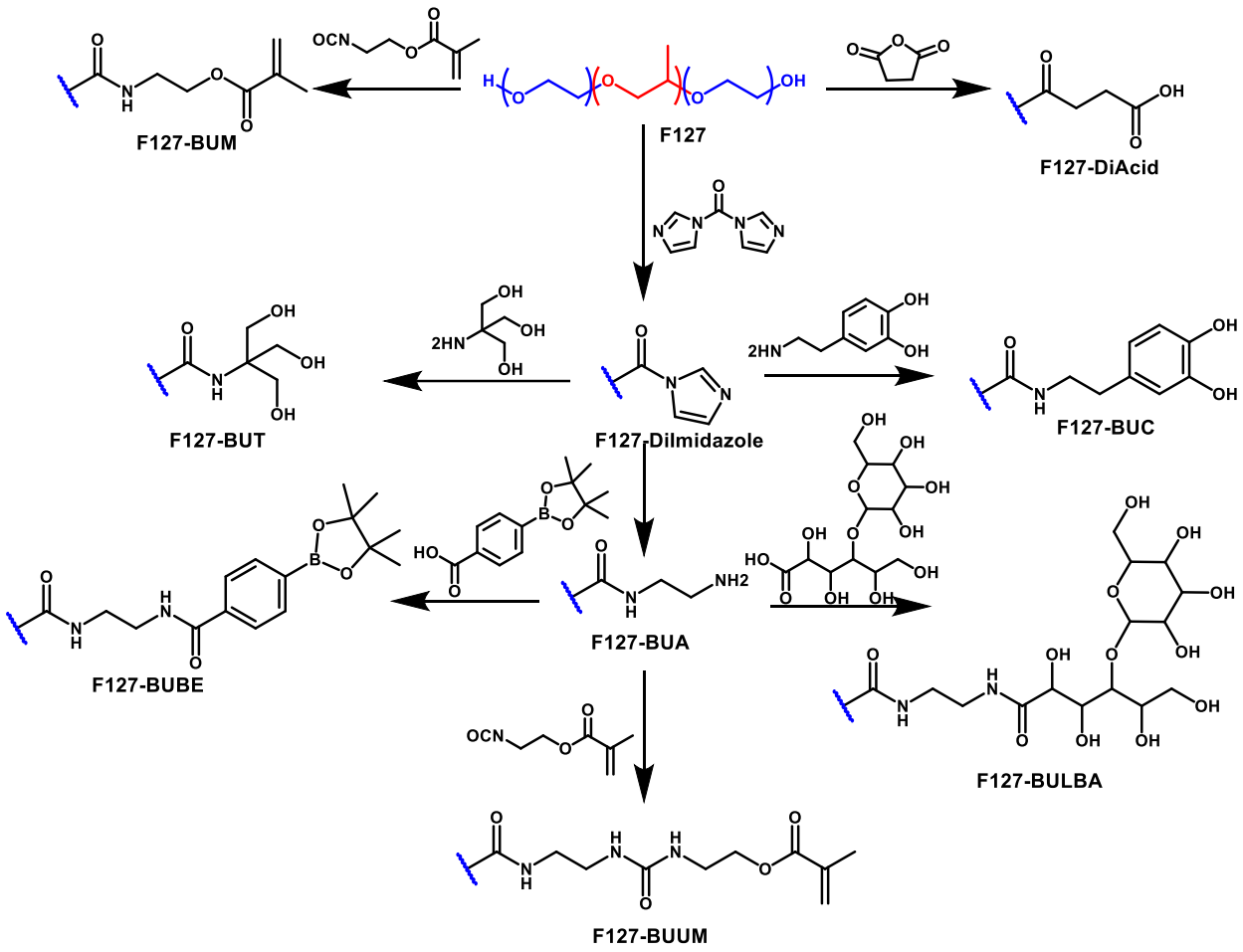

Figure 3.24 Synthetic scheme for the synthesis of telechelic F127 polymers

Abbreviations are as follows: bis-urethane methacrylate (F127-BUM, bis-urethane triol (F127-BUT), bis-urethane catechol (F127-BUC), bis-urethane boronic ester (F127-BUBE), bis-urethane amine (F127-BUA) bis-urethane lactobionic acid (F127-BULBA), and bis-urethane urea methacrylate (F127-BUUM).

3.2 Results and Discussion

Pluronic F127 was functionalized at the chain-end primarily through the activation of the alcohol through either a tin catalyzed isocyanate coupling in the case of F127-Bis-urethane Methacrylate (F127-BUM) or an imidazole intermediate by reacting with carbonyldiimidazole (CDI). From the CDI functionalized polymer, several additional reactions are available to generate

amine, boronic ester, or polyol moieties. The summary of synthetic scope is presented in Figure 3.1.

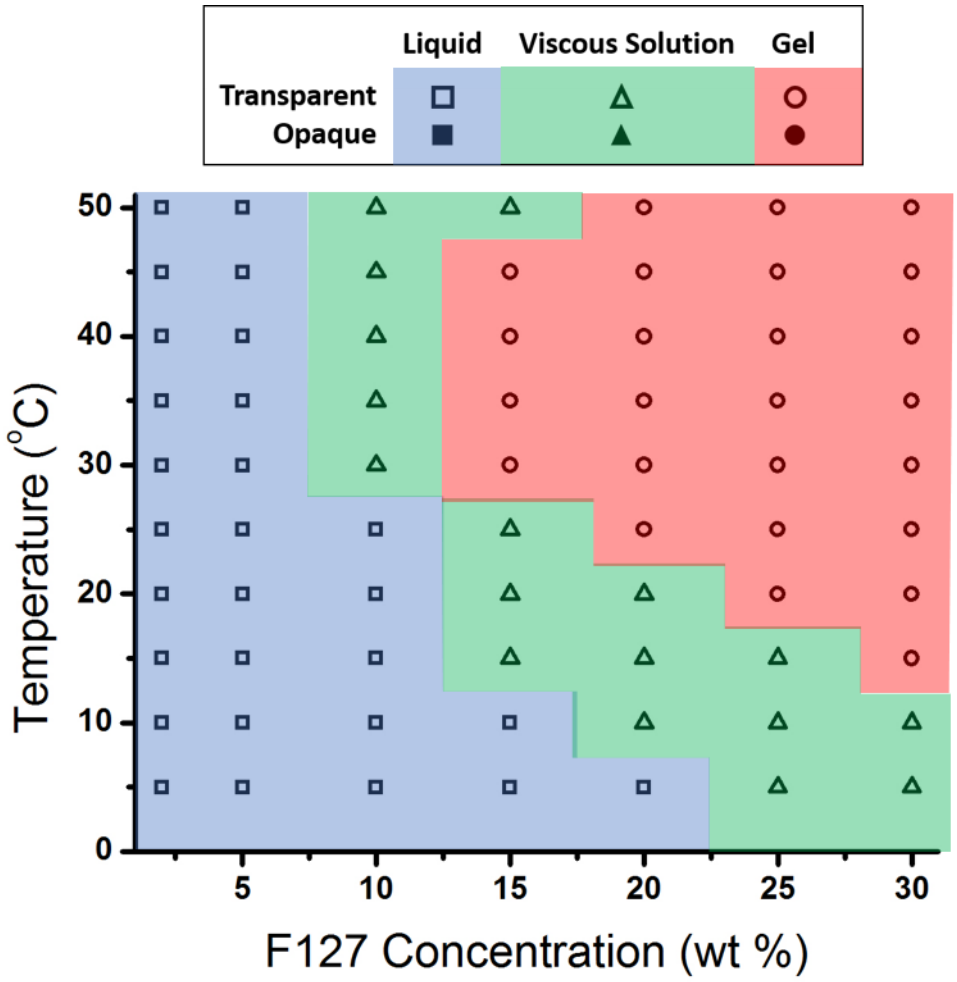

Figure 3.25 Phase diagram of F127 in DI water.

F127 by itself is capable of forming hydrogels at 20-30 wt% and has a gelation temperature (T_{gel}) of around 15-20 °C (Figure 3.2). Early attempts of functionalizing this polymer began with the tin catalyzed isocyanate coupling to achieve F127-Bis-urethane Methacrylate (F127-BUM) with the intention of utilizing the methacrylate end-groups to cross-link the hydrogel network. To determine the influence of the urethane and methacrylate contribution to the assembly behavior, a phase diagram was constructed as is shown in Figure 3.3a. In comparing with native F127, it is

clear that the chain-end functionalization has little effect on the gelation behavior and remains an ideal candidate for extrusion-based printing.

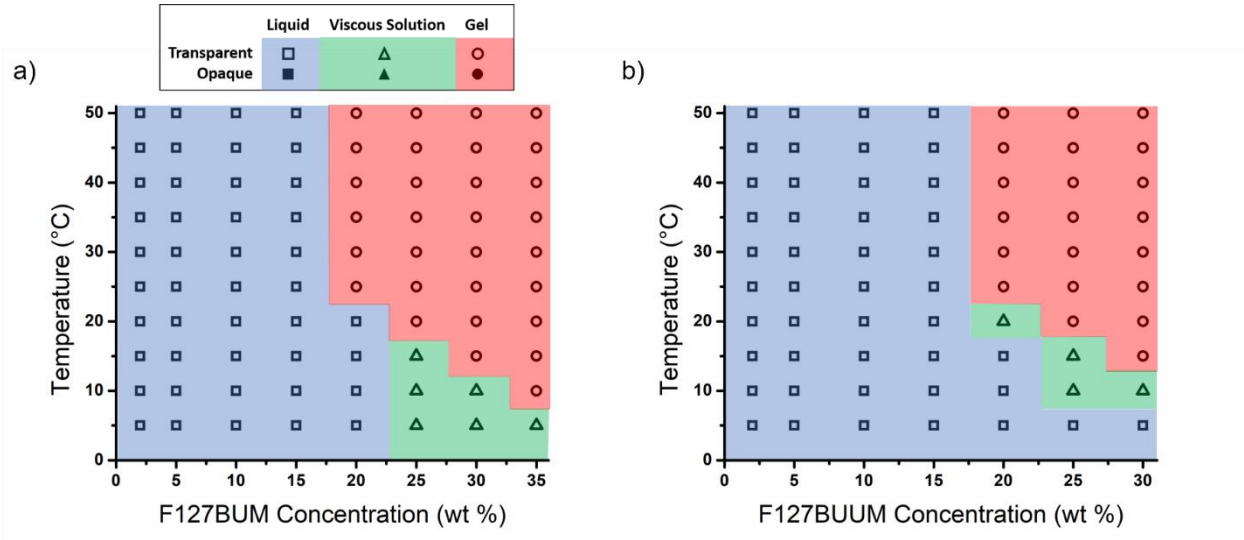

Figure 3.26 Phase diagrams of F127-BUM and F127-BUUM

In exploring methacrylate functionalization of F127 it was hypothesized that including a urea spacer as part of the end-group may influence the self-assembly through hydrogen bond interactions. Therefore, a new synthetic strategy as outlined in Figure 3.1 was developed by functionalizing the chain-ends with CDI to activate the alcohol for a subsequent amide bond formation with ethylene diamine. From here the same isocyanate coupling can be performed without the need for a tin catalyst to achieve F127-Bis-urethane Urea Methacrylate (F127-BUUM). In a similar fashion, a phase diagram was constructed (Figure 3.3b). Again, it is shown that there is little difference between the native F127 and F127-BUUM suggesting that the urea spacer has no effect on the gelation properties of the polymer.

While the gelation was unchanged there was still a question as to whether or not the rheological properties were influenced by the changing end-groups. Figure 3.4 shows the yield stress and viscosity comparisons between F127 and the two methacrylate derivatives. From this data it is clear that the addition of the urea spacer between the urethane and methacrylate portions

contribute to an increased viscosity and a resistance to yielding to applied shear. This led us to the conclusion that F127-BUM was better suited to extrusion-based applications.

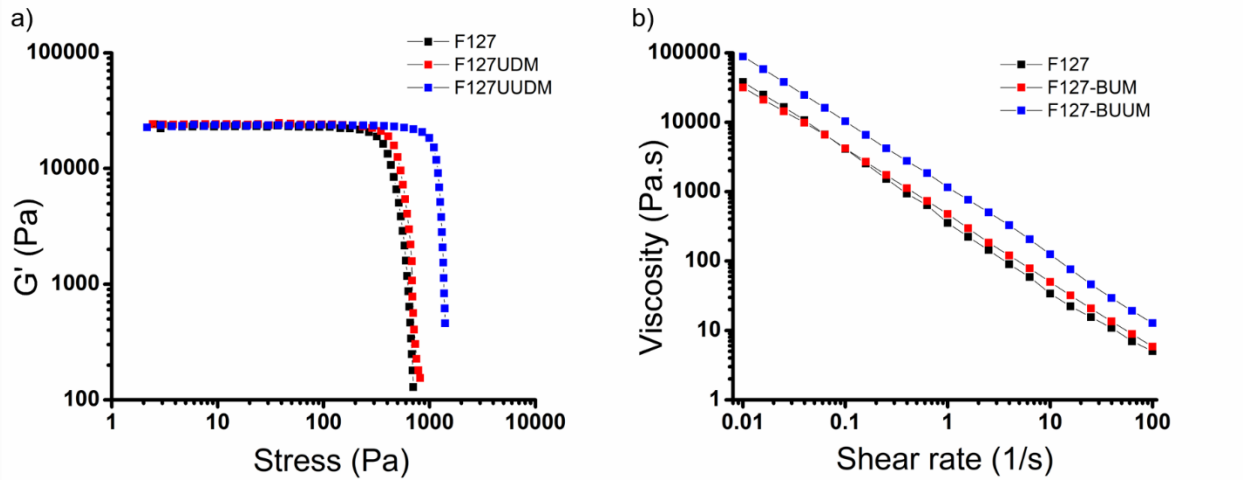

Figure 3.27 Rheology of F127, F127-BUM, and F127-BUUM

Experiments performed at 25 °C in DI water. a) Yield stress showing that the addition of urea into the end-group increases the stress required to break the hydrogel network. b) Viscosity measurements demonstrating that urea also increases the viscosity for all shear rates.

After exploring the physical interactions between urethanes and ureas at the chain-end of F127, there was interest in exploring alternative cross-linking methods between chain-ends by looking at ionic or dynamic covalent linkages. It was hypothesized that by blending F127-Bis-urethane Amine (F127-BUA) with F127-DiAcid in PBS media that the ionic interactions between the carboxylate and ammonium groups would "stick" and therefore lower the required concentrations to induce gelation. The amine chain-ends were synthesized as discussed previously on the route to F127-BUUM but F127-DiAcid was synthesized through the ring opening of succinic anhydride. Phase diagrams are shown in Figure 3.5 and compare F127-BUA and F127-DiAcid by themselves and blended 1:1 in DI and PBS media. As may be expected, the addition of the ionically charged groups slightly reduce the gelation behavior resulting in polymers that are more soluble in water and therefore have a higher T_{gel} than native F127. The blends of F127-BUA and F127-DiAcid in a 1:1 ratio are more interesting in that the hydrogels formulated in PBS offer

a slightly lower gelation temperature than native F127 at 20 wt% but given the propensity for error in these qualitative phase diagrams it is not deemed significant enough for our purposes.

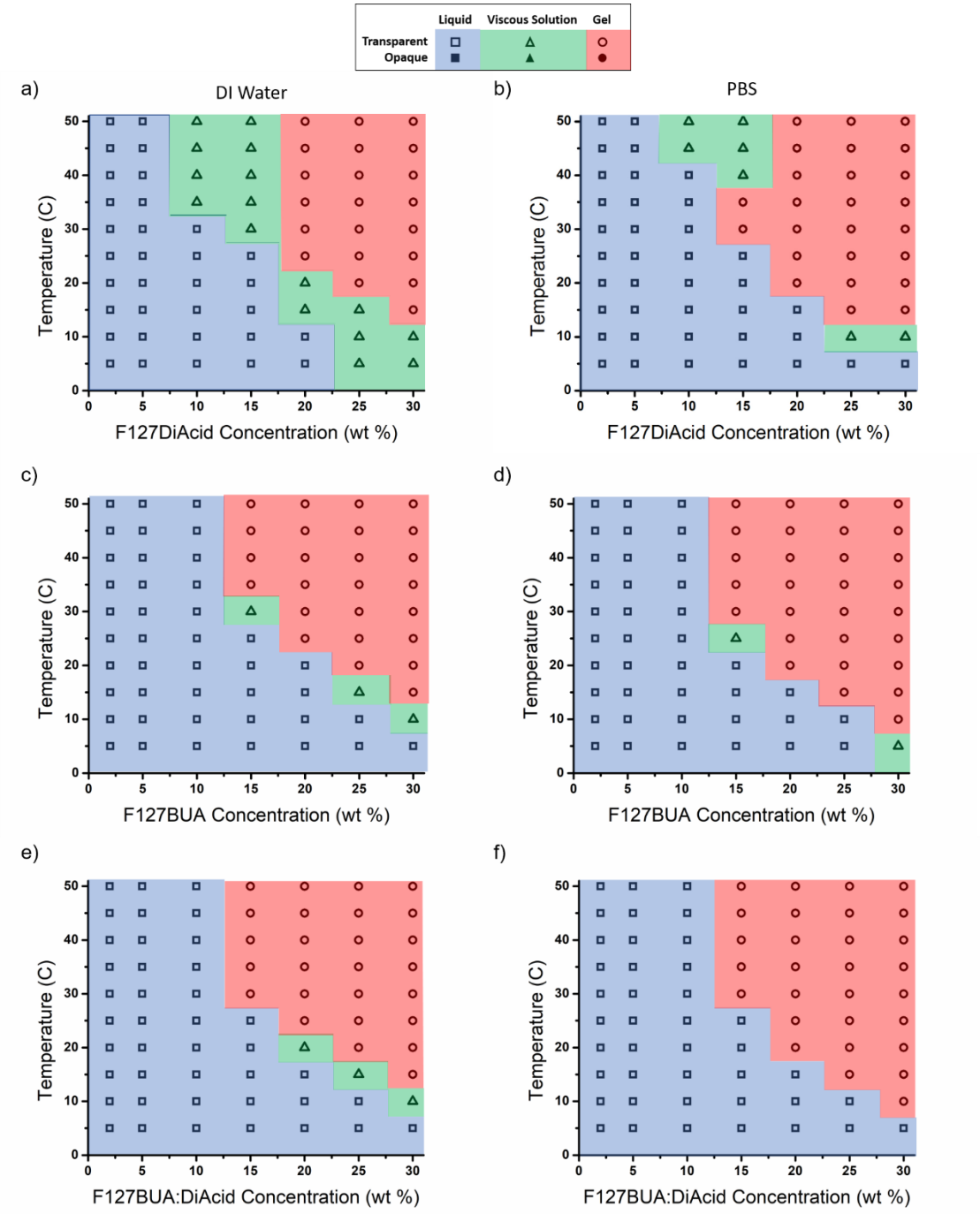

Figure 3.28 Phase diagrams of F127-DiAcid and F127-BUA

Phase diagrams on the left correspond to hydrogels formulated in DI water and phase diagrams on the right correspond to hydrogels formulated in 1x PBS.

After the somewhat dissatisfying investigation into the effects of ionic bonding in polymer hydrogel formation next we considered dynamic covalent bonds. While there are many possibilities, we chose boronic acid and polyol binding as there were fewer examples in the literature and the scope of binding included polysaccharides which may improve cell adhesion and viability for our polymeric hydrogel platform. Initial strategies involved the esterification with boc-protected glycine followed by deprotection with trifluoroacetic acid to yield a chain-end amine. While the synthesis was successful, it was discovered that the ester bond was readily cleaved under basic conditions and therefore incompatible with boronate/diol binding requirements. Instead we opted for the synthesis as outlined in Figure 3.1 to generate a urethane instead of an ester which showed greater tolerance to hydrolysis in basic conditions. The chain-end amine allowed for the use of peptide coupling strategies to amidate various carboxylic acids such as phenyl boronic ester and lactobionic acid.

To begin this investigation, first the effect of boronic ester on gelation properties was explored. Initially we thought that deprotection of the pinacol ester was necessary prior to formulating the hydrogels but due to the relatively low binding affinity of pinacol it was hypothesized that a slow exchange would occur. In addition to DI water, the polymer was tested in synthetic complete media (SCM), with the addition of dextran, and with the addition of curdlan (Figure 3.6**)**. From these results there was little effect in DI water and with the addition of 10 wt% dextran, however the polymer seemed to show increased solubility in the SCM. Interestingly, curdlan, a more soluble dextran, when formulated in 0.25 M NaOH solution, reduced the gelation temperature for concentrations of F127-BUBE greater than 20 wt% but had no effect on lower

concentrations. Given the above results it was suggested that F127 functionalized with polyol end groups may improve the binding at the chain-ends and act as cross-links.

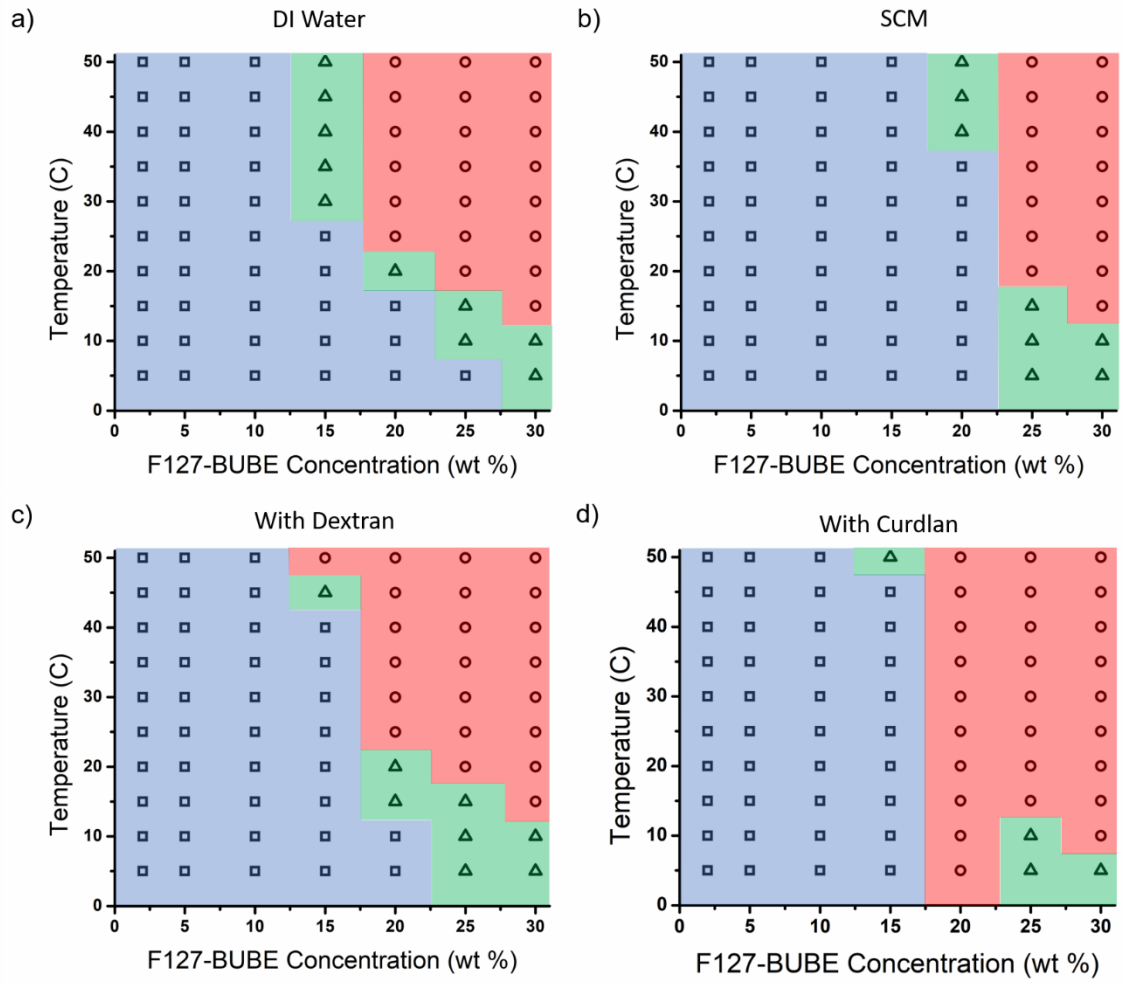

Figure 3.29 Phase diagrams of F127-BUBE in various aqueous media

a) DI water has little effect on the assembly of hydrogel network whereas (b) SCM increases the solubility and requires higher concentrations to form a gel. c) The addition of Dextran (10 wt%) has little effect on the network formation.

With that in mind, a few functional F127 polymers were synthesized, namely those with Tris (F127-Bis-urethane triol, F127-BUT) and lactobionic acid (F127-Bis-urethanelactobionic acid, F127-BULBA) end-groups. A catechol derivative (F127-Bis-urethane catechol, F127-BUC) was also attempted but was unsuccessful due to the oxidation of catechol in basic conditions. While unsatisfying we found there to be little difference between the blends formulated with either F127-

BUT or F127-BULBA in DI water or basic conditions (Figure 3.7). From all of the data described here and in the previous sections, it was determined that attempting to influence the hydrogel's gelation temperature by relying on dynamic covalent bonds in the hydrophilic domain in the presence of an excess of water was a futile effort.

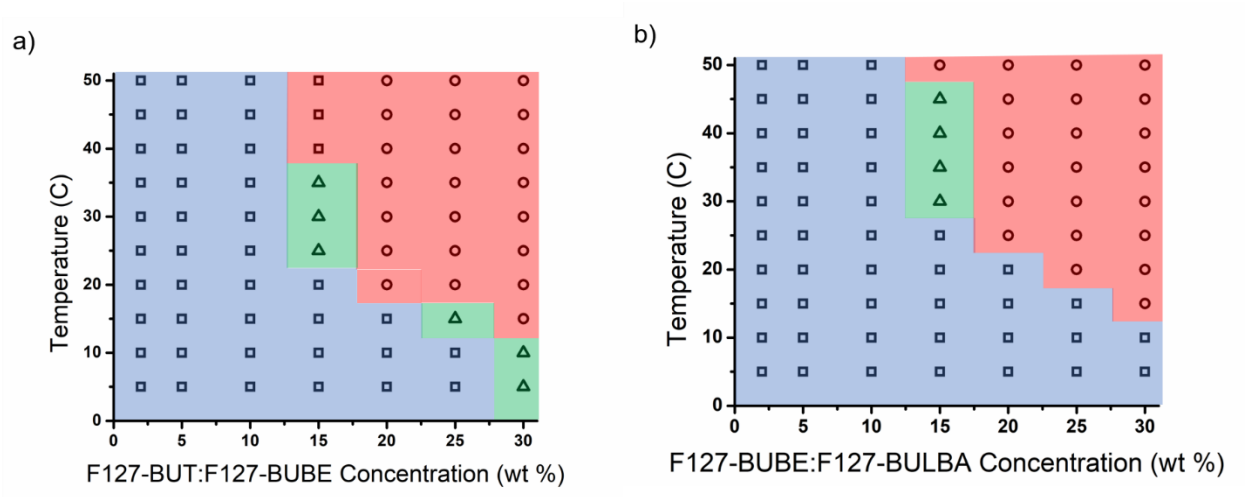

Figure 3.30 Phase diagrams of F127-BUBE blends

a) Blended with F127-BUT and (b) blended with F127-BULBA. Both formulations were blended 1:1 and in pH 10 solution.

While boronic acid binding to diols did not influence the gelation properties of the hydrogel formulations we wanted to explore the rheological properties and determine if any binding was occurring. The primary rheological experiments of interest were that of yield stress and shear-thinning as they give an insight into the shear force required to break physical or covalent cross-links. As can be seen in Figure 3.8, compared to native F127, the formulation with base soluble curdlan or blended with F127-BULBA were the only ones to show an increased yield stress and higher viscosity. Based on the binding affinity for galactose moieties and the number of available diols in curdlan compared to triol this makes sense as the binding affinity is higher for the former

case. However, an increased yield stress and higher viscosity makes it more difficult to extrusion print and therefore these hydrogels are less desirable than native F127 or F127-BUM hydrogels.

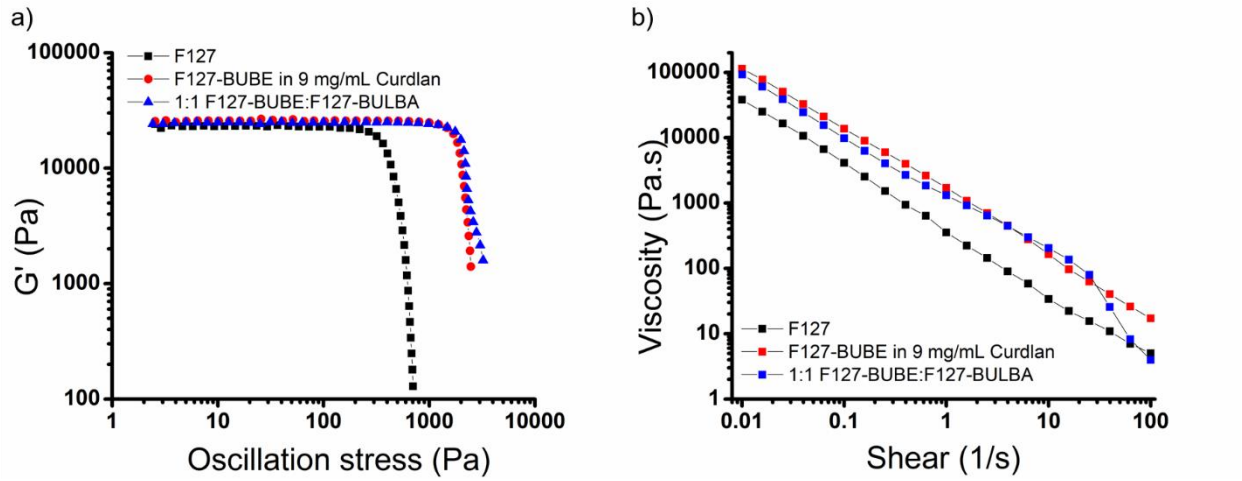

Figure 3.31 Rheology of F127-BUBE blends with F127-BULBA or Curdlan

Curdlan gels were prepared at 9 mg/mL in 0.25 M NaOH solution and F127-BUBE:F127-BULBA blends were mixed in a 1:1 ratio. a) Yield stress showing that the dynamically cross-linked network takes more force to extrude. b) Shear-thinning experiment showing that the dynamically cross-linked network is more viscous at all shear rates, however, the 1:1 mixture of F127-BUBE:F127-BULBA appears to break around 30 1/s.

3.3 CONCLUSIONS

A series of telechelic polymer hydrogels derived from F127 were synthesized and their gelation and rheological properties were explored by qualitative phase diagrams and rheology. Among the polymers tested, F127-BUM was the most promising as a light-responsive hydrogel with minimal interruption of the gelation temperature and yield stress from the original which makes it a great candidate in extrusion-based 3D printing. F127-BUA and DiAcid were preferentially soluble in the aqueous solvent as may be expected and did not show a significant effect of ionic binding in DI or PBS media. Similarly, attempts at utilizing the binding affinity of boronic acid with a series of polyols was met with unsatisfying results as there was little evidence

of effective binding that takes place. Overall, I hope this chapter serves as a useful guide in what not to do if you want to target alternative binding strategies in synthetic polymer hydrogels.

3.4 EXPERIMENTAL

3.4.1 *Materials and Instrumentation*

All chemicals and solvents, unless otherwise stated, were purchased from Sigma-Aldrich or Fisher Scientific and used without further purification unless noted otherwise. Pluronic F127 was dried under reduced pressure overnight prior to functionalization. Dry dichloromethane and tetrahydrofuran was obtained by purification over alumina columns on a Pure Process Technology purification system. 1H NMR spectra were obtained on a Bruker Avance 300 or 500 MHz spectrometer.

3.4.2 *Synthesis of Pluronic F127 Bis-urethane Methacrylate (F127-BUM)*

F127 (60 g, 4.8 mmol) was dried under vacuum, then anhydrous dichloromethane (550 ml) was charged to the flask. The mixture was stirred until complete dissolution of the F127 was observed. The reaction mixture was brought to 30 °C and then dibutyltin dilaurate (12 drops) was added, followed by dropwise addition of 2-isocyanatoethyl methacrylate (3.5 ml, 24.8 mmol) in anhydrous dichloromethane (50 ml). The reaction was allowed to proceed for 2 d before quenching with MeOH. The F127-BUM was precipitated in ether, the precipitate was allowed to settle, and the supernatant was decanted. The F127-BUM precipitate was finally washed in ether twice, dried under ambient conditions and then dried under vacuum.

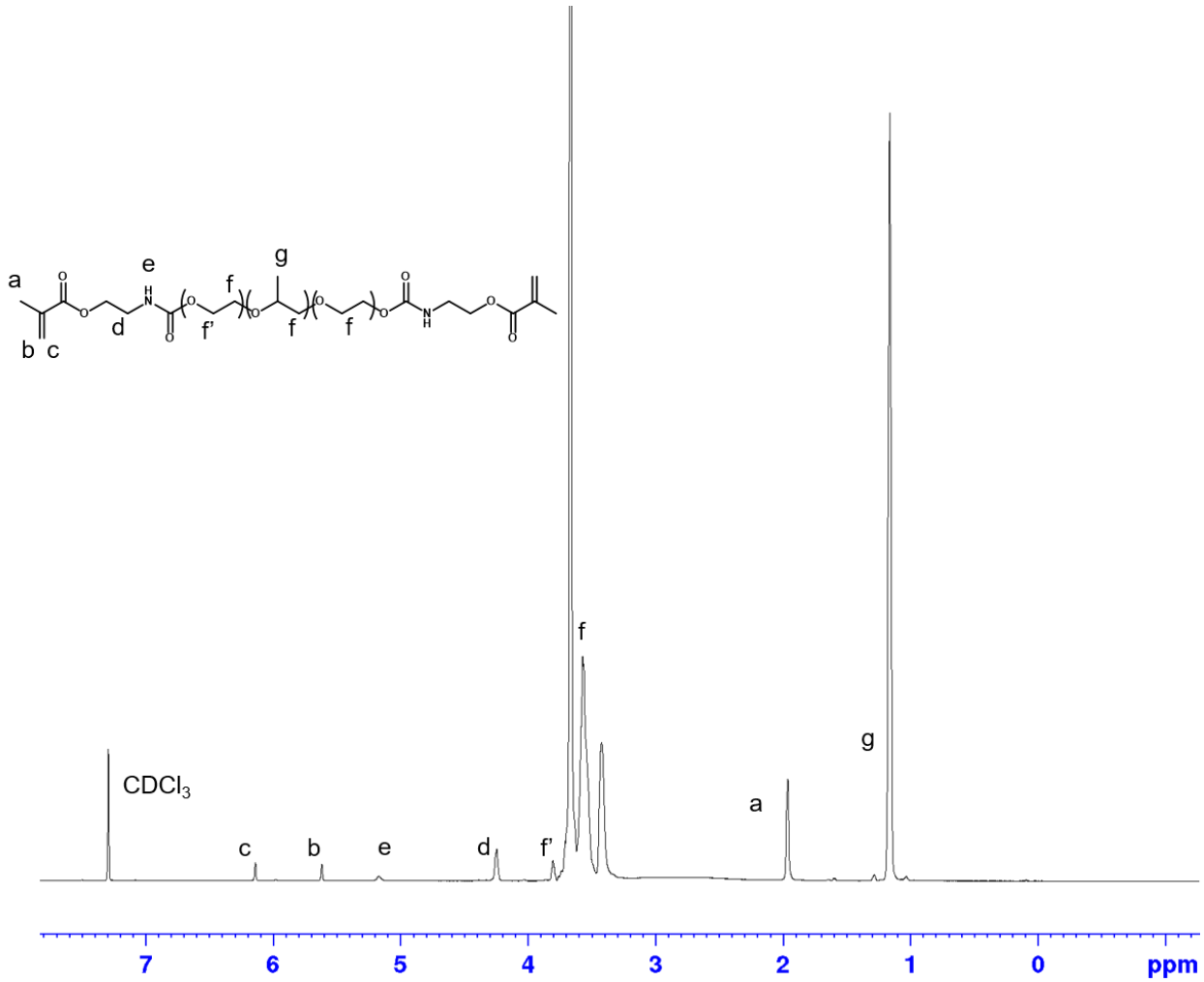

Figure 3.32 ^{1}H NMR spectrum of F127-BUM (500 MHz, 293 K, $CDCl_3$)

3.4.3 *Synthesis of Pluronic F127 DiAcid*

F127 (10 g, 0.8 mmol) was dissolved THF (80 mL) and brought to 50 °C until the polymer was fully dissolved. TEA (285.5 µL, 2 mmol) was added followed by succinic anhydride (820 mg, 8 mmol) dropwise over 45 min. After the addition, the reaction was brought to reflux and run overnight. Water (3 mL) was added to quench the reaction and stirred for an additional hour. The reaction mixture was transferred to a centrifuge tube and spun at 4,400 rpm for 15 minutes. The collected supernatant was combined and concentrated under reduced pressure, redissolved in DCM and extracted with 1M HCl to remove excess reagent. After two additional washes, the DCM layer

was dried with $MgSO_4$, filtered, and concentrated under reduced pressure until viscous. Finally, the polymer was precipitated into diethyl ether, washed twice, and dried under vacuum.

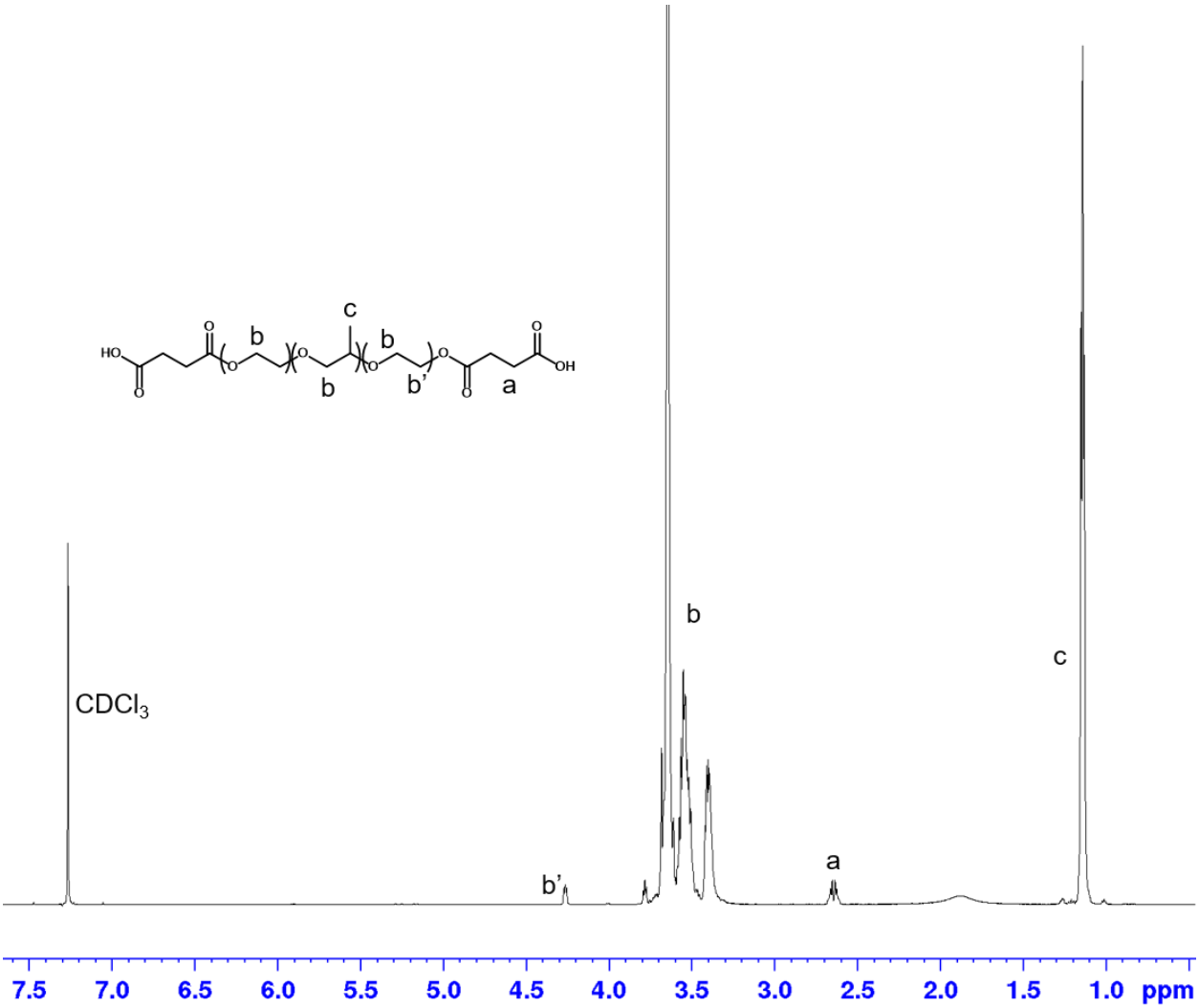

Figure 3.33 ^{1}H NMR spectrum of F127-DiAcid (500 MHz, 293 K, $CDCl_3$)

3.4.4 *Synthesis of Pluronic F127 DiImidazole (F127-DI)*

F127 (20 g, 1.6 mmol) and carbonyldiimidazole (CDI, 2.66 g, 16 mmol) were dissolved in acetonitrile separately (ACN, 100 mL each). The F127/ACN mixture was dropwise added into the CDI/ACN reaction flask over 1 h and was allowed to run for 4 h. The resulting polymer was immediately used in other reactions and was not isolated.

3.4.5 *Synthesis of Pluronic F127 Bis-urethane Triol (F127-BUT)*

F127-DI (10 g, 0.8 mmol) from previous step was used immediately by adding Tris (2 g, 3.2 mmol) and TBAB (5 mg, 0.016 mmol) and allowing the reaction to proceed for 24 h. The reaction mixture was immediately filtered, concentrated under reduced vacuum, and precipitated in diethyl ether. The polymer was dried under ambient conditions and subsequently dialyzed in DI water for 3 d followed by lyophilization to yield a white powder.

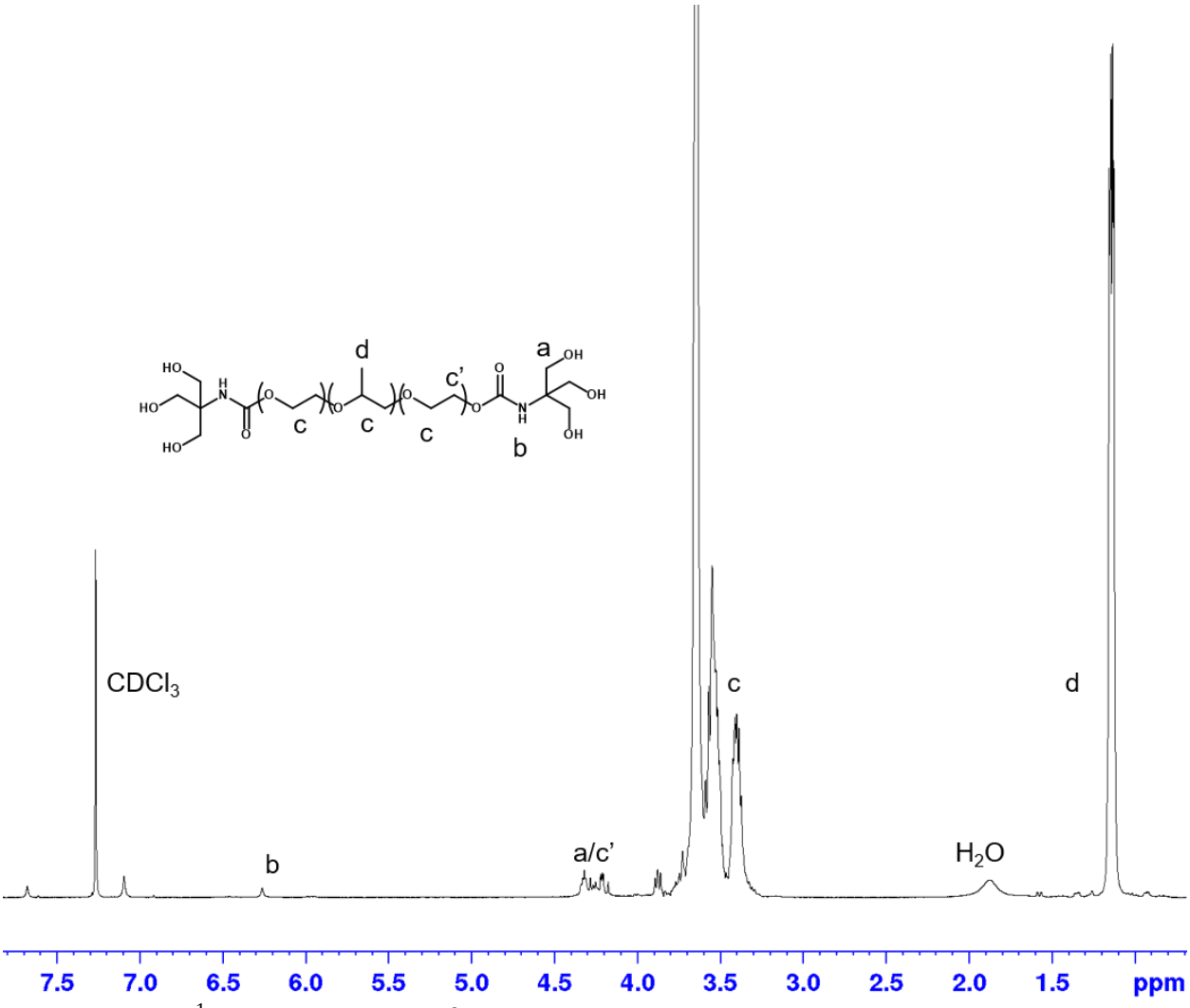

Figure 3.34 ^{1}H NMR spectrum of F127-BUT (500 MHz, 293 K, $CDCl_3$)

3.4.6 *Synthesis of Pluronic F127-Bis urethane Amine (F127-BUA)*

F127-DI (20 g, 1.6 mmol) from previous step was used immediately by adding ethylene diamine (EDA, 16.5 mL, 240 mmol) and allowing the reaction to run overnight. The resulting mixture was filtered, concentrated under reduced vacuum, precipitated into diethyl ether, and washed 3 times. The resulting white polymer was dried under vacuum.

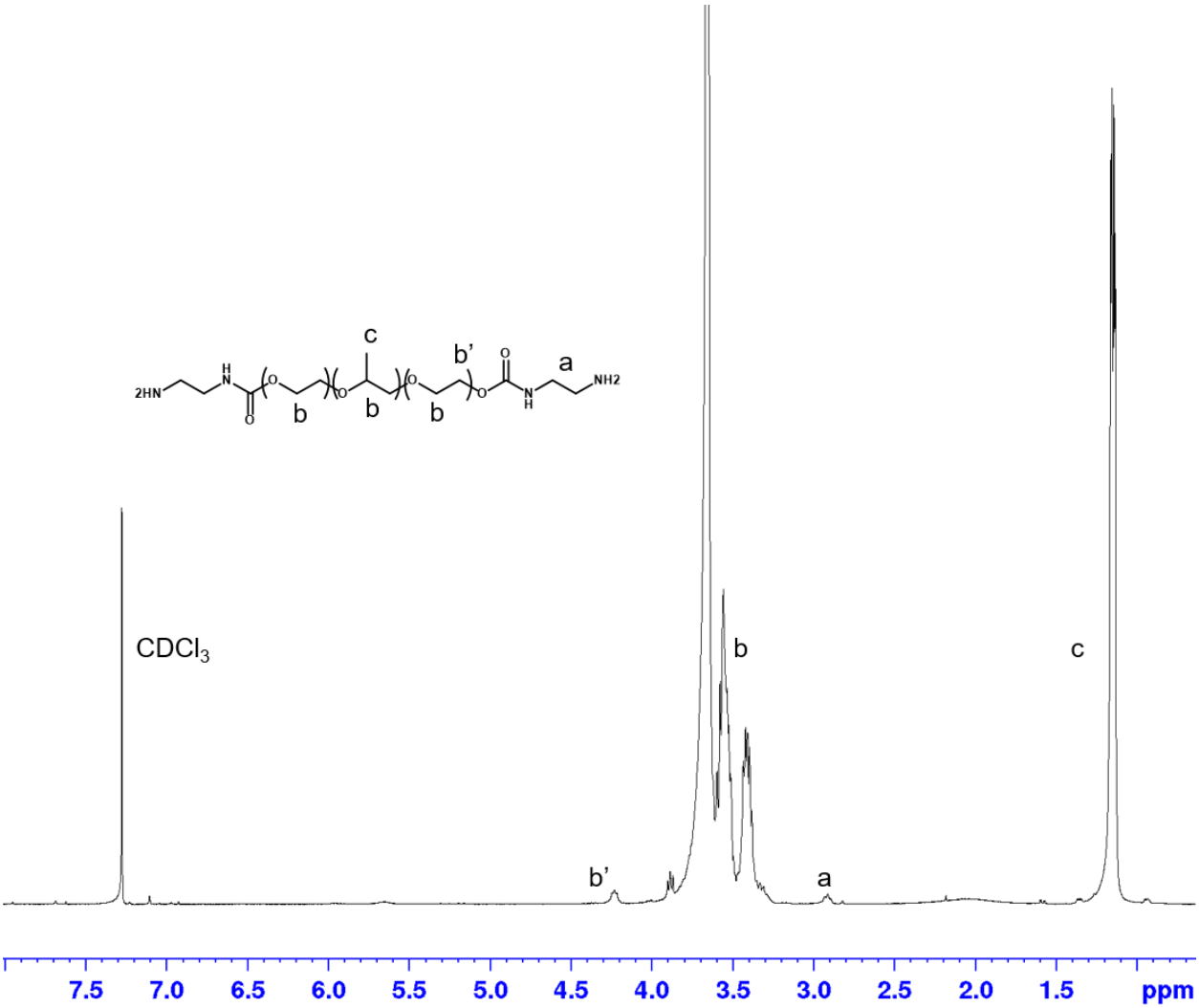

Figure 3.35 ^{1}H NMR spectrum of F127-BUA (500 MHz, 293 K, $CDCl_3$)

3.4.7 *Synthesis of Pluronic F127 Bis-urethane Boronic Acid (F127-BUBA)*

F127-BUA (10 g, 0.8 mmol) from previous step was dissolved in DMF (50 mL) and stirred until completely dissolved. In a separate flask, 4-carboxyphenylboronic acid pinacol ester (CPBE, 437 mg, 1.8 mmol), HATU (852 mg, 2.2 mmol), and DiPEA (697 µL, 4 mmol) were stirred in DMF (50 mL) until dark yellow (30 min). The CPBE mixture was added to the polymer and stirred for 24 h. After the reaction is complete, the solution was concentrated under reduced pressure and precipitated in diethyl ether and dried under vacuum. The polymer was then dissolved in water and dialyzed 3 d and lyophilized to yield a white powder.

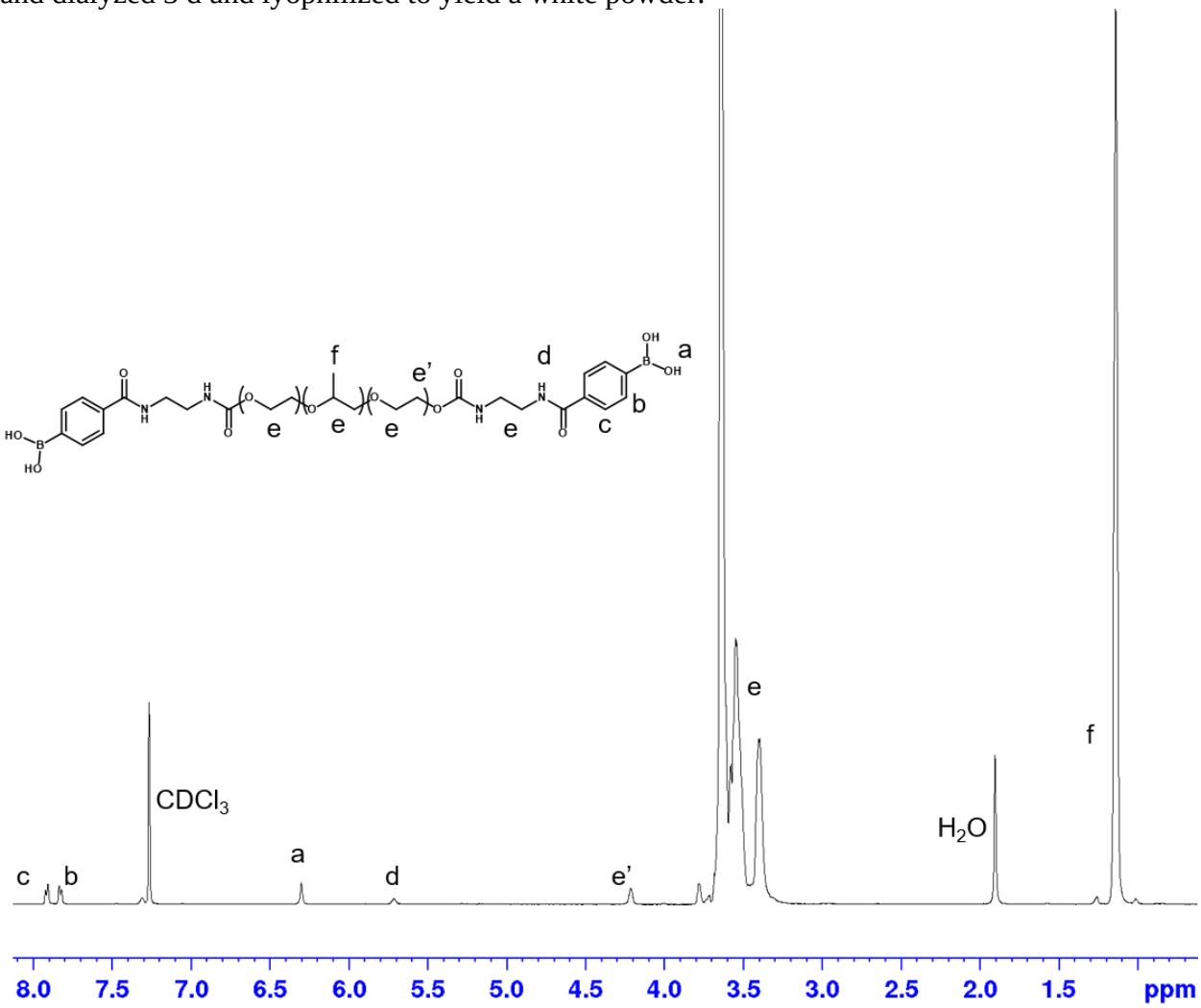

Figure 3.36 ^{1}H NMR spectrum of F127-BUBA (500 MHz, 293 K, $CDCl_3$)

3.4.8 *Synthesis of Pluronic F127 Bis-urethane Urea Methacrylate (F127-BUUM)*

F127-BUA (10 g, 0.8 mmol) was dissolved in DCM (80 mL) and in a separate flask, isocyanatoethyl methacrylate (IEMA, 0.58 µL, 4 mmol) was dissolved in DCM (20 mL) and added dropwise into the polymer mixture over 30 min. The reaction was allowed to proceed at RT overnight and quenched with methanol (10 mL), concentrated under reduced vacuum, precipitated into diethyl ether, washed 2 times and dried under vacuum to obtain a white powder.

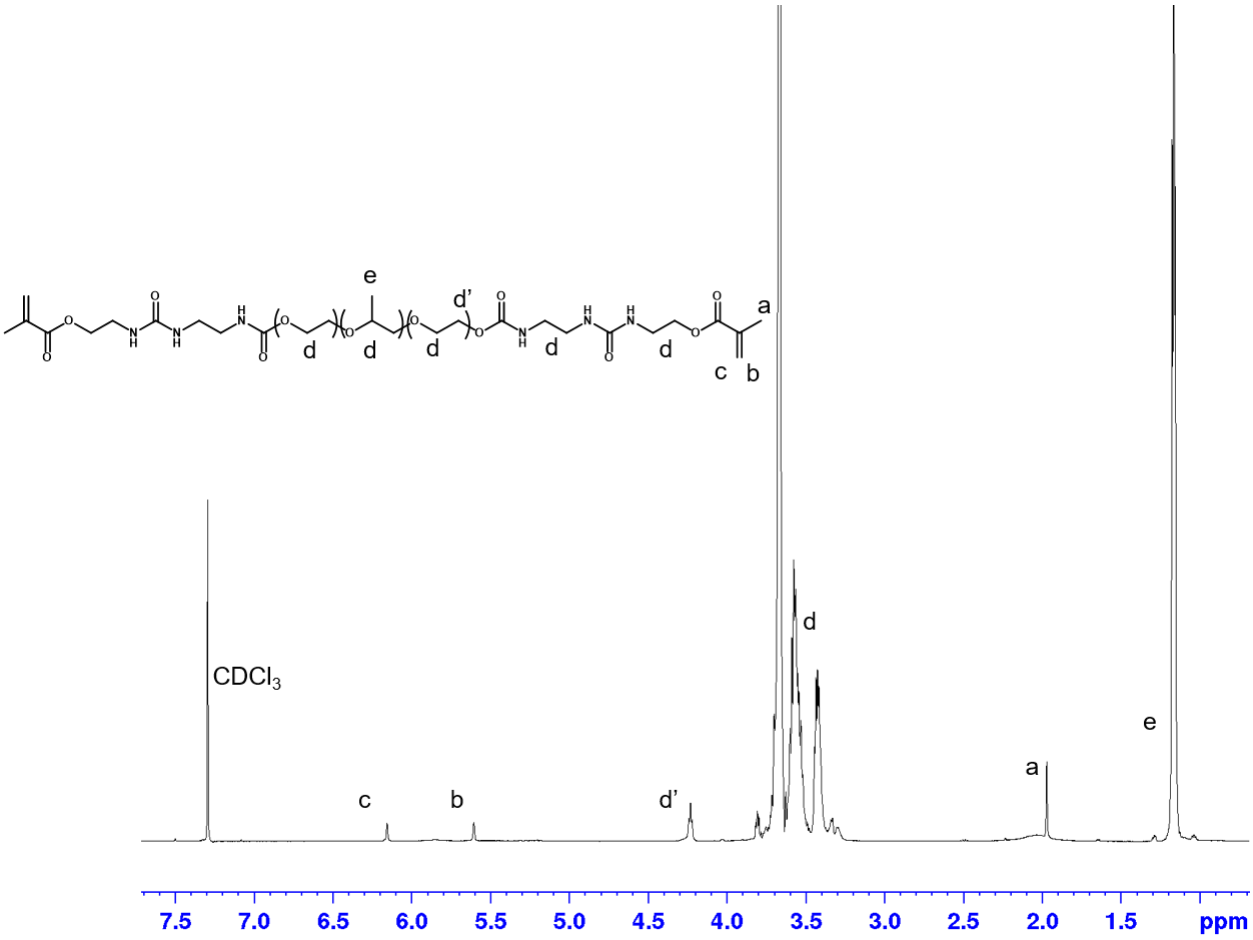

Figure 3.37 ^{1}H NMR spectrum of F127-BUUM (500 MHz, 293 K, $CDCl_3$)

3.4.9 *Synthesis of Pluronic F127 Bis-urethane Lactobionic Acid (F127-BULBA)*

F127-BUA (5 g, 0.4 mmol) was dissolved in DMF (25 mL) and stirred until completely dissolved. In a separate flask, calcium lactobionate hydrate (LBA, 675 mg, 0.9 mmol), HATU (433 mg, 1.1 mmol), and DiPEA (348 µL, 2 mmol) were stirred in DMF (25 mL) until dark yellow (30 min). The LBA mixture was added to the polymer and stirred for 24 h. Once finished, the reaction was filtered, concentrated under reduced vacuum, precipitated in diethyl ether, and dried under vacuum. The dry polymer was dissolved in water and dialyzed for 3 d followed by lyophilization to yield a white powder.

3.4.10 *Phase Diagram Experiments*

Hydrogels were prepared by weighing functionalized F127 (5 mg/ wt%) from 2 to 30 wt% in dram vials. Aqueous media (DI, PBS, SCM, or pH 10) was added to bring the total mass to 200 mg. The 7 vials were then rubber banded together and suspended in a water bath with temperature control. Temperatures below room temperature were regulated by periodically adding ice. Measurements were taken after observing a constant temperature for at least 5 minutes and were obtained by inverting the set of vials and recording which were either free flowing, slow to flow, or a gel. This process was repeated in 5 degree increments from 5 to 50 °C.

3.4.11 *Rheological Experiments.*

Dynamic oscillatory experiments were performed on a TA Instruments Discovery HR-2 equipped with a 20 mm parallel plate geometry. Samples, which were equilibrating in an ice bath for at least 10 minutes, were carefully loaded onto the Peltier plate at 5 °C. A preshear experiment was applied to ensure bubbles were eliminated from the sample cell. The sample was equilibrated at 25 °C for 8 minutes. Strain sweep experiments were performed, and all experiments were conducted using a strain value in the linear viscoelastic regime. Viscosity versus shear rate

experiments were performed with a 20 mm parallel plate geometry at 25 °C. Gel yield strains were measured under oscillatory strain (frequency 1 Hz, 25 °C) starting with an initial strain of 0.01 %.

3.5 REFERENCES

(1) Chatterjee, S.; Hui, P. C. leung. Review of Stimuli-Responsive Polymers in Drug Delivery and Textile Application. *Molecules*. MDPI AG 2019. https://doi.org/10.3390/molecules24142547.

(2) Kondiah, P. J.; Choonara, Y. E.; Kondiah, P. P. D.; Marimuthu, T.; Kumar, P.; Du Toit, L. C.; Pillay, V. A Review of Injectable Polymeric Hydrogel Systems for Application in Bone Tissue Engineering. *Molecules*. MDPI AG November 21, 2016, p 1580. https://doi.org/10.3390/molecules21111580.

(3) Shang, J.; Le, X.; Zhang, J.; Chen, T.; Theato, P. Trends in Polymeric Shape Memory Hydrogels and Hydrogel Actuators. *Polymer Chemistry*. Royal Society of Chemistry March 7, 2019, pp 1036–1055. https://doi.org/10.1039/c8py01286e.

(4) Zhang, D.; Ren, B.; Zhang, Y.; Xu, L.; Huang, Q.; He, Y.; Li, X.; Wu, J.; Yang, J.; Chen, Q.; Chang, Y.; Zheng, J. From Design to Applications of Stimuli-Responsive Hydrogel Strain Sensors. *J. Mater. Chem. B* **2020**, *8* (16), 3171–3191. https://doi.org/10.1039/c9tb02692d.

(5) Yom-Tov, O.; Seliktar, D.; Bianco-Peled, H. PEG-Thiol Based Hydrogels with Controllable Properties. *Eur. Polym. J.* **2016**, *74*, 1–12. https://doi.org/10.1016/j.eurpolymj.2015.11.002.

(6) Rydholm, A. E.; Bowman, C. N.; Anseth, K. S. Degradable Thiol-Acrylate Photopolymers: Polymerization and Degradation Behavior of an in Situ Forming Biomaterial. *Biomaterials* **2005**, *26* (22), 4495–4506. https://doi.org/10.1016/j.biomaterials.2004.11.046.

(7) Zhan, H.; Löwik, D. W. P. M. A Hybrid Peptide Amphiphile Fiber PEG Hydrogel Matrix

for 3D Cell Culture. *Adv. Funct. Mater.* **2019**, *29* (16), 1808505. https://doi.org/10.1002/adfm.201808505.

(8) Moore, E. M.; West, J. L. Bioactive Poly(Ethylene Glycol) Acrylate Hydrogels for Regenerative Engineering. *Regen. Eng. Transl. Med.* **2019**, *5* (2), 167–179. https://doi.org/10.1007/s40883-018-0074-y.

(9) Johnston, T. G.; Yuan, S. F.; Wagner, J. M.; Yi, X.; Saha, A.; Smith, P.; Nelson, A.; Alper, H. S. Compartmentalized Microbes and Co-Cultures in Hydrogels for on-Demand Bioproduction and Preservation. *Nat. Commun.* **2020**, *11* (1), 1–11. https://doi.org/10.1038/s41467-020-14371-4.

(10) Müller, M.; Becher, J.; Schnabelrauch, M.; Zenobi-Wong, M. Nanostructured Pluronic Hydrogels as Bioinks for 3D Bioprinting. *Biofabrication* **2015**, *7* (3), 035006. https://doi.org/10.1088/1758-5090/7/3/035006.

(11) Basu, A.; Saha, A.; Goodman, C.; Shafranek, R. T.; Nelson, A. Catalytically Initiated Gel-in-Gel Printing of Composite Hydrogels. *ACS Appl. Mater. Interfaces* **2017**, *9* (46), 40898–40904. https://doi.org/10.1021/acsami.7b14177.

(12) Smith, P. T.; Basu, A.; Saha, A.; Nelson, A. Chemical Modification and Printability of Shear-Thinning Hydrogel Inks for Direct-Write 3D Printing. *Polymer (Guildf).* **2018**, *152*, 42–50. https://doi.org/10.1016/j.polymer.2018.01.070.

(13) Saha, A.; Johnston, T. G.; Shafranek, R. T.; Goodman, C. J.; Zalatan, J. G.; Storti, D. W.; Ganter, M. A.; Nelson, A. Additive Manufacturing of Catalytically Active Living Materials. *ACS Appl. Mater. Interfaces* **2018**, *10* (16), 13373–13380. https://doi.org/10.1021/acsami.8b02719.

(14) Wong, J.; Gong, A. T.; Defnet, P. A.; Meabe, L.; Beauchamp, B.; Sweet, R. M.; Sardon,

H.; Cobb, C. L.; Nelson, A. 3D Printing Ionogel Auxetic Frameworks for Stretchable Sensors. *Adv. Mater. Technol.* **2019**, *4* (9), 1900452. https://doi.org/10.1002/admt.201900452.

(15) Millik, S. C.; Dostie, A. M.; Karis, D. G.; Smith, P. T.; McKenna, M.; Chan, N.; Curtis, C. D.; Nance, E.; Theberge, A. B.; Nelson, A. 3D Printed Coaxial Nozzles for the Extrusion of Hydrogel Tubes toward Modeling Vascular Endothelium. *Biofabrication* **2019**, *11* (4), 045009. https://doi.org/10.1088/1758-5090/ab2b4d.

(16) Yan, B.; Zhou, H.; Lai, J.; Wang, Z.; Luo, C.; Liu, H.; Jin, X.; Ma, A.; Chen, W. Pluronic F127 Gels Fabricated by Thiol–Ene Click Chemistry: Preparation, Gelation Dynamics, Swelling Behaviors and Mechanical Properties. *Polym. Bull.* **2019**, *76* (12), 6049–6061. https://doi.org/10.1007/s00289-019-02696-0.

Chapter 4. TIME-DEPENDENT POLYMER NETWORK FORMATION IN EXTRUDABLE HYDROGELS

4.1 ABSTRACT

The fabrication of hydrogel materials has gained increased attention for a broad range of biomedical and biotechnological applications. However, one longstanding challenge in the field is to develop hydrogels that can be easily processed into the desired form factor, while achieving the necessary final physical and biochemical properties. Herein, we report a shear-thinning hydrogel ink that can be photo-cured to create a stretchable, suturable hydrogel whose polymer network is formed via the combination of thiol-Michael addition and radical polymerization. A shear-thinning hydrogel based on bis-methacrylated Pluronic® F-127 was modified with varying equivalents of 2,2'-(ethylenedioxy)diethanethiol (EDT) as an additive. We observed that aging the hydrogel over time prior to extrusion allowed the relatively slow thiol-Michael addition to occur (between thiol and methacrylate) prior to UV initiated photopolymerization of the methacrylates. The viscoelastic properties of these hydrogels could be tuned based on the amount of EDT added, and the aging time of the hydrogel formulation. The changes to the physical properties of the hydrogels were attributed to the increased chain length between network junctions that resulted from the thiol-Michael addition reactions. The optimized hydrogel composition was then extruded from a coaxial nozzle to produce hydrogel tubes that, after curing, were resistant to tearing and were suturable. These extrudable synthetic hydrogels with tunable viscoelastic properties are promising for tissue engineering applications and as surgical training models for human vasculature.

4.2 INTRODUCTION

Hydrogels are an important class of material due to their widespread use in biomedical applications such as tissue engineering,[1-13] surgical training models,[14,15] and implantable devices.[14,16–19] Synthetic polymer hydrogels are advantageous over naturally derived hydrogels (such as calcium alginate and gelatin) because they afford materials that can be more specifically tailored to mimic biological materials like human tissue.[20–22] However, one longstanding challenge in the field is to develop hydrogels that can be easily processed into the desired form factor, while achieving the necessary final physical and biochemical properties. Shear-thinning hydrogels[23,24] have shear-dependent viscoelastic behaviors that can facilitate the processing of these materials, and are particularly well-suited as injectable hydrogels for subdermal drug delivery[25–27] and for direct ink write 3D printing.[28–30] These hydrogels can be mechanically or pneumatically pressurized to flow from a syringe, and can quickly recover its gel state via the reformation of reversible covalent or noncovalent bonds upon exiting the nozzle.[31,32] Strategies for designing shear-thinning hydrogels have included incorporation of cyclodextrin to enable host-guest supramolecular interactions,[28] protein directed assembly,[33] and control of block copolymer architectures.[34–36]

Poly(ethylene oxide)-*b*-poly(propylene oxide)-*b*-poly(ethylene oxide) is a triblock copolymer that self-assembles into micelles in water to afford shear-thinning hydrogels. Our group,[29,37–41] and others,[42,43] have used a commercially available form of this polymer known as F127, and the cross-linkable F127-bisurethane methacrylate (F127-BUM) derivative, to afford extrudable hydrogel inks for creating 3D constructs. In a recent example, we extruded hydrogel tubes toward modeling vascular endothelium using customized coaxial nozzles.[38] The nozzles were modeled via computer-aided design and then 3D printed on a commercially available SLA

printer to generate coaxial nozzles with different orifice geometries and dimensions. While the lumen of these tubular hydrogel constructs could be endothelialized with human umbilical vein endothelial cells, the hydrogels were still limited by their brittleness, particularly to needle puncture during suture. Thus, chemical strategies that provide the processability of hydrogels via shear-thinning behavior, but with improved mechanical properties after curing the hydrogels are desirable for engineering *in vitro* models that resemble tubular biological structures (such as blood vessels, airways, and the intestines).

Thiol-Michael "click" chemistry presents an important class of reactions for macromolecular systems[44–46] that has been utilized in bioconjugation reactions,[47–49] the formation of graft polymer architectures,[50,51] and network formation in polymer hydrogels.[11,52–56] The thiol-Michael addition takes place between a free thiol and α,β-unsaturated ester and may be catalyzed by base, or phosphorus and nitrogen centered nucleophiles.[57] As demonstrated in a computational study by Northrop and Coffey, methacrylates are generally less reactive than acrylates, ally ethers, and maleimides in thiol-Michael reactions.[58] Bowman and co-workers experimentally verified this difference in reactivity by using a photobase and show slow addition of thiols onto butyl methacrylate.[59] Additionally, thiols and alkenes can undergo photoradical thiol-Michael reactions. Bunel and co-workers showed that under photoradical conditions, methacrylate homopolymerization was favored over photoradical thiol-Michael addition.[60]

Recently, Long and co-workers showed that the combination of free-radical polymerization with thiol-Michael "click" chemistry could be utilized to afford poly(dimethylsiloxane)-based (PDMS-based) silicones. The chain-ends of PDMS were functionalized with acrylamides or thiols to afford resins that varied in the ratio of thiol to acrylamide. The polymerized network showed a tunable stretchability and Young's modulus that

was dependent upon the extent of thiol-Michael chain-extension between chain-end acrylamide and thiols, versus the free-radical polymerization of the chain-end acrylamides.[61] The Smaldone group has also demonstrated base-catalyzed thiol-Michael addition of a three-arm thiol onto acrylate-functionalized F127. In this work, the concentration of base determined the cross-link density of the final printed construct.[62] Additionally, Anseth and co-workers demonstrated the importance of aging in gels formulated with thiols. Their group used a four-arm thiol and diacrylated PEG to show a time-dependent thiol-Michael addition, which forms the preliminary polymer network before a subsequent UV cure further cross-links the material.[63]

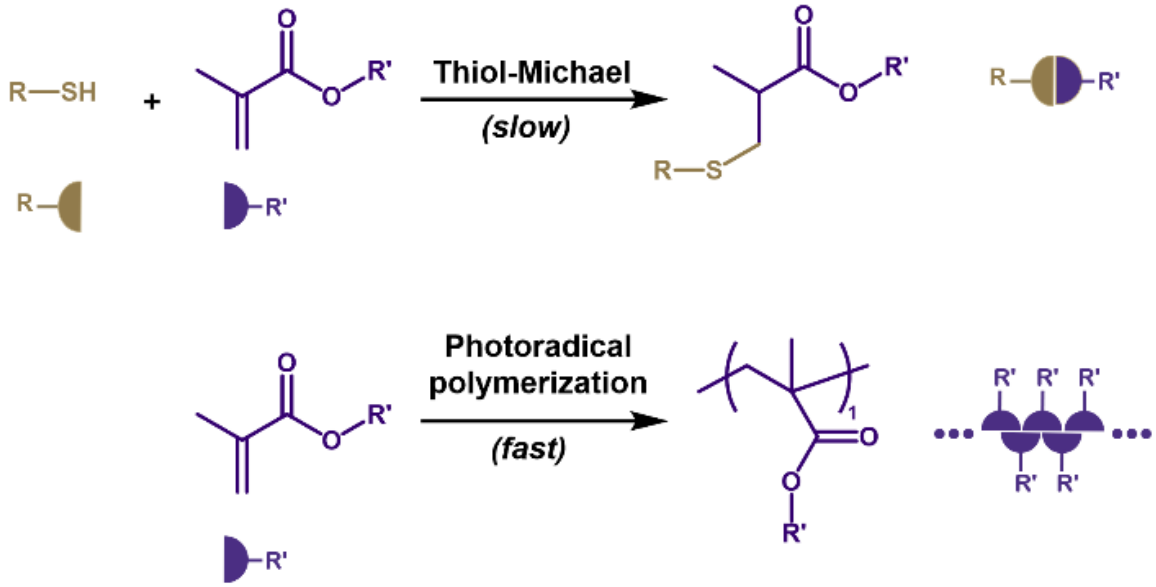

Figure 4.38 The scope of reactions available between thiols and methacrylates.

A slow thiol-Michael reaction takes place spontaneously while introduction of lithium phenyl-2,4,6-trimethylbenzoylphosphinate (LAP) photoinitiator and 365 nm light enables fast photoradical mediated polymerization.

Herein, we report a shear-thinning hydrogel ink that can be photo-cured to create a stretchable, suturable hydrogel whose polymer network is formed via the combination of thiol-Michael addition and radical polymerization. The introduction of a dithiol additive into the F127-

BUM hydrogel was employed to introduce two different covalent bond-forming reactions: the radical polymerization of the methacrylate chain-ends cross-links the polymer network, while the thiol-Michael coupling reaction of the F127 polymer chains with a dithiol additive could effectively increase the molecular weight of the polymer chains between cross-linking sites (Figure 4.1). As a result, the mechanical properties of the hydrogels were dependent upon the contribution of the thiol-Michael addition versus the radical polymerization to the formation of the final network. Although the thiol-Michael addition between thiols and methacrylates is slow, the hydrogel ink can be aged over time to allow the reaction to occur prior to the UV-initiated radical polymerization of the methacrylate end-groups. The hydrogel inks were extruded using a coaxial nozzle to create tubular constructs that were UV-cured to afford suturable hydrogels, which could have future use as models for vascular tissue.

4.3 Results and Discussion

F127-BUM affords shear-thinning hydrogels at concentrations above ~20 w/w %, even in the presence of water-soluble additives.[29] In this investigation, 2,2'-(ethylenedioxy) diethanethiol (EDT) was introduced as an additive to 30 w/w % F127-BUM hydrogel formulations (with 0.1 wt% LAP as photo-initiator) (Figure 4.2) at 0, 0.5, 1.0, 1.5, or 2.0 molar equivalents relative to the polymer. Rheological characterization of these hydrogels confirmed the shear-thinning behavior of all the hydrogels (Figure 4.14-17**)**. Figure 4.1 shows the reactions by which covalent networks can be formed. Thiols can spontaneously react with methacrylates at a slow rate under ambient conditions and neutral pH (in the absence of UV light). This reaction results in a chain-extension that couples F127-BUM polymer chains to form longer bridging chains between points of cross-linking in the network. Photoinitiated radical polymerization of the methacrylate end-groups can also

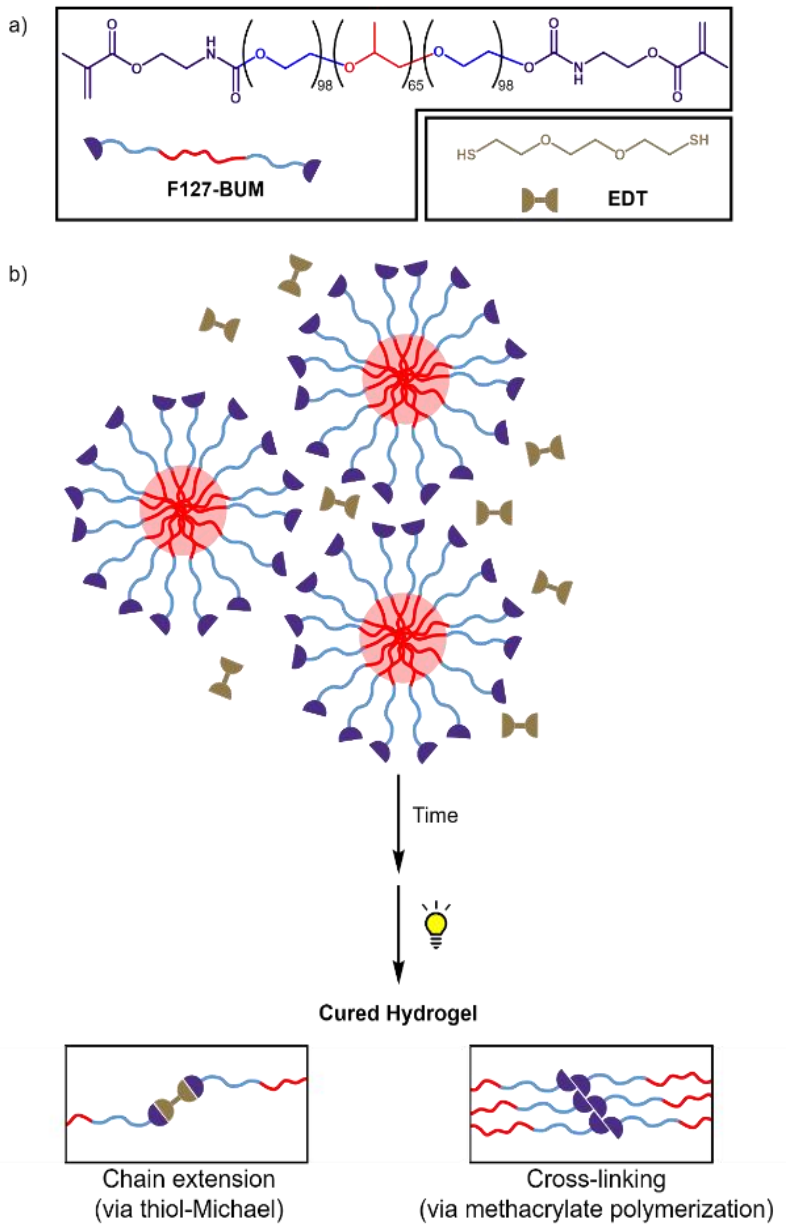

Figure 4.39 Materials used in this work and cartoon describing chain-extension and photoradical cross-linking

a) Materials used in this work. F127 is functionalized with urethane methacrylate end-groups (F127-BUM). At temperatures above the gelation temperature (T_{gel}) and in concentrations greater than 20 wt%, F127-BUM forms core-shell micelles that affords a hydrogel network. 2,2'-(ethylenedioxy)diethane thiol (EDT) was chosen because of its water solubility and commercial availability. b) An F127-BUM hydrogel formulated with EDT slowly undergoes thiol-Michael chain-extension. A UV cure after a set period of ageing affords tunability in the extent of cross-linking by radical polymerization.

occur rapidly and introduces crosslinking sites into the network. As shown in Figure 4.2, the final polymer network is comprised of both physical cross-links (the assembled poly(propylene oxide) blocks of the self-assembled micelle core) and chemical cross-links (the polymerized methacrylate chain-ends) that are separated by the bridging polymer chains.

F127-BUM hydrogels that are chemically cross-linked in the absence of EDT exhibit elasticity, and brittle fracture upon failure. Inspired by recent publications on 3D printed elastomers,[61,64] we hypothesized that increasing the length of the bridging F127-BUM chains via thiol-Michael addition could lead to hydrogel networks tunable stiffness and stretchability. As a method of characterizing hydrogel networks, the affine network theory of unentangled rubber elasticity[65] is a useful tool to help probe the effects of cross-link junctions. This model assumes that the cross-link points between each strand is representative of the entire network and may estimate the molecular weight between cross-link junctions through uniaxial deformation written in terms of the shear modulus. F127 is known to create hydrogel networks by the aggregation of micelles packing into a face-centered cubic (fcc) lattice at concentrations above 20 wt% in aqueous media and above its gelation temperature (T_{gel}).[66] This model does not take into account defects such as loops or dangling ends and may not be representative of a highly entangled micellar network such as F127. Nonetheless, many groups have shown that this is an appropriate model for this type of investigation.[61,67–69] Equation (1) allows us to approximate the molecular weight between cross-links (M_c) by using rheometry to determine the average plateau storage modulus (G_N^0).

$$M_c = \frac{dRT}{G_N^0} \quad (1)$$

Where d is density, T is temperature, and R is the universal gas constant.

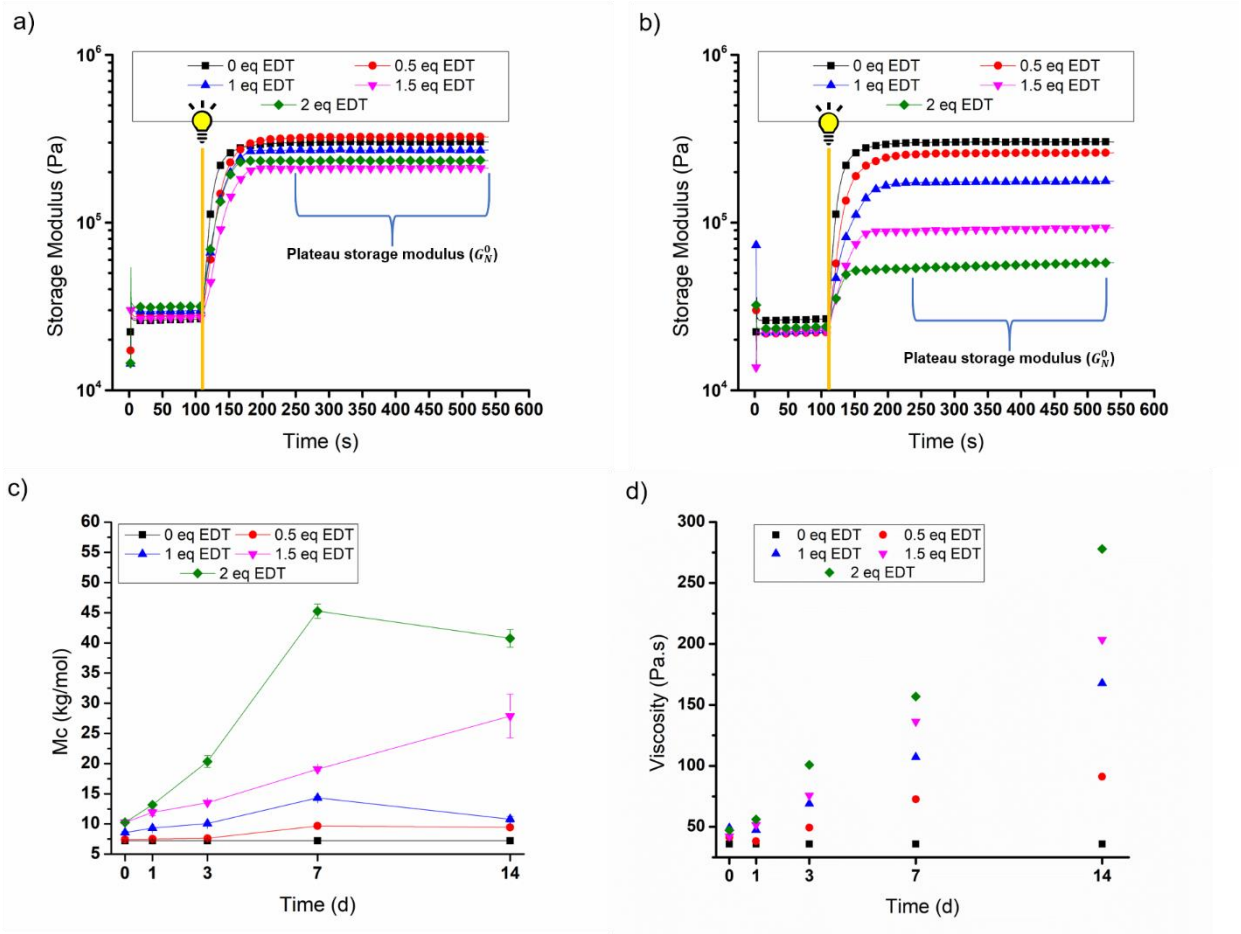

Figure 4.40 Photorheological characterization of 30 wt% F127-BUM hydrogel with varying equivalents of EDT

After (a) 0 and and (b) 7 days of equilibration. At 120 s, the UV light was turned on and left on for the remainder of the experiment. The plateau storage modulus was taken as the average storage modulus in the region between 250 and 550 s. (c) Molecular weight between cross-links (M_c) as calculated from equation (1). A linear increase was shown for 1 to 2 equivalents EDT in the first 7 days. (d) Viscosity measurements taken at 10 s^{-1} at 21 °C. Apart from unmodified F127-BUM, each formulation shows a linear increase in viscosity over time, which suggests an increase in molecular weight prior to UV cure.

The shear moduli of all hydrogel formulations were determined using a photo-rheometer in which the samples were exposed to 365 nm light and the viscoelastic

properties monitored over that time. Given the slow kinetics of thiol-Michael addition in reactions that involve methacrylates in the absence of any catalyst, each hydrogel formulation was characterized over the course of 14 days.

The thiol-Michael reaction (slow rate of reaction) and photo-initiated radical polymerization (fast rate of reaction) occurred during two discrete steps. Upon addition of EDT to each hydrogel formulation the thiols can undergo a spontaneous thiol-Michael addition to extend the polymer chains. After a predetermined period of time (on the order of days) the photopolymerization of the methacrylates was initiated upon UV exposure during the photo-rheology experiment. Representative examples of the photo-rheological experiments from days 0 and 7 are shown in Figure 4.3a,b. Upon UV irradiation (365 nm, 5 mW cm^{-2}) the storage modulus rapidly increased within 2 min to a plateau storage modulus (G_N^0). Initially (at day 0), the (G_N^0) for the hydrogels were similar, independent of the quantity of EDT that was added. In this case, the thiol-Michael reactions were too slow to enable sufficient incorporation of EDT into the polymer network. However, as we increased the time (day 3 and beyond) for the thiol-Michael reaction to occur prior to photo-initiated polymerization, larger differences were observed based on the molar equivalents of EDT (Figure 4.3a,b). For example, in the case of the samples that were incubated for 7 days prior to photo-initiated polymerization, as the molar equivalents of EDT in the hydrogel formulation was increased, the G_N^0 for that hydrogel decreased. Thus, while the F127-BUM hydrogel had a G_N^0 of 347 kPa, the hydrogel formulation with highest amount of EDT (2 molar equivalents) in this study exhibited a decreased stiffness (55 kPa). We attribute this trend to the increase in length of the polymer chains (the total length of bridging chains increase as F127 polymer chains are coupled together via thiol-Michael

addition reactions) relative to free-radical polymerization of the methacrylates as the thiol:alkene ratio increased.

The relative stiffness between the different formulations can be used to determine the molecular weight between cross-links (M_c) by using a calculation derived from the affine theory of rubber elasticity (equation 1). The number average molecular weight for F127-BUM is 12.5 kg/mol, which corresponded well to the values obtained using the affine model for day 0 and day 1 (Figure 3c). During these earlier time periods, there was not a significant change to the molecular weight (8-12 kg/mol) independent of the amount of EDT that was added. The slow kinetics of the thiol-Michael reaction meant that there was negligible chain extension. However, M_c increased over time (see days 3, 7, and 14 in Figure 4.10-12) when 1.5 equivalents or 2.0 equivalents of EDT was included in the formulation. Thus, there was chain extension via bridging thiol-Michael addition over time.

Further support for thiol-Michael addition prior to UV curing was provided by rheometrical evaluation of the changes in the viscosity of the hydrogels (Figure 4.3d). During the early time periods, there was little variation in the viscosity of the hydrogel. However, after 3 days, the viscosity began to deviate from 49 to 100 Pa·s and continued to increase linearly over 14 days to 91 and 278 Pa·s for 0.5 and 2 equivalents, respectively. These results suggest that chain-extension from slow thiol-Michael addition led to an increase in molecular weight in a time-dependent manner prior to polymerization by UV light.

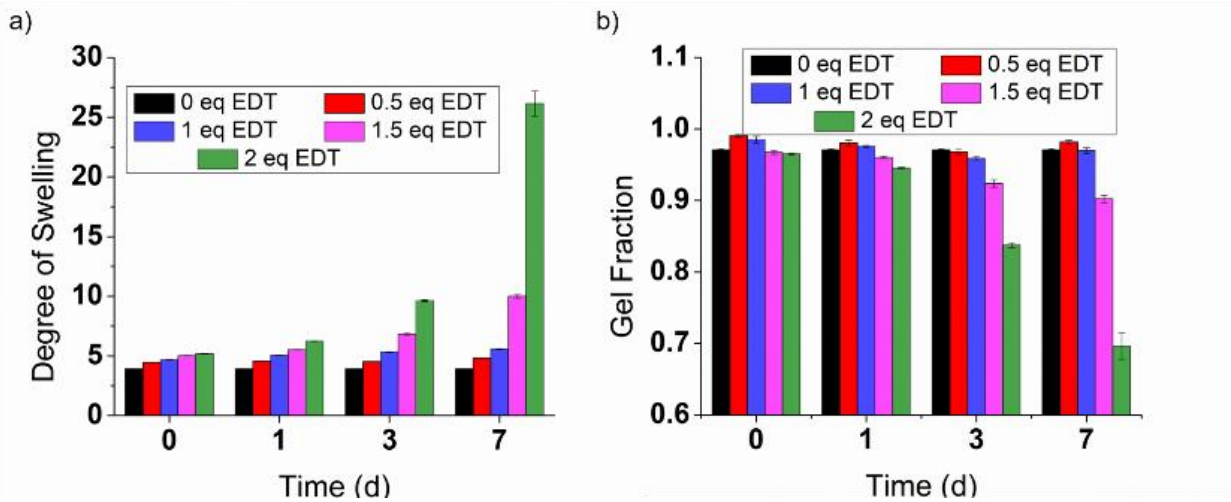

Figure 4.41 Swelling and gel fraction experiments on 30 wt% F127-BUM with varying equivalents of EDT

a) Degree of swelling shows a drasic increase when using 2 equivalents of EDT. b) Gel fraction experiment showing that 30% of the polymer mass is lost when 2 equivalents of EDT are added to the hydrogel formulation.

Given the possibility of dead chain-ends influencing the M_c value, measurements on the degree of swelling and gel fraction were performed to offer insight into the cross-link density and the ability of non-polymerized units to leach out of the network. As shown in Figure 4.4a, the hydrogels with 1 or fewer equivalents of EDT maintain around the same degree of swelling, whereas 1.5 and 2 equivalents aged for 7 days increase to 10 and 26 times their dry mass, respectively. These results are supported by a gel fraction (G_f) experiment (Figure 4.4b) where the swollen gels were then subsequently dried *in vacuo* and weighed. G_f was calculated by taking the dried mass after equilibrium swelling over the initial dried mass to determine the amount of polymer covalently incorporated into the network. Originally, we thought that the high degree of swelling was due solely to the loss of 10 and 30% polymer mass, respectively. To determine the effect of dead chain-ends on M_c, we compared 3 equivalents of mercaptoethanol to 1.5 equivalents of EDT to achieve

the same thiol:alkene ratio. The M_c value was 42 kg/mol after ageing for 3 days compared to 19 kg/mol for the EDT containing sample (Figure 4.13). Additionally, the mercaptoethanol containing gel completely dissolved after 3 days of ageing. Thus, a significant amount of EDT is incorporated and contributes to the network stretchability in addition to the contribution of a low degree of mass loss.

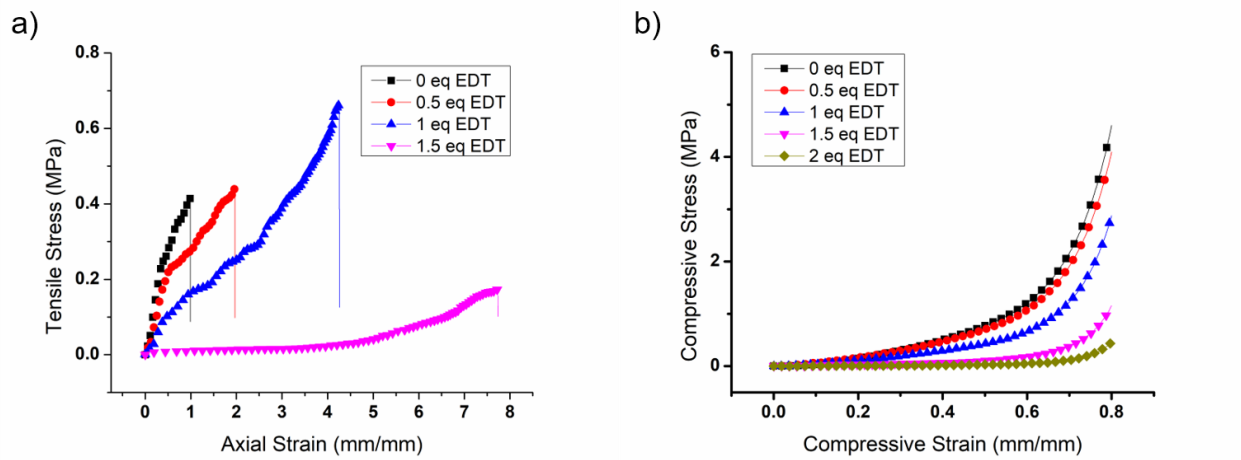

Figure 4.42 Tensile and compression measurements taken on the third day after adding EDT to a 30 wt% F127-BUM hydrogel.

a) Stress-strain tensile curve showing increased stretchability with higher EDT equivalents. 2 eq EDT omitted because the dogbone extended beyond the video extensometer viewing window. (b) Stress-strain compression curve showing a reduction in maximum stress at 80% extension. Tabulated Young's and compressive moduli can be found in Table 1.

Figure 4.5a shows a representative set of tensile measurements from 0 to 1.5 equivalents of EDT for hydrogel formulations that were aged for 3 days. The data for the hydrogel comprising 2 equivalents of EDT is not shown due to elongation beyond the video extensometer's active window. We observed that as the amount of thiol was increased, the Young's modulus (Y) decreased and the elongation at break increased, which suggests a more stretchable hydrogel. Compression experiments on the same set of gels showed similar trends (Figure 4.5b), as summarized in Table 4.1. At higher equivalents of EDT,

there was a greater degree of chain-extension via thiol-Michael addition which reduced the stiffness of a resulting hydrogel.

Table 4.2 Summary of tensile and compression experiments for 30 wt% F127-BUM with varying equivalents of EDT after 3 days of equilibration.

Dithiol Eq	Y (MPa)[a,c]	E (MPa)[a,c]	Max Elongation at Break (mm/mm)	Max Compressive Stress (MPa)[b,c]
0	1.0 ± 0.1	1.1 ± 0.1	0.55 ± 0.08	5 ± 1
0.5	0.78 ± 0.07	0.98 ± 0.03	2.0 ± 0.2	4.6 ± 0.9
1	0.54 ± 0.04	0.654 ± 0.006	3.2 ± 0.5	2.8 ± 0.2
1.5	0.25 ± 0.03	0.26 ± 0.03	8 ± 1	1.1 ± 0.1
2	0.04 ± 0.01	0.039 ± 0.004	24.9 ± 0.9	0.44 ± 0.06

[a]Calculated as the linear region between 0 and 10% extension
[b]Reported at 80% extension
[c]Error given as standard deviation over 3 replicate experiments

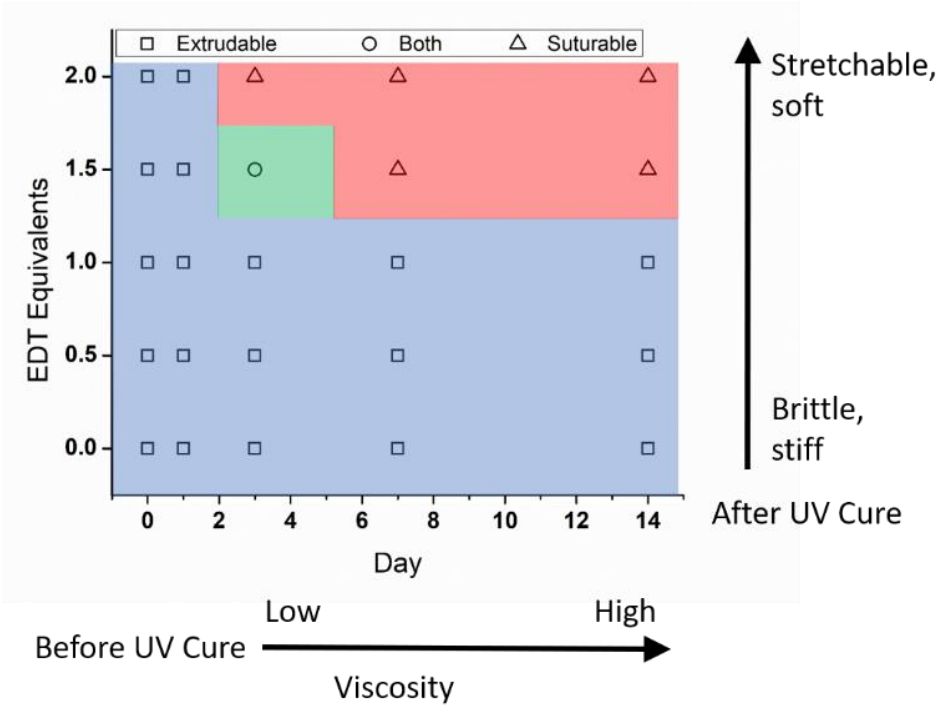

Figure 4.43 Summary of extrudability and Suturability in EDT containing F127-BUM hydrogels.

Ageing the hydrogel increases the viscosity while increasing the EDT equivalents results in a suturable gel. The optimum conditions are 1.5 equivalents EDT aged for 3 days.

In an extrusion-based setup, shear-thinning gel viscosity (Figure 4.14-17) is an important parameter to determine how well the material will flow out of a nozzle. In general, we observed that hydrogel formulations with viscosities greater than 100 Pa/s (Figure 4.3d) did not readily extrude from a pneumatically controlled syringe at 20 psi. Therefore, aging of the hydrogels beyond 7 days and with ≥1.5 equivalents resulted in gels that could not be extruded. Additionally, hydrogels that are stiff are not capable of withstanding a needle puncture without tearing. As evidenced by tensile measurements (Figure 5a), hydrogels with 1 or fewer EDT equivalents resulted in stiff and brittle gels while hydrogels with 2 equivalents underwent plastic deformation. We observed that 1.5 equivalents of EDT in the hydrogel aged for 3 d resulted in an elastic hydrogel that could resist tearing or fracturing when punctured with a needle (Figure 4.6).

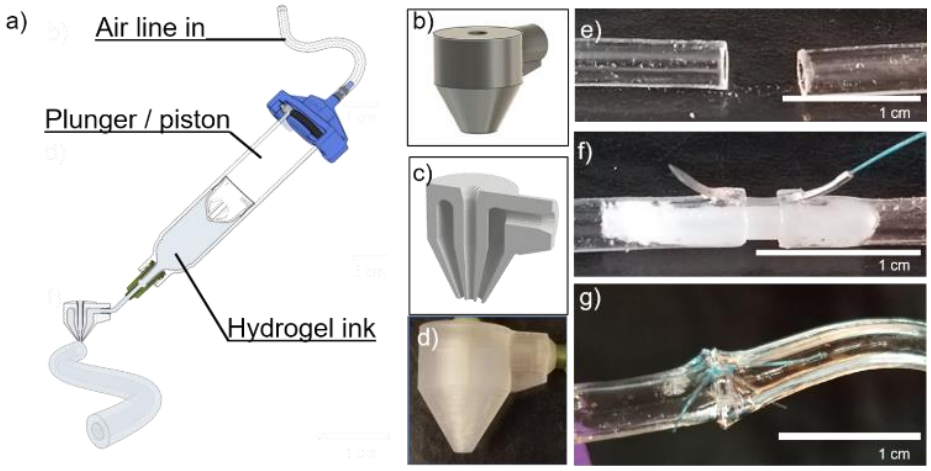

Figure 4.44 Fabrication and suturing of 30 wt% F127-BUM hydrogel with 1.5 equivalents EDT and equilibrated for 3 days

a) Cartoon of coaxial nozzle extrusion setup showing cross-section of nozzle and final printed hollow hydrogel tube. (b) STL rending of nozzle, (c) cross section, and (d) printed nozzle using Form 2 clear resin. (e) After extrusion, the tube is cut down the middle. (f) A plastic insert is placed as a support for the 4/0 nylon monofilament needle to join the two tubes. (g) A simple interrupted suture is placed, the plastic insert is removed, and the hydrogel is washed.

As a final proof of concept, we demonstrated the extrusion of a hydrogel tube using an optimized hydrogel formulation that could be cut, and then sutured. The hydrogel formulation comprising 30 w/w % F127-BUM and 1.5 equivalents of EDT was aged for 3 days prior to extrusion through a custom nozzle[38] that affords tubular hydrogel constructs (Figure 4.7). After irradiation with UV light, the samples were cross-linked via radical polymerization to afford stretchable hydrogel tubes. The extruded hydrogel tube was then cut with a razor blade and a plastic support piece was installed, before a nylon 4/0 monofilament suturing needle was passed through the gel on both ends and set with a simple suture. Finally, the plastic support was removed, and the hydrogel was washed to show the suture remaining in place. The resulting stitched hydrogel was robust and could be manipulated by hand without tearing the suture.

4.4 CONCLUSION

A stretchable, suturable hydrogel was fabricated utilizing a shear-thinning hydrogel that could undergo a combination of thiol-Michael chain-extension and free-radical polymerization. The ratio of dithiol additive to methacrylate was altered to tune the viscoelastic properties of the hydrogel. Through use of the affine network theory of rubber elasticity, the molecular weight between cross-links was calculated and provides support for explaining the difference in mechanical properties of the hydrogels. The proposed mechanism of network formation occurs via a slow thiol-Michael addition during a period of hydrogel aging, followed by free-radical polymerization initiated by UV light. In our study, we observed that 3 days of equilibration with a 1.5:1 thiol:methacrylate ratio was optimal to achieve good stretchability and puncture resistance during suture. This hydrogel was extruded through a custom 3D printed nozzle to afford robust, suturable hydrogel

tubes. These materials represent a promising step toward synthetic vasculature for surgical training and implantable devices.

4.5 EXPERIMENTAL

4.5.1 *Materials and Instrumentation*

All chemicals and solvents, unless otherwise stated, were purchased from Sigma-Aldrich or Fisher Scientific and used without further purification unless noted otherwise. Pluronic® F127 was dried under reduced pressure overnight prior to functionalization. Dry dichloromethane was obtained by purification over alumina columns on a Pure Process Technology purification system. ^{1}H NMR spectra were obtained on a Bruker Avance 300 or 500 MHz spectrometer.

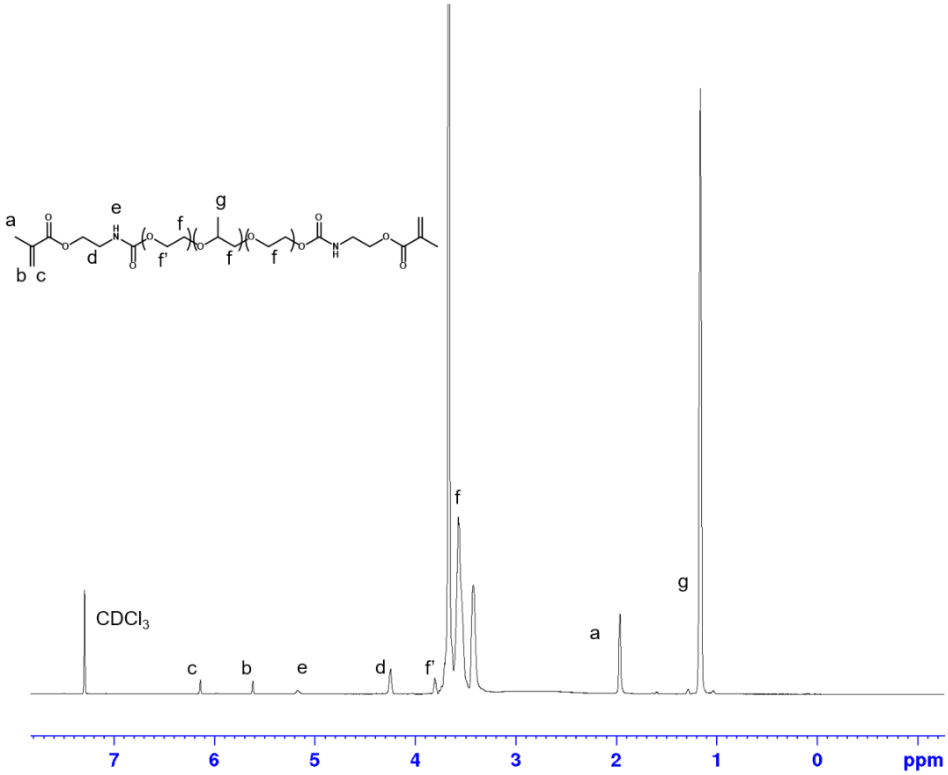

Figure 4.45 ^{1}H NMR spectrum of F127-BUM (500 MHz, 293 K, $CDCl_3$).

4.5.2 *Synthesis of Pluronic® F127-Bis-urethane Methacrylate (F127-BUM)*

The synthesis of F127-bis-urethane methacrylate (F127-BUM) was performed as previously described.[38] Briefly, F127 (60 g, 4.8 mmol) was dried under vacuum, then anhydrous

dichloromethane (550 ml) was charged to the flask. The mixture was stirred until complete dissolution of the F127 was observed. Dibutyltin dilaurate (12 drops) was then added, followed by dropwise addition of 2-isocyanatoethyl methacrylate (3.5 ml, 24.8 mmol) in anhydrous dichloromethane (50 ml). The reaction was allowed to proceed for 2 d before quenching with MeOH. The F127-BUM was precipitated in ether, allowed to settle, and decanted. The F127-BUM precipitate was finally washed in ether twice, prior to being dried under vacuum.

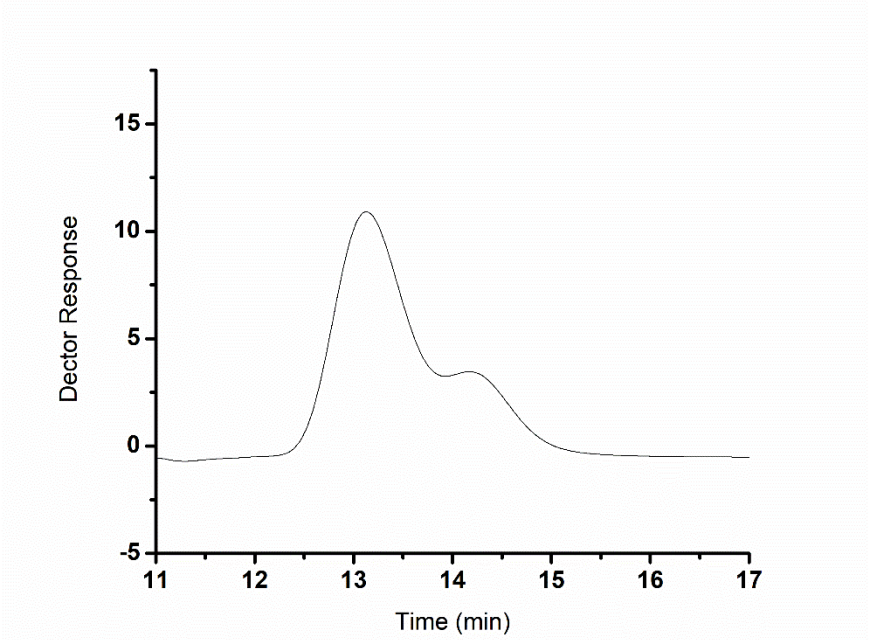

Figure 4.46 GPC trace of F127-BUM in $CHCl_3$ with 0.1 wt/v% TEA as stabilizer.

Smaller peak at higher retention time is due to diblock copolymers present in F127 batches from vendor.

4.5.3 *Preparation of F127-BUM Hydrogels*

F127-BUM (3 g, 0.24 mmol) was added to a scintillation vial, then deionized water or PBS solution (7 mL) was added. The vial was then vortex mixed and placed in an ice box until fully dissolved. To this vial, Lithium phenyl-2,4,6-trimethylbenzoylphosphinate (LAP, 10 mg, 0.03 mmol) and 2,2'-(Ethylenedioxy)diethanethiol (EDT, 58.6 µL, 0.36 mmol) were added and stirred

between 0 and 5 °C until fully dissolved. Samples were stored in a 5 °C refrigerator and only removed at 0, 1, 3, 7, and 14-day time points to be cast into molds or loaded onto the rheometer.

4.5.4 *Rheological Experiments*

Viscous flow experiments were performed on a TA Instruments Discovery HR-2 equipped with a 40 mm cone and plate geometry. Samples, which were equilibrated in an ice bath for at least 10 minutes, were carefully loaded onto a Peltier plate at 5 °C and trimmed. A preshear experiment was conducted to ensure that bubbles were eliminated from the sample cell. The sample was equilibrated at 21 °C for 8 min. The experiments were conducted in a logarithmic sweep from 0.01 to 100 1/s with 5 points per decade. Data was collected using steady state sensing with a 30 s sample period, 5% tolerance, and 3 consecutive measurements. Photorheological experiments were performed with an 8 mm parallel plate geometry and loaded onto a UV curing stage. A preshear experiment was conducted to ensure that bubbles were eliminated from the sample cell. The sample was equilibrated at room temperature for 8 min. The photorheological experiments were conducted using constant 1% strain and a frequency of 1 Hz which lies in the linear viscoelastic regime. A 120 s dwell time elapsed before the UV lamp (365 nm LED with an irradiation intensity of 5 mW cm^{-2}) was turned on for 7 min.

4.5.5 *Tensile Measurements*

An Instron 5585H 250 kN electro-mechanical test frame with a 50 N load cell was used to evaluate the tensile properties of the cross-linked hydrogels. The ASTM D638 type V specimen specifications were used to prepare dogbone samples by casting in approximately 2 g of 30 wt% gel into a Teflon dogbone mold. The gel was then exposed to 365 nm light for 10 min. The chemically cross-linked structure was then removed from the mold and placed into a falcon tube with a hydrated KimWipe to maintain humidity before testing. The sample was then placed on

pneumatic self-aligning grips fixed on the load frame, and the sample was subjected to increasing strain at a constant rate of 10 mm/min until mechanical failure of the sample. Axial strain was measured with a video extensometer accessory. Young's modulus was calculated from the slope of the linear region between 0 to 10% strain.

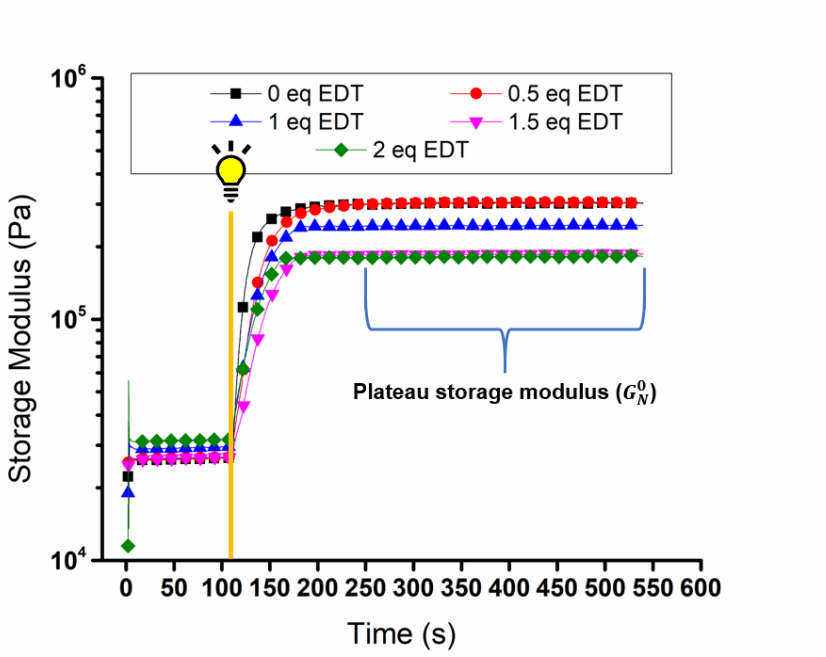

Figure 4.47 Photorheological experiment on 30 wt% F127-BUM hydrogel with varying equivalents of EDT after 1 day of equilibration.

At 120 s, the UV light is turned on and left on for the remainder of the experiment.

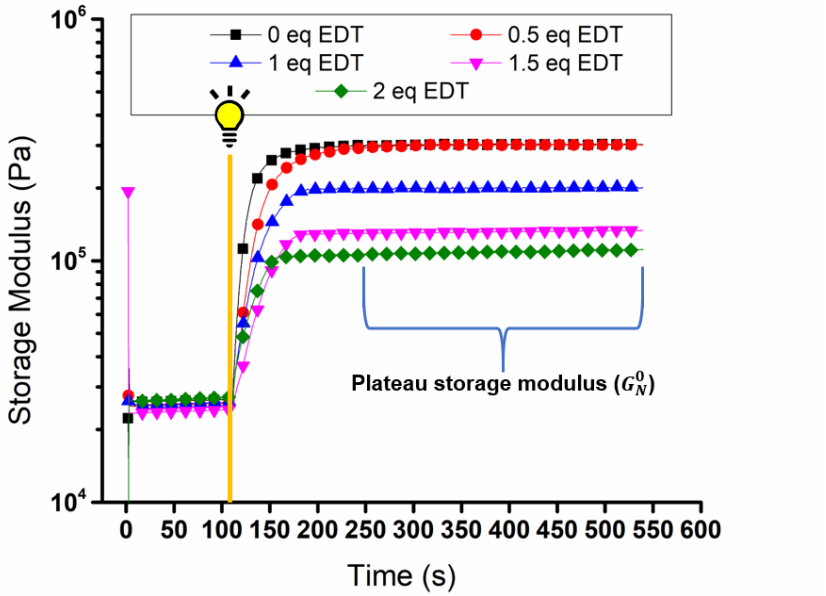

Figure 4.48 Photorheological experiment on 30 wt% F127-BUM hydrogel with varying equivalents of EDT after 3 days of equilibration.

At 120 s, the UV light is turned on and left on for the remainder of the experiment.

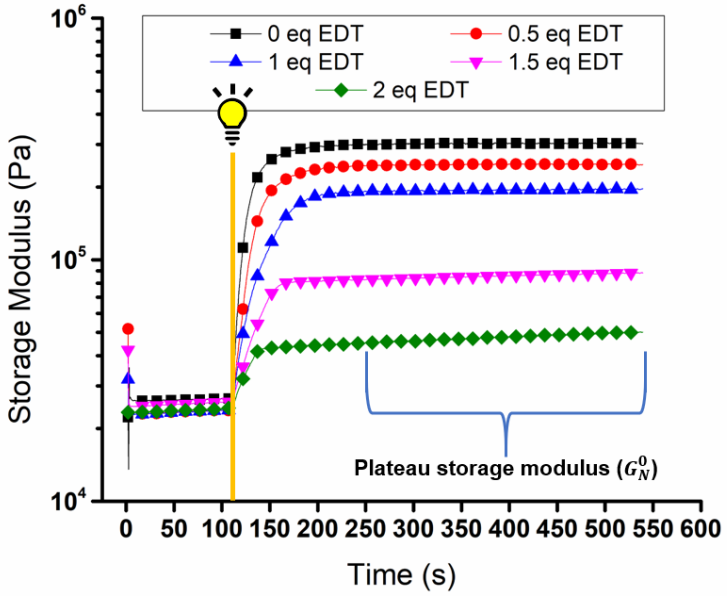

Figure 4.49 Photorheological experiment on 30 wt% F127-BUM hydrogel with varying equivalents of EDT after 14 days of equilibration.

At 120 s, the UV light is turned on and left on for the remainder of the experiment.

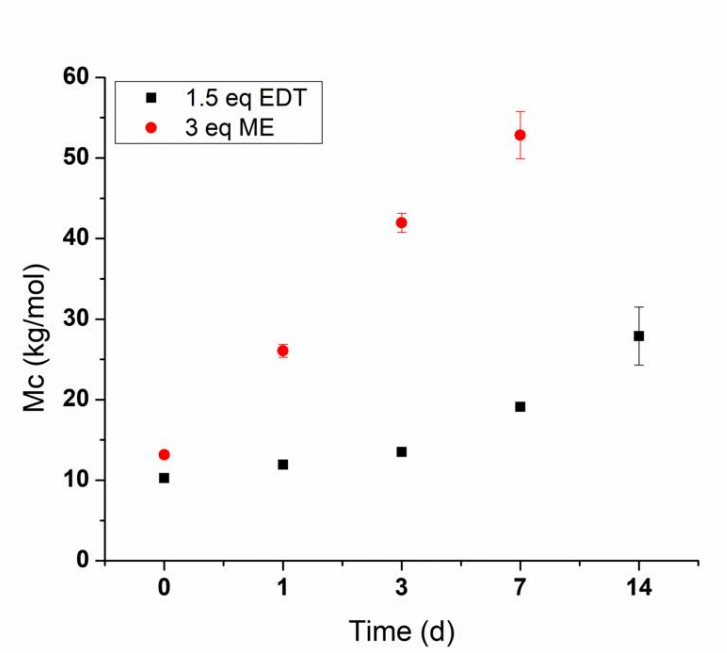

Figure 4.50 Molecular weight between cross-links control with mercaptoethanol.

M_c calculated from equation (1). Mercaptoethanol (ME) shows the effect of dead chain-ends on the Mc value as ME does not contribute to the hydrogel network.

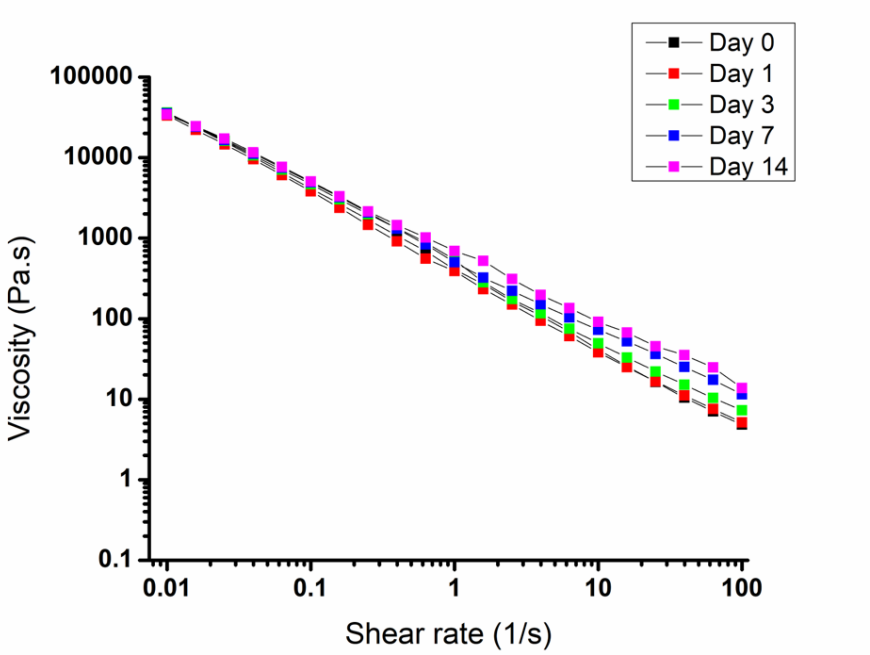

Figure 4.51 Viscous flow measurement of 30 wt% F127-BUM at 21 °C with 0.5 equivalents of EDT measured over the course of 14 days.

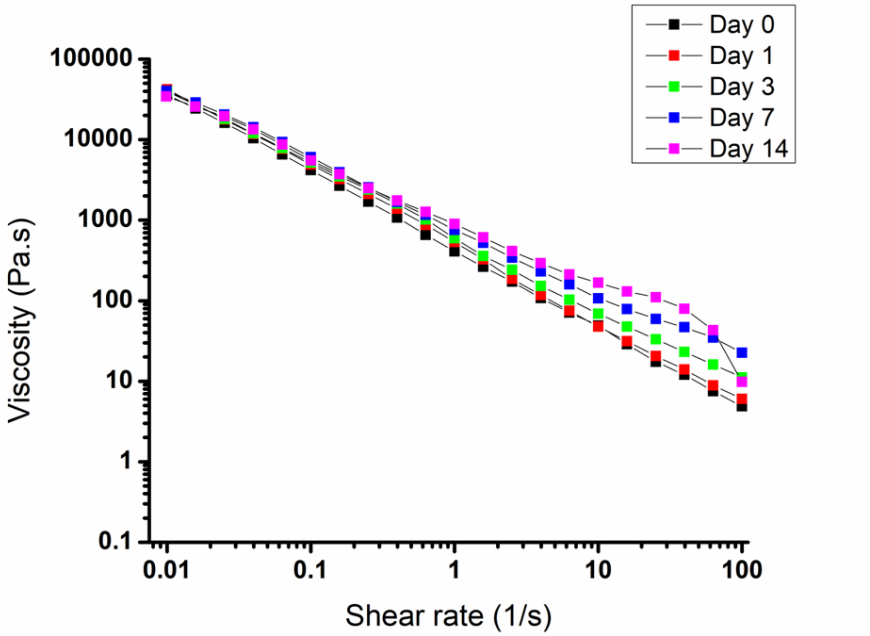

Figure 4.52 Viscous flow measurement of 30 wt% F127-BUM at 21 °C with 1 equivalent of EDT measured over the course of 14 days.

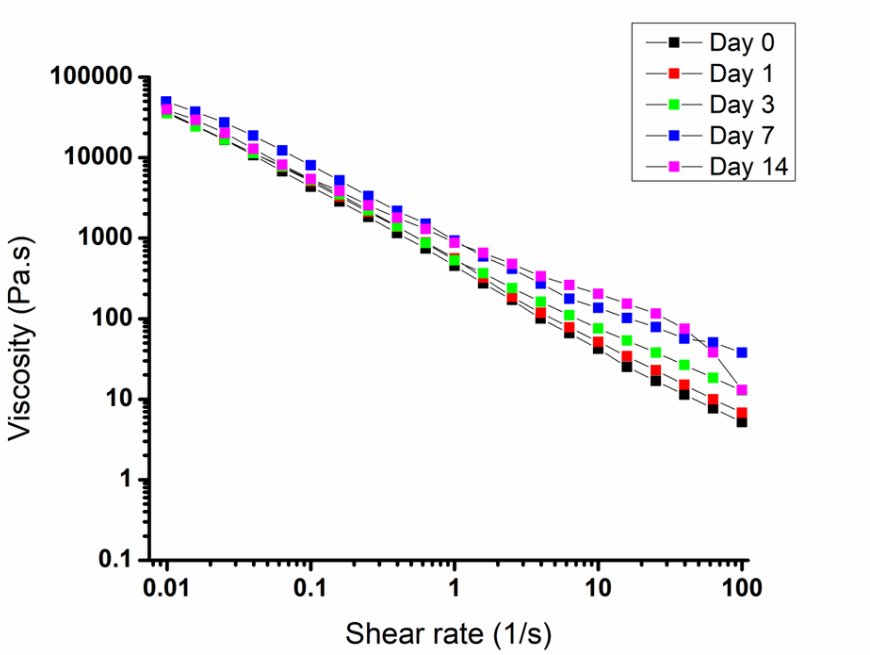

Figure 4.53 Viscous flow measurement of 30 wt% F127-BUM at 21 °C with 1.5 equivalents of EDT measured over the course of 14 days.

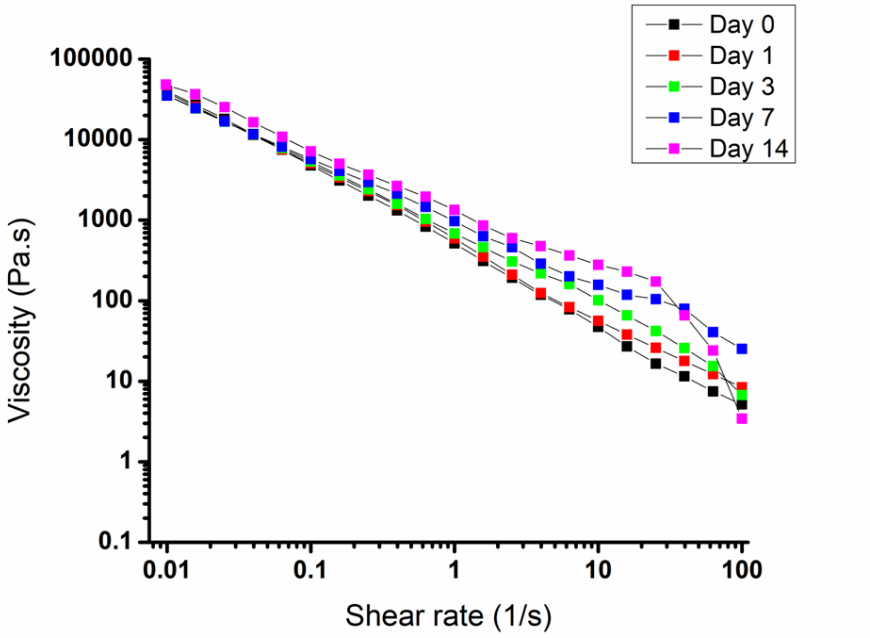

Figure 4.54 Viscous flow measurement of 30 wt% F127-BUM at 21 °C with 2 equivalents of EDT measured over the course of 14 days.

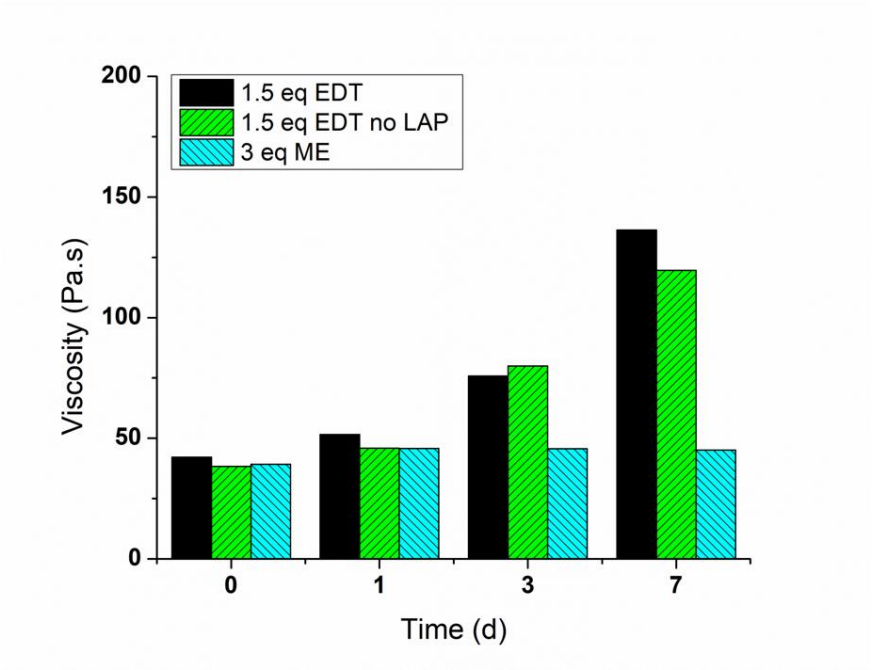

Figure 4.55 Viscous flow controls.

Measurements of 30 wt% F127-BUM taken at 10 s^{-1} and at 21 °C. The photoinitiator LAP does not influence the viscosity change over time. Mercaptoethanol has no effect on the viscosity of the hydrogel.

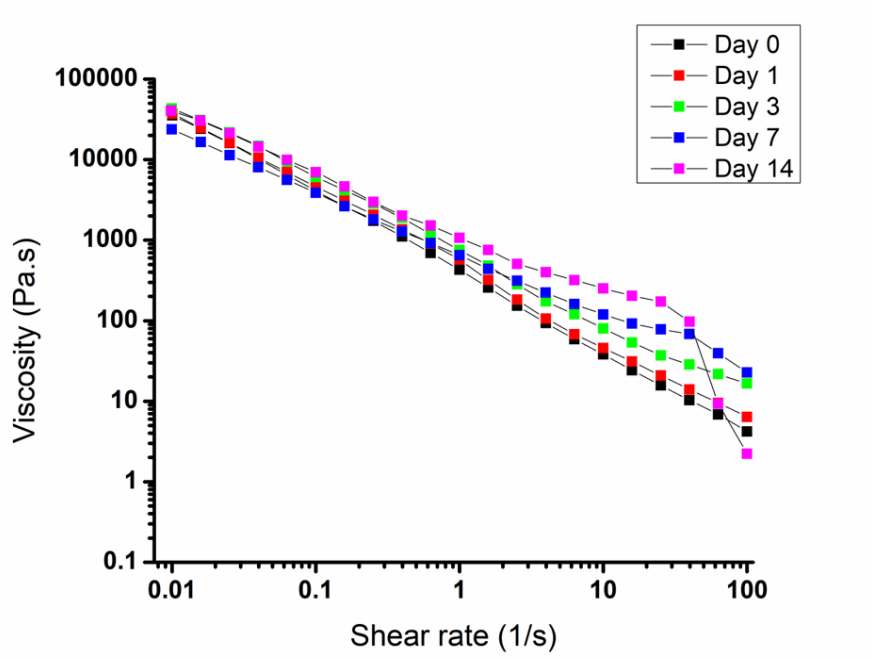

Figure 4.56 Viscous flow measurement of 30 wt% F127-BUM at 21 °C with 1.5 equivalents of EDT without LAP photoinitator measured over the course of 7 days.

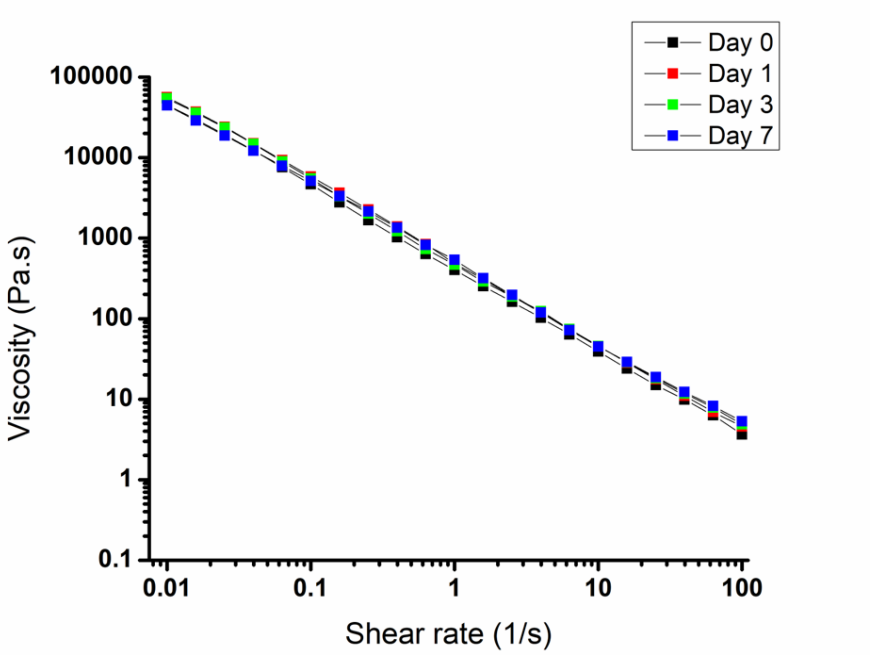

Figure 4.57 Viscous flow measurement of 30 wt% F127-BUM at 21 °C with 3 equivalents of mercaptoethanol measured over the course of 7 days.

4.5.6 *Compressive Measurements*

An Instron 5585H 250 kN electro-mechanical test frame with a 1 kN load cell was used to evaluate the compressive properties of the cross-linked hydrogel. Cylindrical compression samples (10 mm diameter x 5 mm height) were cast into PDMS molds and then exposed to 365 nm light for 10 min. The chemically cross-linked structure was then removed from the mold and placed into a falcon tube with a hydrated tissue to maintain humidity before testing. All tests were conducted at room temperature (21 °C) using a crosshead rate of 1.3 mm/min until 80% strain. Compressive modulus was calculated from the slope of the linear region between 0 to 10% strain.

4.5.7 *Extrusion Through Coaxial Nozzle*

All tubes were extruded through custom printed coaxial nozzles with a Form 2 SLA 3D printer. Gels chilled on ice were loaded into syringes (Nordson EFD), and once the gels reached room temperature, the extrusion set-up was assembled. Syringe barrel adapters (Nordson EFD)

were then attached to each syringe. Pressure to drive the syringe pistons (10-12 psi) was supplied by an in-house N_2 line. To adjust pressures prior to extrusion, the tubing of each syringe barrel adapter was clamped using a pinch-clamp, and the regulators were set to the desired pressures. To begin extrusion, the tubing of each adapter was unclamped, and after waiting a moment for the coaxial extrusion rate to stabilize, a 4 in x 6 in glass sheet was manually translated under the nozzle to catch the coaxial gel filament. The shell of the coaxial filament was then photo cross-linked for 10 min under a UV lamp (365 nm, 3.3 mW cm^{-2}).

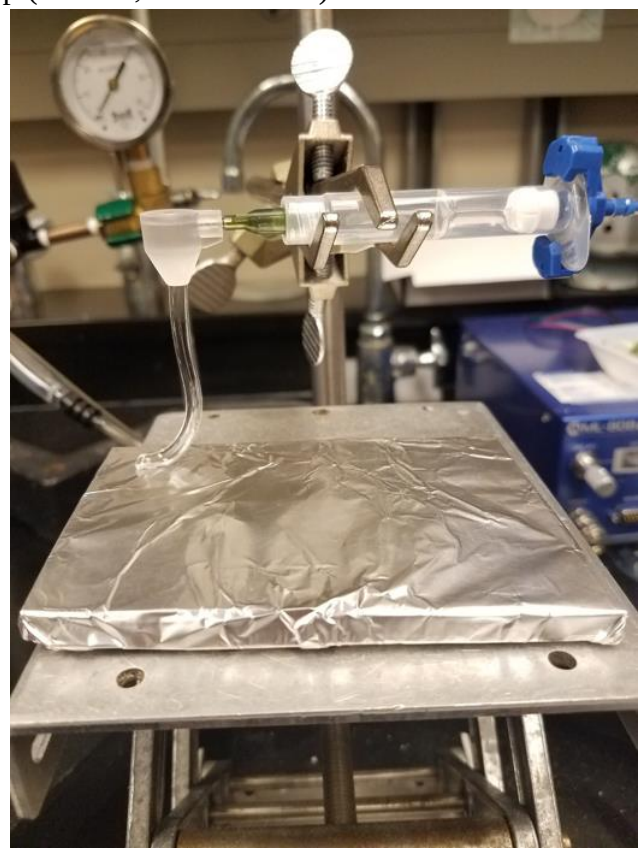

Figure 4.58 Hydrogel tube extrusion setup using coaxial nozzle

4.5.8 *Degree of Swelling and Gel Fraction Experiments*

Cylindrical samples (10 mm diameter x 5 mm height) were cast into PDMS molds and then exposed to 365 nm light for 10 min. The resulting cross-linked gel was extracted and wiped down to remove residual uncross-linked polymer on the surface and weighed. The disks were then dried

in a vacuum oven for 1 d and weighed to obtain the initial dry mass. Equilibrium swelling was achieved by soaking the disks in DI water over 3 d and weighed to obtain the degree of swelling. The swollen gels were then dried in a vacuum oven for 2 d and weighed to obtain a second dry mass which was used to calculate the gel fraction (G_f).

4.5.9 *Suturability Tests*

Hydrogel tubes printed using a coaxial nozzle were first cut using a razor blade. To the middle of the tube, a plastic insert was placed to provide structural support. A 4/0 nylon suture was used to rejoin the material. The simple interrupted suture method was used to demonstrate suturability. The final sutured tube was washed in DI water and the plastic insert was removed.

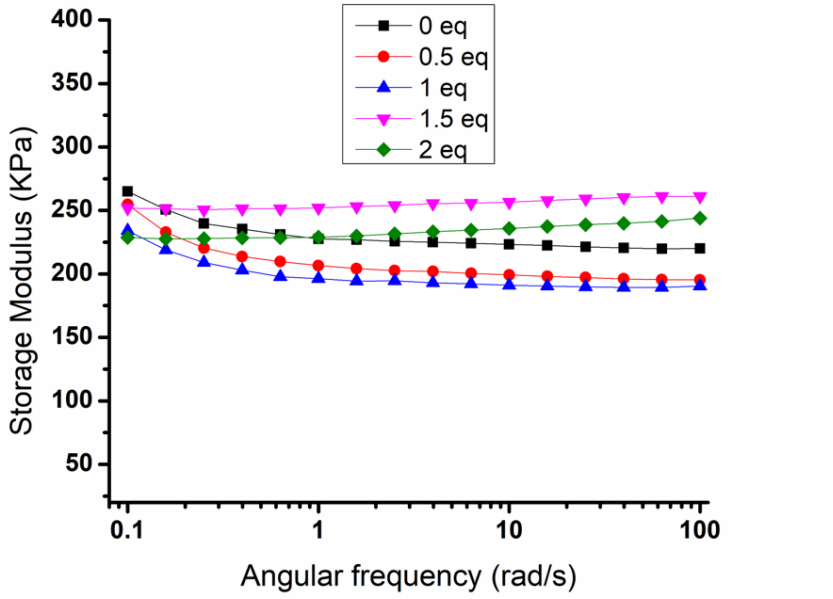

Figure 4.59 Frequency sweep measurement of 30 wt% F127-BUM at 1% strain and 21 °C with varying equivalents of EDT immediately after EDT addition.

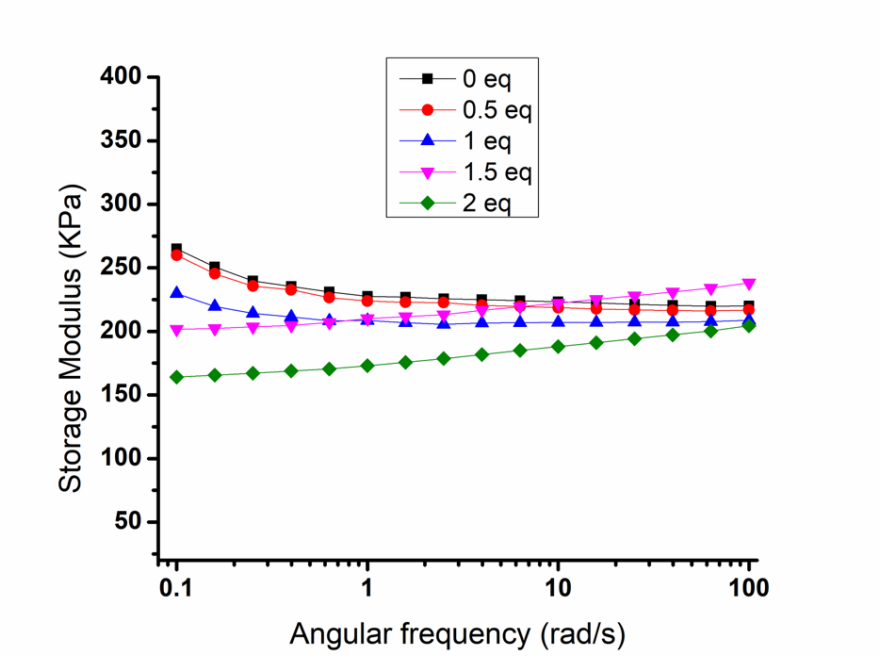

Figure 4.60 Frequency sweep measurement of 30 wt% F127-BUM at 1% strain and 21 °C with varying equivalents of EDT 1 day after EDT addition.

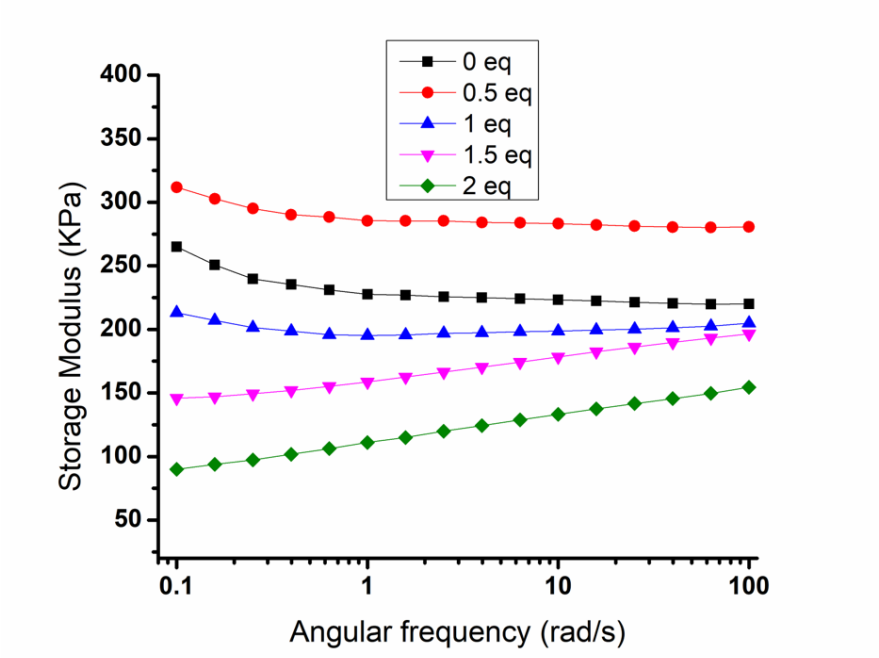

Figure 4.61 Frequency sweep measurement of 30 wt% F127-BUM at 1% strain and 21 °C with varying equivalents of EDT 3 days after EDT addition.

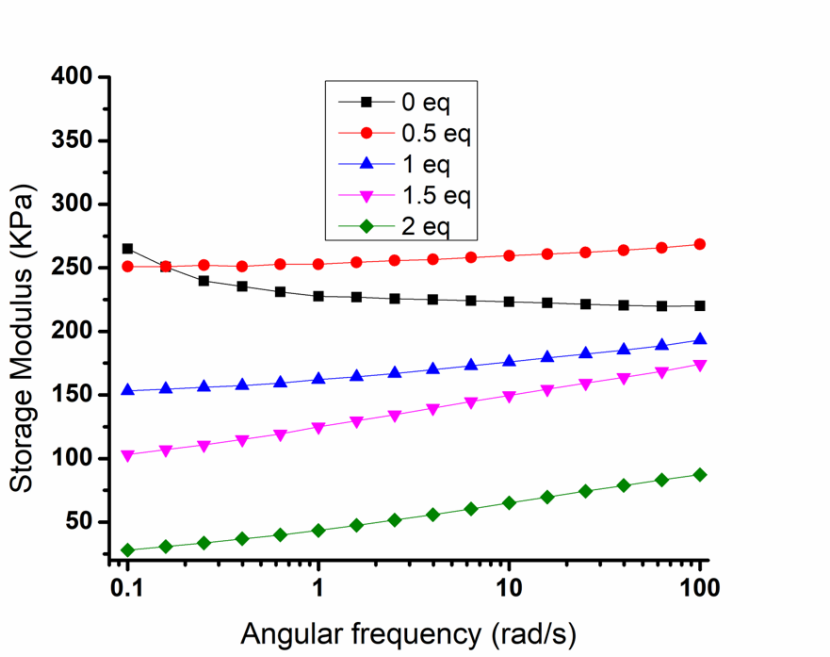

Figure 4.62 Frequency sweep measurement of 30 wt% F127-BUM at 1% strain and 21 °C with varying equivalents of EDT 7 days after EDT addition.

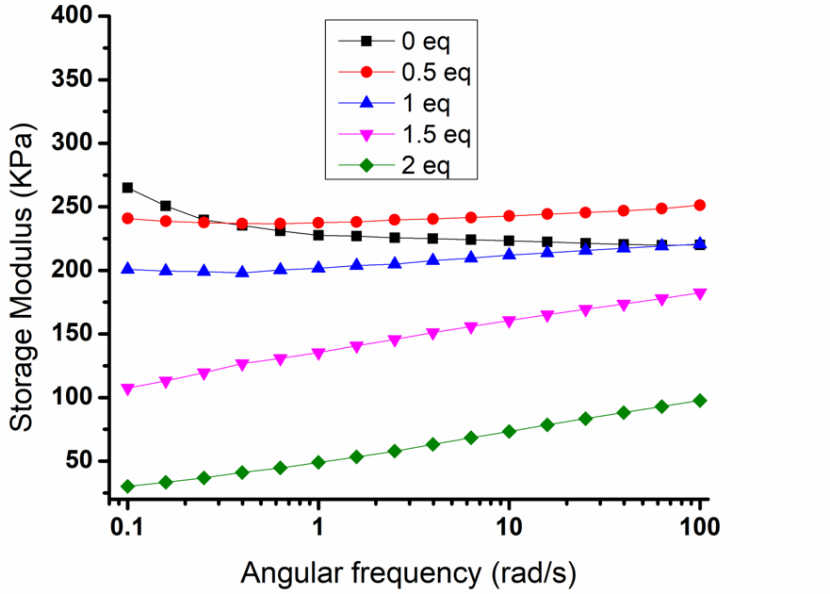

Figure 4.63 Frequency sweep measurement of 30 wt% F127-BUM at 1% strain and 21 °C with varying equivalents of EDT 14 days after EDT addition.

4.6 ACKNOWLEDGEMENTS

Adapted as manuscript in progress with permission from Karis, D.; Nelson, A. Time-Dependent Polymer Network Formation in Extrudable Hydrogels. *Manuscript submitted*

4.7 REFERENCES

(1) Joung, D.; Lavoie, N. S.; Guo, S.; Park, S. H.; Parr, A. M.; McAlpine, M. C. 3D Printed Neural Regeneration Devices. *Adv. Funct. Mater.* **2020**, *30* (1), 1906237. https://doi.org/10.1002/adfm.201906237.

(2) Pedde, R. D.; Mirani, B.; Navaei, A.; Styan, T.; Wong, S.; Mehrali, M.; Thakur, A.; Mohtaram, N. K.; Bayati, A.; Dolatshahi-Pirouz, A.; Nikkhah, M.; Willerth, S. M.; Akbari, M. Emerging Biofabrication Strategies for Engineering Complex Tissue Constructs. *Adv. Mater.* **2017**, *29* (19), 1606061. https://doi.org/10.1002/adma.201606061.

(3) Cleversey, C.; Robinson, M.; Willerth, S. M. 3D Printing Breast Tissue Models: A Review of Past Work and Directions for Future Work. *Micromachines* **2019**, *10* (8), 501. https://doi.org/10.3390/mi10080501.

(4) Ahadian, S.; Sadeghian, R. B.; Salehi, S.; Ostrovidov, S.; Bae, H.; Ramalingam, M.; Khademhosseini, A. Bioconjugated Hydrogels for Tissue Engineering and Regenerative Medicine. *Bioconjugate Chemistry*. American Chemical Society October 21, 2015, pp 1984–2001. https://doi.org/10.1021/acs.bioconjchem.5b00360.

(5) Jabbari, E.; Leijten, J.; Xu, Q.; Khademhosseini, A. The Matrix Reloaded: The Evolution of Regenerative Hydrogels. *Materials Today*. Elsevier B.V. May 1, 2016, pp 190–196. https://doi.org/10.1016/j.mattod.2015.10.005.

(6) Guan, X.; Avci-Adali, M.; Alarçin, E.; Cheng, H.; Kashaf, S. S.; Li, Y.; Chawla, A.; Jang, H. L.; Khademhosseini, A. Development of Hydrogels for Regenerative Engineering. *Biotechnol. J.* **2017**, *12* (5), 1600394. https://doi.org/10.1002/biot.201600394.

(7) Gungor-Ozkerim, P. S.; Inci, I.; Zhang, Y. S.; Khademhosseini, A.; Dokmeci, M. R. Bioinks for 3D Bioprinting: An Overview. *Biomaterials Science*. Royal Society of Chemistry May 1, 2018, pp 915–946. https://doi.org/10.1039/c7bm00765e.

(8) Knipe, J. M.; Peppas, N. A. Multi-Responsive Hydrogels for Drug Delivery and Tissue Engineering Applications. *Regen. Biomater.* **2014**, *1* (1), 57–65. https://doi.org/10.1093/rb/rbu006.

(9) Neves, M. I.; Wechsler, M. E.; Gomes, M. E.; Reis, R. L.; Granja, P. L.; Peppas, N. A. Molecularly Imprinted Intelligent Scaffolds for Tissue Engineering Applications. *Tissue Engineering - Part B: Reviews*. Mary Ann Liebert Inc. February 1, 2017, pp 27–43. https://doi.org/10.1089/ten.teb.2016.0202.

(10) Elkhoury, K.; Russell, C. S.; Sanchez-Gonzalez, L.; Mostafavi, A.; Williams, T. J.; Kahn, C.; Peppas, N. A.; Arab-Tehrany, E.; Tamayol, A. Soft-Nanoparticle Functionalization of Natural Hydrogels for Tissue Engineering Applications. *Advanced Healthcare Materials*. Wiley-VCH Verlag September 12, 2019, p 1900506. https://doi.org/10.1002/adhm.201900506.

(11) Jiang, Z.; Shaha, R.; McBride, R.; Jiang, K.; Tang, M.; Xu, B.; Goroncy, A. K.; Frick, C.; Oakey, J. Crosslinker Length Dictates Step-Growth Hydrogel Network Formation Dynamics and Allows Rapid on-Chip Photoencapsulation. *Biofabrication* **2020**, *12* (3), 035006. https://doi.org/10.1088/1758-5090/ab7ef4.

(12) Kang, H. W.; Lee, S. J.; Ko, I. K.; Kengla, C.; Yoo, J. J.; Atala, A. A 3D Bioprinting System to Produce Human-Scale Tissue Constructs with Structural Integrity. *Nat. Biotechnol.* **2016**, *34* (3), 312–319. https://doi.org/10.1038/nbt.3413.

(13) Lee, A.; Hudson, A. R.; Shiwarski, D. J.; Tashman, J. W.; Hinton, T. J.; Yerneni, S.; Bliley, J. M.; Campbell, P. G.; Feinberg, A. W. 3D Bioprinting of Collagen to Rebuild Components of the Human Heart. *Science (80-.).* **2019**, *365* (6452), 482–487. https://doi.org/10.1126/science.aav9051.

(14) Qiu, K.; Haghiashtiani, G.; McAlpine, M. C. 3D Printed Organ Models for Surgical Applications. *Annu. Rev. Anal. Chem.* **2018**, *11* (1), 287–306. https://doi.org/10.1146/annurev-anchem-061417-125935.

(15) Maruyama, H.; Yokota, Y.; Hosono, K.; Arai, F. Hydrogel Heart Model with Temperature Memory Properties for Surgical Simulation. *Sensors* **2019**, *19* (5), 1102. https://doi.org/10.3390/s19051102.

(16) Hu, W.; Zhang, Z.; Zhu, L.; Wen, Y.; Zhang, T.; Ren, P.; Wang, F.; Ji, Z. Combination of Polypropylene Mesh and in Situ Injectable Mussel-Inspired Hydrogel in Laparoscopic Hernia Repair for Preventing Post-Surgical Adhesions in the Piglet Model. *ACS Biomater. Sci. Eng.* **2020**, *6* (3), 1735–1743. https://doi.org/10.1021/acsbiomaterials.9b01333.

(17) Sultana, T.; Van Hai, H.; Abueva, C.; Kang, H. J.; Lee, S. Y.; Lee, B. T. TEMPO Oxidized Nano-Cellulose Containing Thermo-Responsive Injectable Hydrogel for Post-Surgical Peritoneal Tissue Adhesion Prevention. *Mater. Sci. Eng. C* **2019**, *102*, 12–21. https://doi.org/10.1016/j.msec.2019.03.110.

(18) Wang, Y.; Zhu, W.; Xiao, K.; Li, Z.; Ma, Q.; Li, W.; Shen, S.; Weng, X. Self-Healing and Injectable Hybrid Hydrogel for Bone Regeneration of Femoral Head Necrosis and Defect. *Biochem. Biophys. Res. Commun.* **2019**, *508* (1), 25–30. https://doi.org/10.1016/j.bbrc.2018.11.097.

(19) Chen, X.; Wang, M.; Yang, X.; Wang, Y.; Yu, L.; Sun, J.; Ding, J. Injectable Hydrogels for the Sustained Delivery of a HER2-Targeted Antibody for Preventing Local Relapse of HER2+ Breast Cancer after Breast-Conserving Surgery. *Theranostics* **2019**, *9* (21), 6080–6098. https://doi.org/10.7150/thno.36514.

(20) Sawicki, L. A.; Ovadia, E. M.; Pradhan, L.; Cowart, J. E.; Ross, K. E.; Wu, C. H.; Kloxin, A. M. Tunable Synthetic Extracellular Matrices to Investigate Breast Cancer Response to Biophysical and Biochemical Cues. *APL Bioeng.* **2019**, *3* (1), 016101. https://doi.org/10.1063/1.5064596.

(21) Tibbitt, M. W.; Anseth, K. S. Hydrogels as Extracellular Matrix Mimics for 3D Cell Culture. *Biotechnology and Bioengineering*. NIH Public Access July 1, 2009, pp 655–663. https://doi.org/10.1002/bit.22361.

(22) Papavasiliou, G.; Sokic, S.; Turturro, M. Synthetic PEG Hydrogels as Extracellular Matrix Mimics for Tissue Engineering Applications. In *Biotechnology - Molecular Studies and Novel Applications for Improved Quality of Human Life*; InTech, 2012. https://doi.org/10.5772/31695.

(23) Guvendiren, M.; Lu, H. D.; Burdick, J. A. Shear-Thinning Hydrogels for Biomedical Applications. *Soft Matter*. The Royal Society of Chemistry January 14, 2012, pp 260–272. https://doi.org/10.1039/c1sm06513k.

(24) Jalalvandi, E.; Shavandi, A. Shear Thinning/Self-Healing Hydrogel Based on Natural Polymers with Secondary Photocrosslinking for Biomedical Applications. *J. Mech. Behav. Biomed. Mater.* **2019**, *90*, 191–201. https://doi.org/10.1016/j.jmbbm.2018.10.009.

(25) Chen, M. H.; Wang, L. L.; Chung, J. J.; Kim, Y. H.; Atluri, P.; Burdick, J. A. Methods to Assess Shear-Thinning Hydrogels for Application As Injectable Biomaterials. *ACS Biomater. Sci. Eng.* **2017**, *3* (12), 3146–3160. https://doi.org/10.1021/acsbiomaterials.7b00734.

(26) Sisso, A. M.; Boit, M. O.; DeForest, C. A. Self-healing Injectable Gelatin Hydrogels for Localized Therapeutic Cell Delivery. *J. Biomed. Mater. Res. Part A* **2020**, *108* (5), 1112–1121. https://doi.org/10.1002/jbm.a.36886.

(27) Samimi Gharaie, S.; Dabiri, S.; Akbari, M. Smart Shear-Thinning Hydrogels as Injectable Drug Delivery Systems. *Polymers (Basel).* **2018**, *10* (12), 1317. https://doi.org/10.3390/polym10121317.

(28) Highley, C. B.; Rodell, C. B.; Burdick, J. A. Direct 3D Printing of Shear-Thinning Hydrogels into Self-Healing Hydrogels. *Adv. Mater.* **2015**, *27* (34), 5075–5079. https://doi.org/10.1002/adma.201501234.

(29) Smith, P. T.; Basu, A.; Saha, A.; Nelson, A. Chemical Modification and Printability of Shear-Thinning Hydrogel Inks for Direct-Write 3D Printing. *Polymer (Guildf).* **2018**, *152*, 42–50. https://doi.org/10.1016/j.polymer.2018.01.070.

(30) Lewis, J. A. Direct Ink Writing of 3D Functional Materials. *Adv. Funct. Mater.* **2006**, *16* (17), 2193–2204. https://doi.org/10.1002/adfm.200600434.

(31) Jalaal, M.; Cottrell, G.; Balmforth, N.; Stoeber, B. On the Rheology of Pluronic F127 Aqueous Solutions. *J. Rheol. (N. Y. N. Y).* **2017**, *61* (1), 139–146. https://doi.org/10.1122/1.4971992.

(32) Chimene, D.; Kaunas, R.; Gaharwar, A. K. Hydrogel Bioink Reinforcement for Additive Manufacturing: A Focused Review of Emerging Strategies. *Adv. Mater.* **2020**, *32* (1), 1902026.

https://doi.org/10.1002/adma.201902026.

(33) Loebel, C.; Ayoub, A.; Galarraga, J. H.; Kossover, O.; Simaan-Yameen, H.; Seliktar, D.; Burdick, J. A. Tailoring Supramolecular Guest-Host Hydrogel Viscoelasticity with Covalent Fibrinogen Double Networks. *J. Mater. Chem. B* **2019**, *7* (10), 1753–1760. https://doi.org/10.1039/c8tb02593b.

(34) Fellin, C. R.; Adelmund, S. M.; Karis, D. G.; Shafranek, R. T.; Ono, R. J.; Martin, C. G.; Johnston, T. G.; DeForest, C. A.; Nelson, A. Tunable Temperature- and Shear-Responsive Hydrogels Based on Poly(Alkyl Glycidyl Ether)S. *Polym. Int.* **2019**, *68* (7), 1238–1246. https://doi.org/10.1002/pi.5716.

(35) Shafranek, R. T.; Leger, J. D.; Zhang, S.; Khalil, M.; Gu, X.; Nelson, A. Sticky Ends in a Self-Assembling ABA Triblock Copolymer: The Role of Ureas in Stimuli-Responsive Hydrogels. *Mol. Syst. Des. Eng.* **2019**, *4* (1), 91–102. https://doi.org/10.1039/c8me00063h.

(36) Karis, D. G.; Ono, R. J.; Zhang, M.; Vora, A.; Storti, D.; Ganter, M. A.; Nelson, A. Cross-Linkable Multi-Stimuli Responsive Hydrogel Inks for Direct-Write 3D Printing. *Polym. Chem.* **2017**, *8* (29), 4199–4206. https://doi.org/10.1039/c7py00831g.

(37) Basu, A.; Saha, A.; Goodman, C.; Shafranek, R. T.; Nelson, A. Catalytically Initiated Gel-in-Gel Printing of Composite Hydrogels. *ACS Appl. Mater. Interfaces* **2017**, *9* (46), 40898–40904. https://doi.org/10.1021/acsami.7b14177.

(38) Millik, S. C.; Dostie, A. M.; Karis, D. G.; Smith, P. T.; McKenna, M.; Chan, N.; Curtis, C. D.; Nance, E.; Theberge, A. B.; Nelson, A. 3D Printed Coaxial Nozzles for the Extrusion of Hydrogel Tubes toward Modeling Vascular Endothelium. *Biofabrication* **2019**, *11* (4), 045009. https://doi.org/10.1088/1758-5090/ab2b4d.

(39) Johnston, T. G.; Yuan, S. F.; Wagner, J. M.; Yi, X.; Saha, A.; Smith, P.; Nelson, A.; Alper, H. S. Compartmentalized Microbes and Co-Cultures in Hydrogels for on-Demand Bioproduction and Preservation. *Nat. Commun.* **2020**, *11* (1), 1–11. https://doi.org/10.1038/s41467-020-14371-4.

(40) Wong, J.; Gong, A. T.; Defnet, P. A.; Meabe, L.; Beauchamp, B.; Sweet, R. M.; Sardon, H.; Cobb, C. L.; Nelson, A. 3D Printing Ionogel Auxetic Frameworks for Stretchable Sensors. *Adv. Mater.*

Technol. **2019**, *4* (9), 1900452. https://doi.org/10.1002/admt.201900452.

(41) Saha, A.; Johnston, T. G.; Shafranek, R. T.; Goodman, C. J.; Zalatan, J. G.; Storti, D. W.; Ganter, M. A.; Nelson, A. Additive Manufacturing of Catalytically Active Living Materials. *ACS Appl. Mater. Interfaces* **2018**, *10* (16), 13373–13380. https://doi.org/10.1021/acsami.8b02719.

(42) Dutta, S.; Cohn, D. Temperature and PH Responsive 3D Printed Scaffolds. *J. Mater. Chem. B* **2017**, *5* (48), 9514–9521. https://doi.org/10.1039/c7tb02368e.

(43) Müller, M.; Becher, J.; Schnabelrauch, M.; Zenobi-Wong, M. Nanostructured Pluronic Hydrogels as Bioinks for 3D Bioprinting. *Biofabrication* **2015**, *7* (3), 035006. https://doi.org/10.1088/1758-5090/7/3/035006.

(44) Fairbanks, B. D.; Love, D. M.; Bowman, C. N. Efficient Polymer-Polymer Conjugation via Thiol-Ene Click Reaction. *Macromolecular Chemistry and Physics*. Wiley-VCH Verlag September 1, 2017, p 1700073. https://doi.org/10.1002/macp.201700073.

(45) Resetco, C.; Hendriks, B.; Badi, N.; Du Prez, F. Thiol-Ene Chemistry for Polymer Coatings and Surface Modification-Building in Sustainability and Performance. *Materials Horizons*. Royal Society of Chemistry November 1, 2017, pp 1041–1053. https://doi.org/10.1039/c7mh00488e.

(46) Lowe, A. B. Thiol-Ene "Click" Reactions and Recent Applications in Polymer and Materials Synthesis: A First Update. *Polymer Chemistry*. Royal Society of Chemistry September 7, 2014, pp 4820–4870. https://doi.org/10.1039/c4py00339j.

(47) Alonso, R.; Jiménez-Meneses, P.; García-Rupérez, J.; Bañuls, M. J.; Maquieira, Á. Thiol-Ene Click Chemistry towards Easy Microarraying of Half-Antibodies. *Chem. Commun.* **2018**, *54* (48), 6144–6147. https://doi.org/10.1039/c8cc01369a.

(48) Grim, J. C.; Brown, T. E.; Aguado, B. A.; Chapnick, D. A.; Viert, A. L.; Liu, X.; Anseth, K. S. A Reversible and Repeatable Thiol-Ene Bioconjugation for Dynamic Patterning of Signaling Proteins in Hydrogels. *ACS Cent. Sci.* **2018**, *4* (7), 909–916. https://doi.org/10.1021/acscentsci.8b00325.

(49) Liu, Y.; Hou, W.; Sun, H.; Cui, C.; Zhang, L.; Jiang, Y.; Wu, Y.; Wang, Y.; Li, J.; Sumerlin, B. S.; Liu, Q.; Tan, W. Thiol-Ene Click Chemistry: A Biocompatible Way for Orthogonal Bioconjugation

of Colloidal Nanoparticles. *Chem. Sci.* **2017**, *8* (9), 6182–6187. https://doi.org/10.1039/c7sc01447c.

(50) Killops, K. L.; Campos, L. M.; Hawker, C. J. Robust, Efficient, and Orthogonal Synthesis of Dendrimers via Thiol-Ene "Click" Chemistry. *J. Am. Chem. Soc.* **2008**, *130* (15), 5062–5064. https://doi.org/10.1021/ja8006325.

(51) Colak, B.; Di Cio, S.; Gautrot, J. E. Biofunctionalized Patterned Polymer Brushes via Thiol-Ene Coupling for the Control of Cell Adhesion and the Formation of Cell Arrays. *Biomacromolecules* **2018**, *19* (5), 1445–1455. https://doi.org/10.1021/acs.biomac.7b01436.

(52) Stichler, S.; Jungst, T.; Schamel, M.; Zilkowski, I.; Kuhlmann, M.; Böck, T.; Blunk, T.; Teßmar, J.; Groll, J. Thiol-Ene Clickable Poly(Glycidol) Hydrogels for Biofabrication. *Ann. Biomed. Eng.* **2017**, *45* (1), 273–285. https://doi.org/10.1007/s10439-016-1633-3.

(53) Shih, H.; Lin, C. C. Cross-Linking and Degradation of Step-Growth Hydrogels Formed by Thiol-Ene Photoclick Chemistry. *Biomacromolecules* **2012**, *13* (7), 2003–2012. https://doi.org/10.1021/bm300752j.

(54) Sawicki, L. A.; Kloxin, A. M. Design of Thiol-Ene Photoclick Hydrogels Using Facile Techniques for Cell Culture Applications. *Biomater. Sci.* **2014**, *2* (11), 1612–1626. https://doi.org/10.1039/c4bm00187g.

(55) Lee, S.; Tae, H.; Ki, C. S. Fabrication of Schizophyllan Hydrogel via Orthogonal Thiol-Ene Photopolymerization. *Carbohydr. Polym.* **2017**, *167*, 270–279. https://doi.org/10.1016/j.carbpol.2017.03.042.

(56) Maleki, L.; Edlund, U.; Albertsson, A. C. Synthesis of Full Interpenetrating Hemicellulose Hydrogel Networks. *Carbohydr. Polym.* **2017**, *170*, 254–263. https://doi.org/10.1016/j.carbpol.2017.04.091.

(57) Nair, D. P.; Podgórski, M.; Chatani, S.; Gong, T.; Xi, W.; Fenoli, C. R.; Bowman, C. N. The Thiol-Michael Addition Click Reaction: A Powerful and Widely Used Tool in Materials Chemistry. *Chemistry of Materials*. American Chemical Society January 14, 2014, pp 724–744. https://doi.org/10.1021/cm402180t.

(58) Northrop, B. H.; Coffey, R. N. Thiol-Ene Click Chemistry: Computational and Kinetic Analysis of

the Influence of Alkene Functionality. *J. Am. Chem. Soc.* **2012**, *134* (33), 13804–13817. https://doi.org/10.1021/ja305441d.

(59) Huang, S.; Sinha, J.; Podgórski, M.; Zhang, X.; Claudino, M.; Bowman, C. N. Mechanistic Modeling of the Thiol-Michael Addition Polymerization Kinetics: Structural Effects of the Thiol and Vinyl Monomers. *Macromolecules* **2018**, *51* (15), 5979–5988. https://doi.org/10.1021/acs.macromol.8b01264.

(60) Lecamp, L.; Houllier, F.; Youssef, B.; Bunel, C. Photoinitiated Cross-Linking of a Thiol-Methacrylate System. *Polymer (Guildf).* **2001**, *42* (7), 2727–2736. https://doi.org/10.1016/S0032-3861(00)00700-X.

(61) Sirrine, J. M.; Meenakshisundaram, V.; Moon, N. G.; Scott, P. J.; Mondschein, R. J.; Weiseman, T. F.; Williams, C. B.; Long, T. E. Functional Siloxanes with Photo-Activated, Simultaneous Chain Extension and Crosslinking for Lithography-Based 3D Printing. *Polymer (Guildf).* **2018**, *152*, 25–34. https://doi.org/10.1016/j.polymer.2018.02.056.

(62) Berry, D. R.; Díaz, B. K.; Durand-Silva, A.; Smaldone, R. A. Radical Free Crosslinking of Direct-Write 3D Printed Hydrogels through a Base Catalyzed Thiol-Michael Reaction. *Polym. Chem.* **2019**. https://doi.org/10.1039/c9py00953a.

(63) Rydholm, A. E.; Bowman, C. N.; Anseth, K. S. Degradable Thiol-Acrylate Photopolymers: Polymerization and Degradation Behavior of an in Situ Forming Biomaterial. *Biomaterials* **2005**, *26* (22), 4495–4506. https://doi.org/10.1016/j.biomaterials.2004.11.046.

(64) Scott, P. J.; Meenakshisundaram, V.; Chartrain, N. A.; Sirrine, J. M.; Williams, C. B.; Long, T. E. Additive Manufacturing of Hydrocarbon Elastomers via Simultaneous Chain Extension and Cross-Linking of Hydrogenated Polybutadiene. *ACS Appl. Polym. Mater.* **2019**, *1* (4), 684–690. https://doi.org/10.1021/acsapm.8b00150.

(65) Rubinstein, M.; Colby, R. Polymer Physics; Oxford University Press: New York, 2003; p 440.

(66) Jiang, J.; Burger, C.; Li, C.; Li, J.; Lin, M. Y.; Colby, R. H.; Rafailovich, M. H.; Sokolov, J. C. Shear-Induced Layered Structure of Polymeric Micelles by SANS. *Macromolecules* **2007**, *40* (11),

4016–4022. https://doi.org/10.1021/ma062654j.

(67) Rodriguez, C. G.; Chwatko, M.; Park, J.; Bentley, C. L.; Freeman, B. D.; Lynd, N. A. Compositionally Controlled Polyether Membranes via Mono(μ-Alkoxo)Bis(Alkylaluminum)-Initiated Chain-Growth Network Epoxide Polymerization: Synthesis and Transport Properties. *Macromolecules* **2020**. https://doi.org/10.1021/acs.macromol.9b02318.

(68) Jimenez-Vergara, A. C.; Lewis, J.; Hahn, M. S.; Munoz-Pinto, D. J. An Improved Correlation to Predict Molecular Weight between Crosslinks Based on Equilibrium Degree of Swelling of Hydrogel Networks. *J. Biomed. Mater. Res. - Part B Appl. Biomater.* **2018**, *106* (3), 1339–1348. https://doi.org/10.1002/jbm.b.33942.

(69) Sen, M.; Yakar, A.; Güven, O. Determination of Average Molecular Weight between Cross-Links ($\bar{M}$(c)) from Swelling Behaviours of Diprotic Acid-Containing Hydrogels. *Polymer.* **1999**, *40* (11), 2969–2974. https://doi.org/10.1016/S0032-3861(98)00251-1.c